Studies on the Encephalomyocarditis Virus Leader and 2A Proteins' Cooperative Interactions for Host Cell Control

By

Ryan Virgil Petty

A dissertation submitted in partial fulfillment

of the requirements for the degree of

Doctor of Philosophy

Biochemistry

at the

University of Wisconsin – Madison

2014

Date of final oral examination: 12-11-14

The dissertation is approved by the following members of the Final Oral Committee:

Ann C. Palmenberg, Professor, Biochemistry

Paul D. Friesen, Professor, Biochemistry

M. Thomas Record, Professor, Biochemistry

Robert T. Striker, Associate Professor, Infectious Disease

Julie C. Mitchell, Associate Professor, Biochemistry

Acknowledgements

Dr. Ann Palmenberg

For her infectious enthusiasm, guidance, and giving us enough space to grow

Dr. Paul Friesen

For fostering a passion and appreciation for viruses and teaching

Drs. Tom Record, Rob Striker, and Julie Mitchel

For their advice, support, and encouragement to become a better scientist

Marchel Hill, Brad Brown, Kelly Watters, Valjean Bacot-Davis, Holly Basta, and Jessica Ciomperlik

For being the best coworkers and family I could have hoped for

Drs. Tom Neal, Tom German, and Tom Sharkey

For being mentors and passionate about science

To all my friends (fencers, gamers, OutReach, etc) in Madison and beyond

For keeping me mostly sane

To my mom, dad, and brother

I simply wouldn't be here without your love and support

Table of Contents

Abstract

Studies on the Encephalomyocarditis Virus Leader and 2A Proteins' Cooperative Interactions for Host Cell Control

Ryan V. Petty

Under the supervision of Professor Ann C. Palmenberg

At the University of Wisconsin-Madison

Encephalomyocarditis virus (EMCV), a Picornavirus, encodes two primary host antagonists, the Leader (L) and 2A proteins. In this thesis, we sought to further define the biochemical mechanism of host cell shutdown induced by these two viral proteins.

L (67 amino acids) binds cellular RanGTPase and induces hyperphosphorylation of nuclear pore proteins, which shuts down active nucleocytoplasmic trafficking of critical antiviral signaling proteins. We showed that L and Ran bind tightly with a low K_D (equilibrium dissociation constant) of 3 nM. RCC1 facilitated this binding and overcame GDP and GTP inhibition of recombinant L:Ran binding. The *in vitro* requirement of RCC1, an exclusively nuclear protein, suggests an active localization of L to the nucleus, despite L lacking a nuclear localization signal (NLS).

We showed that 2A (143 amino acids), which encodes an NLS, binds L with a K_D=1.5 μM, far less so than L:Ran, suggesting a more transient interaction. This binding is unaffected by the phosphorylation status of L, but requires several residues in the L hinge region and the first fifty amino acids of 2A. L:2A binding may explain previously observed phenotypes of 2A mutant viruses, instead impacting L localization to the pore or proper processing of the L-P1-2A precursor by the viral 3C protease.

2A induces a general shutdown of translation through an unresolved mechanism. Addition of recombinant 2A to translation extracts with translation reporter constructs favored viral IRES-driven over host 5' cap-driven translation. The first fifty amino acids of 2A were sufficient for inducing this IRES:cap shift, but not for the general translation shutdown observed with full 2A. 2A contains a C-terminal eIF4E binding site and disruption of eIF4E:4G interactions enhanced 2A-induced cap-dependent translation shutdown. 2A also induces the formation of salt-sensitive 80S ribosomes, suggesting that 2A may be assembling translation-deficient initiation complexes.

Taken together, these studies have further defined the biochemical mechanism of L, the only known direct inhibitor of Ran, and protein 2A, a potent viral inhibitor of cellular translation. We have also shown that L and 2A activities should not necessarily be considered independent of one another, but instead cooperative.

List of Figures and Tables

Appendix

List of Abbreviations

$2A^{pro}$	2A protease
$3C^{pro}$	3C protease
4EBP1	eIF4E-binding protein 1
AMPK	AMP-activated protein kinase
CK2	casein kinase 2
CRE	cis-acting replication element
DNA	deoxyribonucleic acid
eIF	eukaryotic initiation factor
EMCV	encephalomyocarditis virus
F/G	phenylalanine/glycine
F/R	firefly/Renilla luciferase
GB1	protein G B-domain
GDP	guanosine diphosphate
GEF	guanine-nucleotide exchange factor
GNP	guanosine di- or triphosphate
GST	glutathione-s-transferase
GTP	guanosine triphosphate
HIV	human immunodeficiency virus
HPLC	high-pressure liquid chromatography
IC_{50}	50% inhibitory concentration
IFN	interferon
IPTG	isopropyl β-D-1-thiogalactopyranoside
IRES	internal ribosome entry site
ITAF	IRES trans-activating factor
k_a	on-rate
k_d	off-rate
K_D	dissociation constant
L	leader
LY	LY294002
mAb	monoclonal antibody
mant	2'/3'-O-N-methylanthraniloyl
MAPK	mitogen-activated protein kinase
MBP	maltose-binding protein
mRNA	messenger RNA
mTOR	mammalian target of rapamycin
NCT	nucleocytoplasmic trafficking
NE	nuclear envelope
NES	nuclear export signal
NLS	nuclear localization signal
NMR	nuclear magnetic resonance
NPC	nuclear pore complex
NTF-2	nuclear transport factor 2
NTP	nucleotide triphosphate

Nup	nuclear pore protein
PFU	plaque-forming unit
PI	phosphotidylinositol
PI3K	phosphoinositide 3 kinase
PTB	polypyrimidine tract-binding protein
RanGAP	Ran GTPase-activating protein
Rap	rapamycin
RCC1	regulator of chromatin condensation 1
RdRp	RNA-dependent RNA polymerase
RNA	ribonucleic acid
SPR	surface plasmon resonance
SYK	spleen tyrosine kinase
TMEV	Theiler's murine encephalomyelitis virus
UTR	untranslated region
VCAM-1	vascular cell adhesion molecule 1
vRNA	viral RNA
VSV	vesicular stomatitis virus
Wort	wortmannin

Chapter 1

Introduction

Virus-host interactions

Viruses are small, obligate, intracellular parasites that contain a genome consisting of single- or double-stranded DNA or RNA. Lacking the full complement of translational machinery required for life, viruses *must* utilize host components to replicate their genomes and produce virus progeny. Consequently, viruses compete with host mRNAs and have evolved diverse mechanisms for shutting down host mRNA translation in favor of viral RNAs (either genomic or transcribed). Cells have themselves evolved numerous mechanisms for combatting viral infections, including broadly targeted innate systems (e.g., interferon) and pathogen-specific adaptive systems (e.g., antibodies and cytotoxic T-lymphocytes). Not surprisingly, viruses have also fought back in this arms race and have evolved further countermeasures in order to maintain an advantage against the host.

For picornaviruses, the family of viruses studied here, these anti-host countermeasures can involve any of several genetic components. Among them is the IRES (internal ribosome entry site), which is a highly structured RNA element that facilitates 5' methylguanosine cap-independent translation. In the absence of additional viral factors, host ribosomes will preferentially translate an IRES-driven over a cap-driven gene by ~10 fold. Some picornaviruses, such as enteroviruses, have evolved

accessory proteins that further enhance IRES-driven translation. Enterovirus $2A^{pro}$ specifically cleaves host eIF4G, the 5' mRNA cap-binding component of cellular translation, which results in a shutdown of host mRNA translation. This cleavage has a two-fold effect: IRES-driven translation is further enhanced, and the host is unable to produce antiviral proteins such as interferon (1).

Cardioviruses, the genera of focus for this work, also shut down cap-dependent translation and antiviral protein production through a different series of mechanisms, including the viral proteins Leader (L) and 2A (which in this case is *not* a protease). The experimental focus of this thesis is to dissect the biochemical mechanisms by which these particular viral proteins act, both independently and cooperatively, to shutdown host defenses and prime the infected the cell for optimal viral replication.

Picornaviruses

Taxonomy:

Picornaviruses are a family of single-stranded, positive-sense RNA viruses that infect a wide range of animal hosts. There are currently 26 (and growing) identified genera of picornaviruses, among the most important to human health are *Hepatovirus* (Hepatits A virus), *Enterovirus* (Enterovirus C [Poliovirus], Enterovirus A [EV-71], and Rhinovirus [A, B, and C]), *Parechovirus* (Human parechovirus), and the viruses of this study, *Cardiovirus* (Encephalomyocarditis virus and Theilovirus [Theiler's murine encephalomyelitis virus and Saffold virus]) (ICTV Report 2013, Table 1-1).

Genome organization:

Picornaviruses follow a well-conserved genome organization (Fig 1-1). The first component of the genome is the viral protein VPg that acts as a primer for genome replication and is incorporated during virion production. The 5' UTR (un-translated region) of the genome contains the IRES which facilitates cap-independent translation and also includes the AUG start codon. Picornaviruses are translated into a single open reading frame consisting of three regions (P1, P2, and P3) that is cleaved co- and post-translationally by either virus-encoded proteases ($2A^{pro}$ and $3C^{pro}$) (2-5) or by a "ribosome skipping" mechanism encoded between the P1 and P2 (often the C-terminus of the 2A gene) (6). The first region, P1, contains the structural proteins 1A, 1B, 1C, and 1D (also known as VP4, VP2, VP3, and VP1, respectively). These proteins coalesce around the RNA genome to form the non-enveloped icosahedral capsid that is transmitted from cell to cell (and host to host). The aphtho-, kobu-, tescho-, and cardiovirus genera all include a "Leader" protein at the N-terminus of the polyprotein. These proteins share a name but vary drastically in structure and function. The aphthovirus Leader is a protease that cleaves eIF4G (aphthoviruses and cardioviruses lack a proteolytic activity in their 2A) (7) whereas the cardiovirus Leader binds cellular proteins, including Ran GTPase and cardiovirus 2A (detailed in this thesis), ultimately shutting down nucleocytoplasmic trafficking (NCT) (8, 9).

The P2 region contains the non-structural proteins 2A, 2B, and 2C whose roles deal primarily with viral replication and host shutdown. The 2A of enteroviruses (as discussed above) is a protease that cleaves itself from the polyprotein (as the initial P1/P2 cleavage) and host eIF4G. In addition, $2A^{pro}$ cleaves nuclear pore proteins

(Nups) that result in the shutdown of NCT and diffusion of normally nuclear host proteins to the cytoplasm, some of which are required for optimal viral translation (10-12). For aphtho- and cardioviruses, the 2A contains at its C-terminus a “primary cleavage cassette” which prevents the nascent polypeptide chain from forming a new peptide bond (6). The ribosome then continues on translating 2B and the remainder of the polyprotein. The cardiovirus 2A has additional anti-host activities during infection, which includes the general shutdown of cap-dependent translation that will be discussed later in this chapter. The function of 2B is poorly understood. Its activity appears to be related to developing the membrane environment wherein viral RNA replication occurs (13). 2C likewise has been shown to affect membranes in the cell and contains helicase and NTPase motifs (13-17).

The P3 region contains proteins required for genome replication and anti-host activities, 3A, 3B, 3C, and 3D. 3A is poorly understood; however, mutations in this region have been shown to attenuate the virus (18, 19). 3B is the VPg that acts as the primer for RNA replication (20, 21). VPg is uridylated on a tyrosine residue, where the polymerase then begins transcribing from the template strand (22). The 3C protein (or its precursor, 3CD) is the primary protease of the virus, responsible for the majority of polypeptide cleavages (23-25) (Fig 1-2). In addition, 3C/3CD can cleave several host transcription and translation factors (26-28). The 3D protein is the RNA-dependent RNA polymerase (RdRp) for the virus and is responsible for production of both the negative strand (replication intermediate) and the positive strand (genome, mRNA) (29-31).

The final component of the RNA genome is the 3’ UTR that contains a virus-encoded poly-A tail in addition to regions involved in RNA replication. Picornaviruses

also contain a CRE (cis-acting replication element) that is located within the coding sequence at various locations in the genome, depending on the genera of virus (32-34). This element functions as a structured RNA during replication.

Lifecycle:

The initial step in a picornaviral lifecycle at the cellular level is attachment to a host receptor followed by entry into the cell (Fig 1-3). Cardioviruses utilize the cell surface VCAM-1 (vascular cell adhesion molecule) as well as other sialoglycoproteins to attach to cells and initiate receptor-mediated endocytosis (35-38). Upon entering the cell, the viral capsid uncoats and releases the genomic RNA into the cytoplasm (39). Being messenger-active, the genome may immediately be translated by ribosomes in a 5' cap-independent manner. Cardioviruses use a Type-II IRES (Enteroviruses use a Type-I and Hepatitis C virus uses a Type-III, differing by the cellular factors required for optimal translation). The IRES directly recruits cellular translation initiation factors including eIF4G and 4A, but not 4E (40, 41) (Fig 1-5). Enteroviruses take this a step further by cleaving eIF4G, eliminating the N-terminal eIF4E-binding domain required for forming the initiation complex with cellular capped transcripts (42). In addition to canonical translation initiation factors, the IRES also recruits additional proteins named ITAFs (IRES trans-activating factor), which include PTB (polypyrimidine tract binding protein) for Type-II and La autoantigen and nucleolin for Type I IRES (43-46). It is interesting to note that many of these proteins have exclusively nuclear lifecycles during normal cell function, but are relocated during viral infection.

The nascent polyprotein is cleaved by the viral 3C protease (and partially by 2A in some genera) and processed into the mature viral proteins. These proteins may go on to modulate the host cell to inhibit antiviral defenses and/or prime the cell for viral replication, or directly assemble on membranes to form viral replication complexes (consisting of 3A, 3B, and 3D) producing both negative sense intermediates and positive sense genomes (13, 47, 48). These newly transcribed genomes may then be used as messages for additional rounds of translation or can be incorporated into assembling capsids. The protomers consist of one copy each of 1A, 1B, 1C, and 1D, which then assemble into pentamers (five protomers per pentamer). Twelve pentamers ultimately form the mature virions, which are released from the cell via lysis (49).

Cardioviruses

History:

Encephalomyocarditis virus (EMCV) and Mengo (a major strain of EMCV) were first isolated nearly 70 years ago (50, 51). Numerous outbreaks have since been observed in farms, zoos, and wildlife reserves, though attenuated strains have been used over the past twenty years to help control outbreaks (52-55). In addition to being a significant agricultural pathogen, EMCV (specifically the IRES) has been used for decades as an important laboratory tool for studying eukaryotic translation and as a model for other picornaviruses that may be more difficult to culture and study *in vitro* (e.g. Hepatitis C virus) (56-59).

Host modulation by Cardioviruses:

While all picornaviruses modify their host cell to varying degrees, there are several viral proteins and molecular events that are unique to cardioviruses: namely, hyperphosphorylation of Nups with subsequent shutdown of NCT by L and modulation of host translation machinery by the 2A protein (8, 60, 61).

Leader-induced NCT shutdown:

L is the first protein produced in the cardiovirus polyprotein (Fig. 1-1). It is a small (67 amino acid in EMCV), highly acidic protein (pI=3.8) with no known sequence or structural homology to any protein yet observed in nature (9, 62, 63). L has distinct domains which function by binding several host proteins (Fig. 1-4A). The N-terminus of L contains a novel CHCC zinc finger fold, mutations of which completely inactivate the protein and disrupt its structure (9, 62, 64). A central “hinge” domain is important for binding the cellular NCT factor Ran GTPase (65). In addition, several residues located in this region are phosphorylated by cellular kinases. For EMCV/Mengo, T_{47} is phosphorylated by Casein Kinase II (CK2) while Y_{41} is phosphorylated by Spleen Tyrosine Kinase (SYK) (66). For TMEV (BeAn) and Saffold, AMP-activated Protein Kinase (AMPK) appears to be a dominant kinase for phosphorylation of L (67). Mutation of these residues to non-phosphorylatable cognates abrogates L activity, which can be partially restored by mutation to phosphomimetic residues (66). Finally, the C-terminus of L contains a stretch of acidic residues (Asp/Glu) that impart the low pI of this protein. Mutations in this region likewise reduce anti-host activities (8). The NMR structure has been solved for full-length Mengo L and is shown in Fig. 1-4B (63).

L has many ascribed anti-host activities, including the disruption of NCT, host translation, mitotic spindle assembly, stress-granule formation, and α/β interferon production, many of which may be linked to the hyperphosphorylation of Nups (8, 9, 68-73). For enteroviruses, disruption of NCT is a proteolytic cleavage of Nups catalyzed by the 2A protease (11, 12, 74, 75). Cardioviruses take a different approach. Instead of a virus-encoded enzymatic activity, L affects Nups by the misdirection of cellular kinases. ERK and p38 are members of the mitogen-activated protein kinase (MAPK) family, and have been implicated through drug screens to be directly or indirectly (via downstream kinases) responsible for the aberrant hyperphosphorylation induced by L (60).

Nucleocytoplasmic Trafficking:

One of the identified binding partners of L is the small GTPase Ran (9). In an uninfected cell, Ran is a molecular switch that is found predominantly in the GTP-bound form in the nucleus and GDP-bound form in the cytoplasm, thus creating a gradient across the nuclear envelope. In the nucleus, Ran forms a trimeric complex with an exportin (karyopherin), which are large adaptor proteins that bind and interact with the F/G (phenylalanine/glycine) repeats of Nups, and a cargo that contains a nuclear export signal (NES) (Fig 1-5). Examples of NES-containing molecules include spliced mRNA ribonucleoprotein complexes and the HIV Rev protein (76-79). Once these complexes have traversed the nuclear pore, the cytoplasmic RanGAP (RanGTPase activating protein) catalyzes the conversion of RanGTP to RanGDP. The inactive RanGDP then dissociates the complex and the exportin and cargo are released into the cytoplasm. Inactive Ran is imported back into the nucleus via the Ran-specific importin NTF-2

(nuclear transport factor-2). Once RanGDP enters the nucleus, it binds the GEF (guanine-nucleotide exchange factor) RCC1 (regulator of chromatin condensation-1). RCC1 then swaps out GDP for GTP, generating active Ran and continuing the export/import cycle. For import, a trimeric complex forms between Importin α, Importin β (of which there are at least six identified in cells), and the cargo, which contains a nuclear localization signal (NLS). Once this heterotrimer enters the nucleus, active RanGTP binds and dissociates the complex.

2A-induced cellular translation shutdown:

For enteroviruses, the mechanism of cap-dependent shutdown again is enzymatic. The 2A protease cleaves eIF4G, retaining only the segment required for IRES-driven translation and eliminating the domain that recruits the cap-binding factor eIF4E. Here, cardioviruses have evolved to use an alternate, non-proteolytic approach. The 2A of cardioviruses (143 amino acids for EMCV) contains identified domains that interact with several cellular components (Fig 1-6). The N-terminus (amino acids 1-50) is a highly basic region (pI=10.1) that has been shown to bind to RNA with high affinity, though in a non-sequence-specific manner. The central portion of the protein (amino acids 51-100) contains predominantly hydrophobic residues, as well as a “yeast ribosome protein”-like nuclear localization signal (80). The C-terminus of 2A (amino acids 101-143) contains a verified eIF4E-binding site (80) and the final dozen amino acids are the cleavage cassette that releases the L-P1-2A precursor from the nascent polypeptide through a “ribosome skipping” mechanism (6, 81, 82) (Fig 1-2).

During infection, 2A is predominantly localized to nucleoli (the nuclear sites of ribosome biogenesis), possibly due to its NLS and RNA-binding activities (80, 83). However, the functional importance of this localization is very poorly understood. 2A can incorporate into pre-40S ribosomes during infection (but does not saturate them) and can also induce a general reduction in cap-dependent translation (61). In a bicistronic reporter plasmid containing a cap-driven firefly luciferase and an IRES-driven *Renilla* luciferase, expression of 2A decreases translation of both reporters, but represses cap-driven translation more than IRES-driven translation (61). Deleting portions of 2A or specifically mutating the NLS or eIF4E-binding site dramatically reduces viral titers, plague sizes, and can cause severe defects polyprotein processing (80).

Cellular vs. viral translation initiation:

The initiation of eukaryotic translation has been a major area of biochemical study for over 50 years (84). Similarly, the effects of viruses (specifically picornaviruses) on eukaryotic translation has been studied for a similar period of time (85). The "canonical" factors required for translation of mRNAs are collectively known as eukaryotic initiation factors (eIFs) (86). Briefly, the vast majority of cellular mRNAs contain a 5' 7-methyl guanosine cap, which is first bound by eIF4E. eIF4E then binds the scaffold protein eIF4G that in turn binds the RNA helicase eIF4A (Fig. 1-7). These three proteins are together known as eIF4F (87). eIF4G then recruits the 43S initiation complex, which consist of the 40S ribosome, eIF2α, eIF3, and the start methionine-tRNA. This complex scans along the mRNA until it reaches the appropriate initiation sequence proximal to the "AUG" start codon (88). Once the AUG is reached, the 60S

ribosome binds, the initiation factors are released, and the mRNA is translated. The rate of initiation, as well as translation itself, is highly regulated by a series of kinases, phosphatases, and accessory binding proteins (88).

EMCV IRES-driven translation requires fewer canonical components (Fig 1-7). In fact, excess eIF4E has been shown to be inhibitory to IRES translation, whereas expression of 4EBP1, a protein that binds and sequesters eIF4E, was shown to enhance IRES translation (1). 4EBP1 has even been shown to be hypophosphorylated during EMCV and poliovirus infection, suggesting a sequestration of eIF4E (89). The fundamental mechanism by which the 2A protein modulates the host translational landscape is a major experimental focus of this thesis.

Thesis Preview

Recent studies have detailed the broad outcomes of Cardiovirus L and 2A proteins in the cell during infection. Little is known, however, about the cellular factors and biochemical mechanisms involved in the host shutdown induced by these proteins. **In this thesis, we examined the role that these two proteins play in interacting with cellular factors, as well as one another, to shut down host translation and antiviral defenses.** In Chapter 2, we evaluated the effect of exogenous nucleotide and the Ran guanine-nucleotide exchange factor, RCC1, on L and cellular Ran binding. In Chapter 3, we demonstrated that L and 2A can also bind one another and detailed this interaction through point mutations, truncations, and phosphorylation inhibition. We also showed that this interaction is conserved among Cardioviruses, though with differing affinities. In Chapter 4, we examined the influence that 2A has on translational complexes. We used a number of methods including ribosome profiling, subcellular fractionation, luciferase assays, and 2A mutant viruses to demonstrate that 2A is necessary and sufficient for inducing translation shutdown and shifting translational components from cap-dependent towards IRES-driven translation. Together, these studies further detail the potent anti-host activities of Cardiovirus L and 2A proteins.

Genus	Example Species
Aphthovirus	Foot-and-mouth disease virus
Aquamavirus	Aquamavirus A
Avihepatovirus	Duck hepatitis A virus
Avisivirus	Avisivirus A
Cardiovirus	Encephalomyocarditis virus, Theilovirus
Cosavirus	Cosavirus A
Dicipivirus	Cadicivirus A
Enterovirus	Enterovirus C (Poliovirus), Rhinovirus
Erbovirus	Equine rhinitis B virus
Gallivirus	Gallivirus A
Hepatovirus	Hepatitis A virus
Hunnivirus	Hunnivirus A
Kobuvirus	Aichivirus A
Megrivirus	Melegrivirus
Mischivirus	Mischivirus A
Mosavirus	Mosavirus A
Oscivirus	Oscivirus A
Parechovirus	Human parechovirus
Pasivirus	Pasivirus A
Passerivirus	Passerivirus A
Rosavirus	Rosavirus
Salivirus	Salivirus A
Sapelovirus	Porcine sapelovirus
Senecavirus	Seneca Valley virus
Teschivirus	Porcine teschovirus
Tremovirus	Avian encephalomyelitis virus

Table 1-1: Picornavirus genera and representative species. Adapted from ICTV Virus Taxonomy, 2013 Release. EC 45, Edinburgh, July 2013.

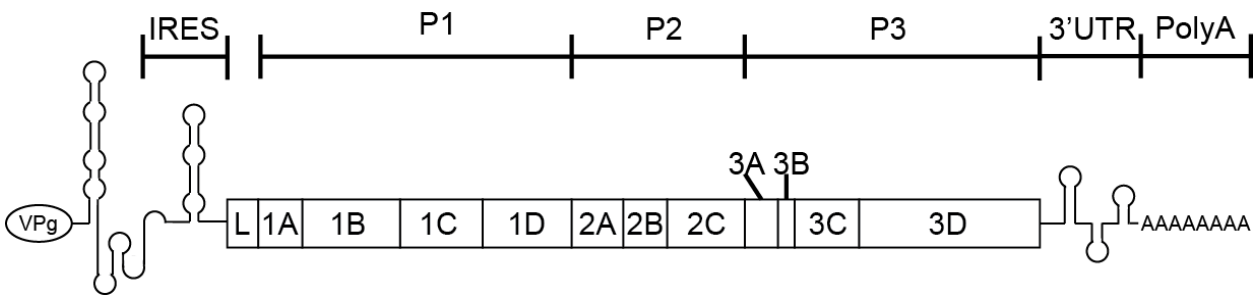

Figure 1-1: Cardiovirus genome layout. A schematic of the cardiovirus genome is presented. The 5' UTR contains replication elements, the pathogenic poly-C tract, and the IRES. The 3' end contains replication elements and is polyadenylated.

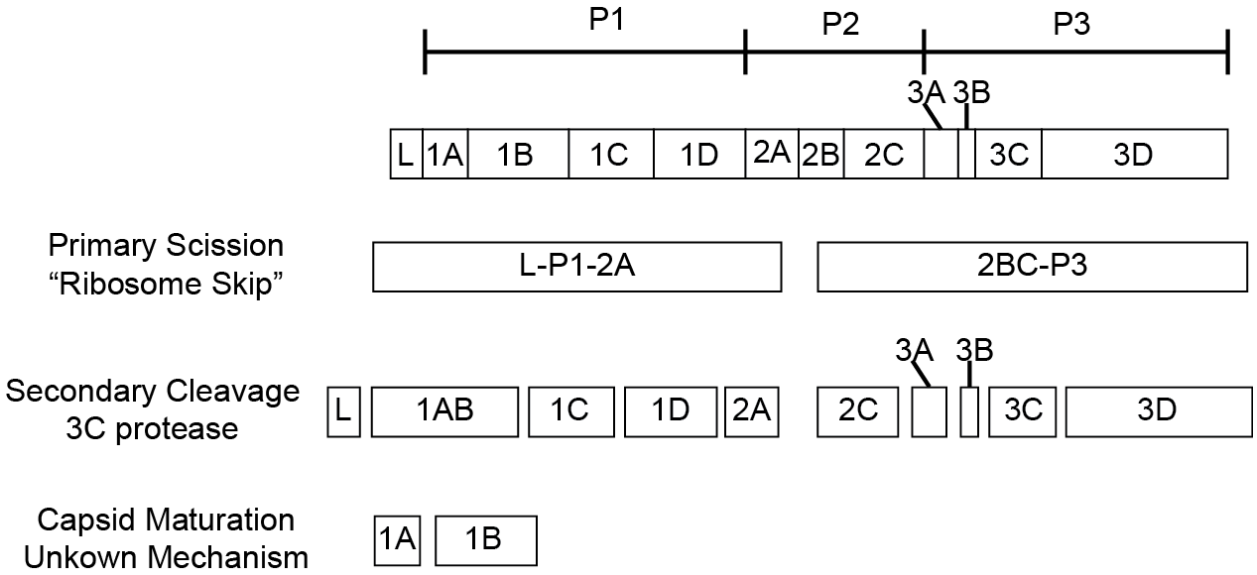

Figure 1-2: Polyprotein processing cascade. The cardiovirus genome is translated as a single polyprotein. The C-terminal NPG/P of 2A induces scission of L-P1-2A from the nascent peptide chain. 3C protease cleaves all subsequent junctions (except 1A/1B) to produce the mature viral proteins. Cleavage of 1AB is required for capsid maturation.

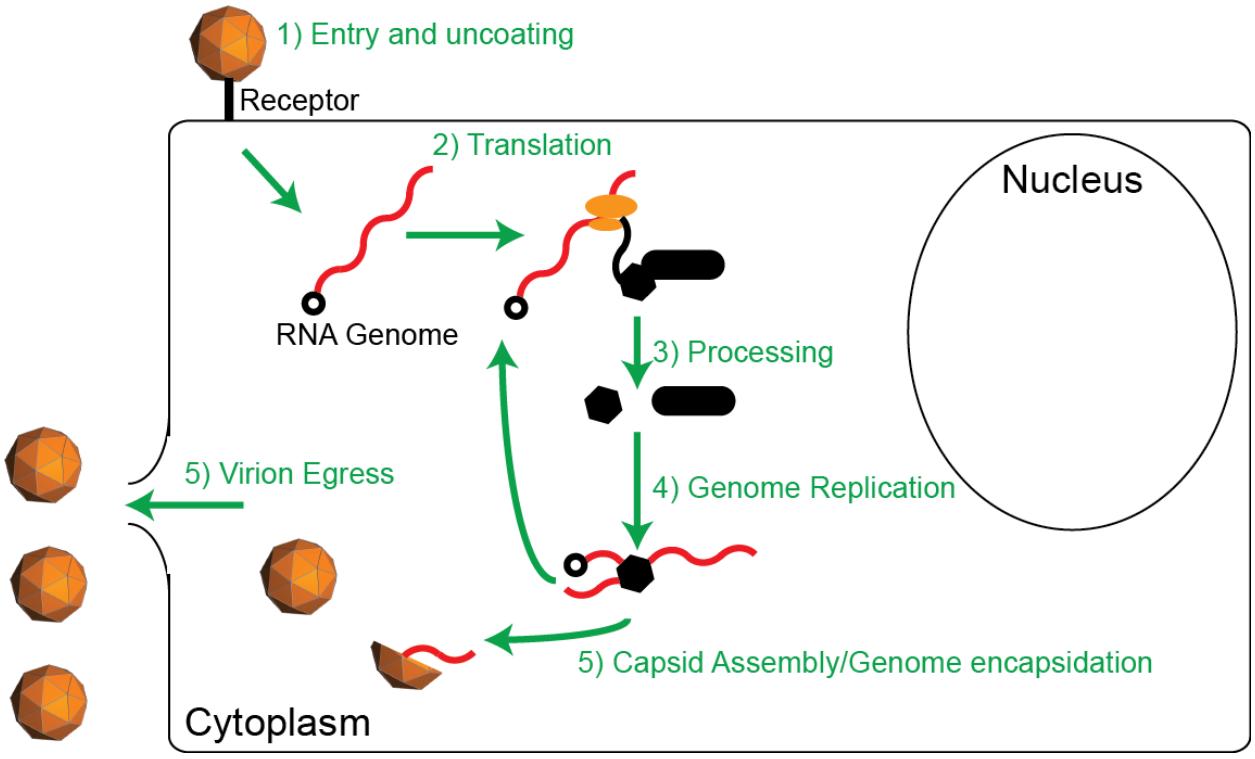

Figure 1-3: The picornavirus lifecycle. A schematic of the general lifecycle of picornaviruses is presented. Major events are highlighted in green.

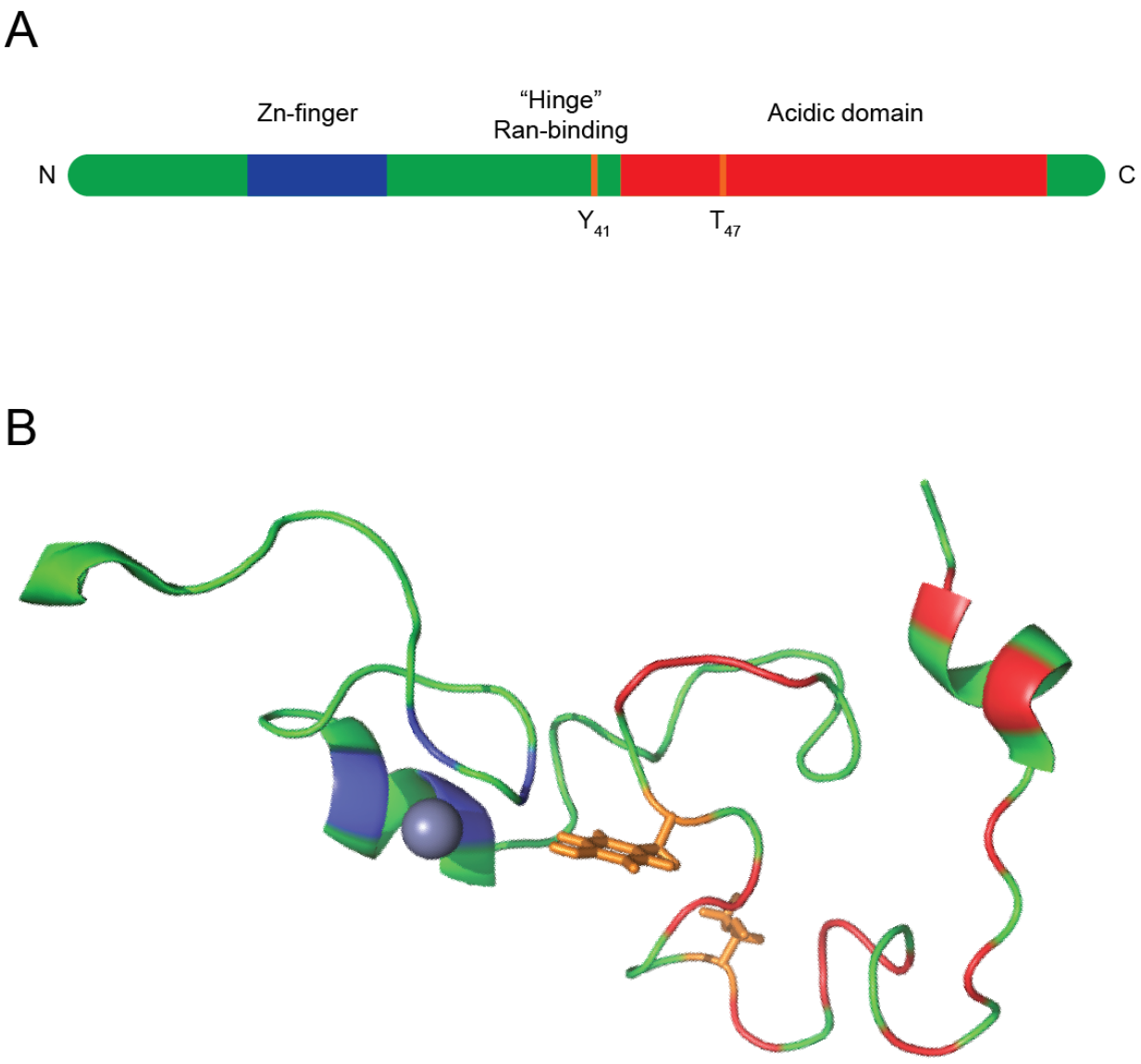

Figure 1-4: EMCV (Mengo) Leader structure and interactions. A) Diagram of L with zinc finger (CHCC, blue), hinge, and acidic domain (D/E, red) as well as phosphorylated residues Y41 and T47 (orange) indicated. B) The NMR structure of full-length, non-phosphorylated EMCV (Mengo strain) L is shown (PDB: 2MMH). Domains and residues are colored as in A.

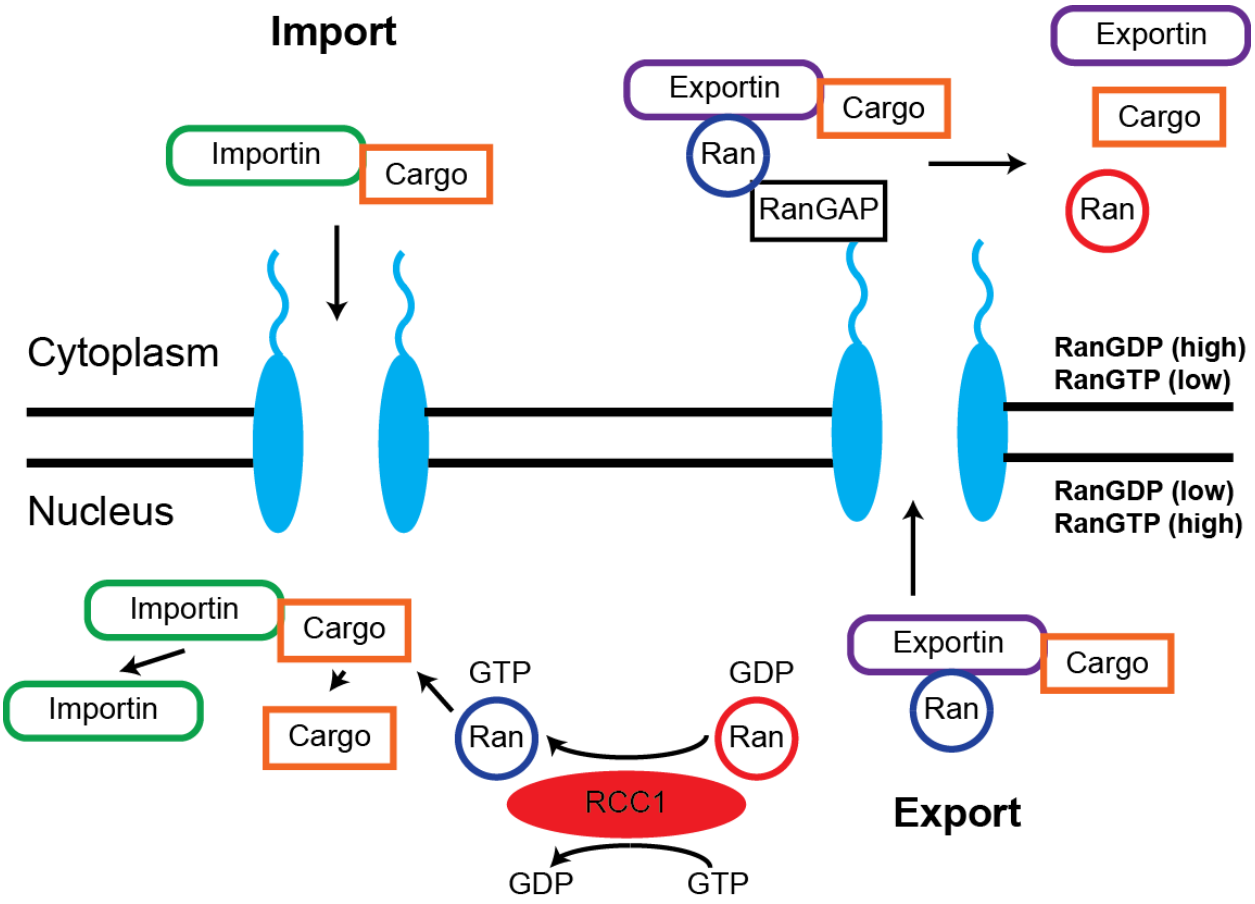

Figure 1-5: Nucleocytoplasmic Trafficking. An overview of the nuclear import/export cycle is presented. Nuclear RCC1 and cytoplasmic RanGAP generate a RanGDP/GTP gradient across the nuclear pore. This gradient facilitates the assembly/disassembly of complexes between importins/exportins and their cargos.

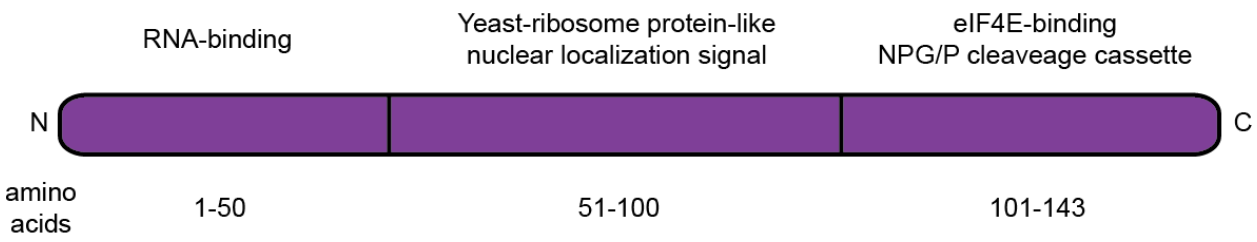

Figure 1-6: EMCV 2A and protein interactions. A schematic of EMCV 2A is shown. The first 50 amino acids ($2A_{1-50}$) have been shown to bind RNA (K_D=23 nM) non-specifically (unpublished). $2A_{51-100}$ contains the nuclear localization signal. $2A_{101-143}$ contains the eIF4E-binding site and NPG/P primary cleavage cassette.

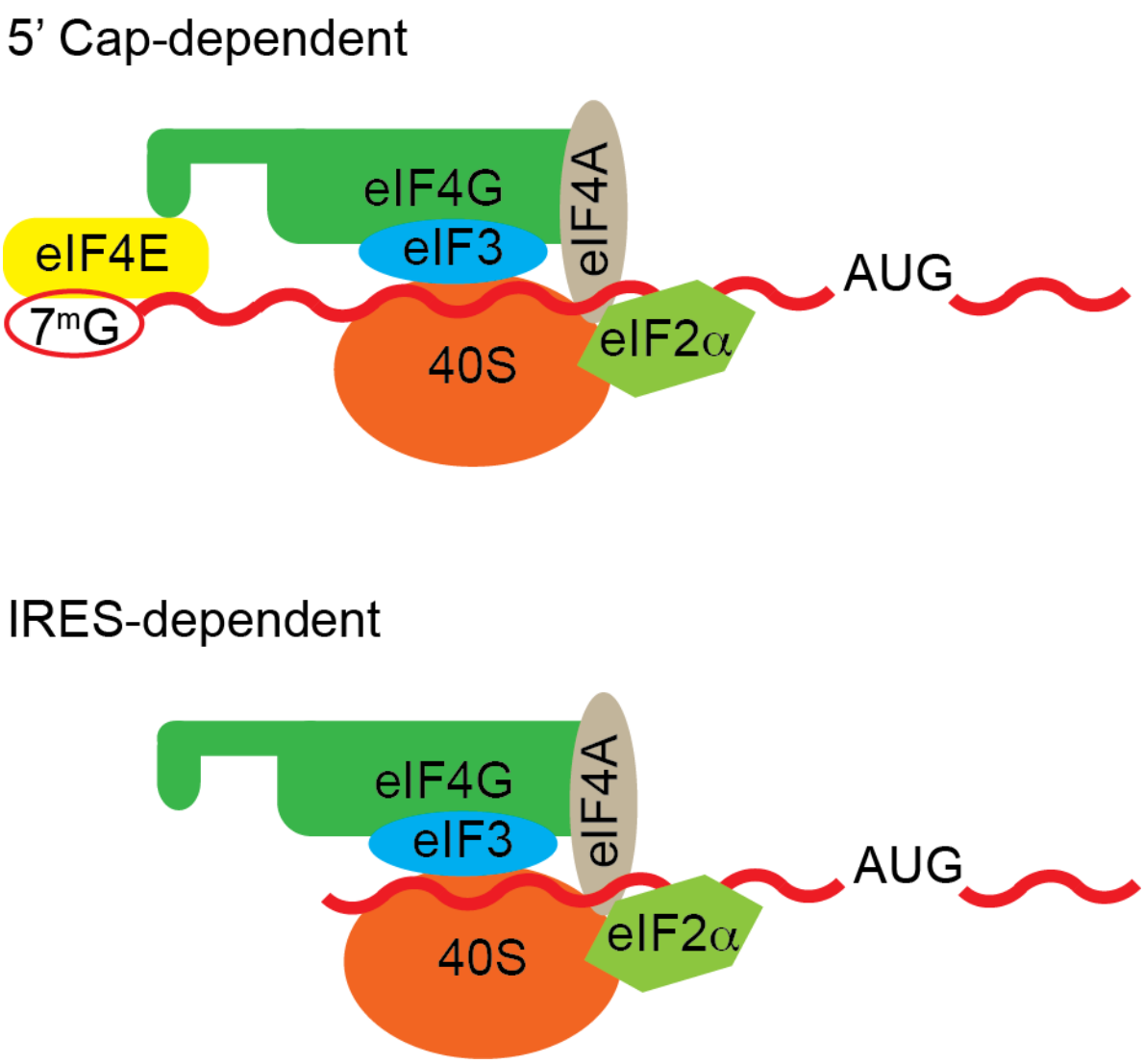

Figure 1-7: Cellular and viral translation initiation. Cellular capped mRNAs require initiation factors to assemble and recruit the 40S ribosome. Cardiovirus RNAs contain an IRES which can directly recruit the factors required (excluding eIF4E) to begin translation.

Chapter 2

Guanine-nucleotide exchange factor RCC1 facilitates a tight binding between EMCV Leader and cellular Ran GTPase

A condensed version of this work was published as a "note" in:

The Journal of Virology, Volume 87, Pages 6517-6520 (2013)

The published version contained Figures 2-1, 2-3, 2-5 and Table 2-1

Abstract

The Leader (L) protein of encephalomyocarditis virus (EMCV) is able to shut off host cell nucleocytoplasmic trafficking (NCT) by inducing hyperphosphorylation of nuclear pore proteins. The mechanism by which this non-enzymatic viral protein of 7 kDa can achieve such dramatic effects during infection is not well understood, but the requisite processes clearly involve L binding to the small GTPase Ran, a critical cellular factor of active NCT. Here, several *in vitro* methods are described, including nucleotide spectrofluorimetry and surface plasmon resonance, to probe the interactions between L and Ran. The experiments demonstrate that excess GDP and GTP in solution are strongly inhibitory to L:Ran binding but the guanine-nucleotide exchange factor for Ran, RCC1, is capable of relieving this inhibition. Using recombinant proteins, L binds Ran with a K_D of ~3 nM and reaches equilibrium binding within 15 minutes, but only in the

presence of RCC1. Fluorescent nucleotide experiments also suggest that L binds at or near the nucleotide-binding pocket of Ran. As the only known direct protein inhibitor of Ran, L presents a unique opportunity for the study of nuclear trafficking events that are dependent on Ran for proper function. The results suggest a mechanism whereby L enters the nucleus early during infection, binds Ran near the nuclear rim at the sites of RCC1 localization, and subsequently subverts NCT by kinase activation to prevent the expression of antiviral signals.

Introduction

In eukaryotes, transcription and translation are spatially separated by the nuclear envelope (NE). The selective gateways for the transport of proteins and RNA complexes between the nucleus and cytoplasm are called nuclear pore complexes (NPC). Each NPC is a 125 MDa association of over 30 unique proteins arranged in 8-fold radial symmetry (90). Proteins larger than 40 kDa require active transport to traverse the pore, and are typically shuttled across the NE after binding to transport proteins called karyopherins. These complexes pass through the NPC via karyopherin-dependent interactions with sequential phenylalanine-glycine (FG) repeat domains on certain nuclear pore proteins (Nups) (91).

The transport bottleneck of the NPC provides a unique target for viruses to selectively shut off anti-viral cytokine signals, because many such proteins originate from signal cascades in the cytoplasm or require transcriptional activation in the nucleus. For instance, cellular IRF7 or IRF7/IRF3 heterodimers must enter the nucleus

after translation and phosphorylation in the cytoplasm to turn on transcription of interferon-α or -β (IFN), which subsequently induces an anti-viral state in infected and surrounding cells (70, 71, 92, 93). To prevent IFN or other cytokine activation, many RNA viruses, despite being primarily or exclusively cytoplasmic in their own replication cycles, encode proteins that target specific nuclear transcription functions or inhibit NPC transport. The M protein of vesicular stomatitis virus (VSV), a rhabdovirus, is one such example. M binds to RAE1, a karyopherin, and prevents mRNA-RAE1 interactions, thus shutting down cellular mRNA export and translation (94). Likewise, the 2A protease of rhinovirus and poliovirus (both of the genus *Enterovirus*), enzymatically cleaves certain FG-containing Nups to inhibit karyopherin transport, mRNA export, and subsequently, cytokine activation (11, 94).

Encephalomyocarditis virus (EMCV) is a member of the *Cardiovirus* genus in the *Picornaviridae* family. It has a (+) sense, single stranded RNA genome whose translation is IRES-driven and occurs immediately in the cytoplasm after uncoating (95). EMCV infection shuts down active nucleocytoplasmic trafficking (NCT), by inducing the hyperphosphorylation of FG-containing Nups, potentially blocking an otherwise toxic IFN α/β production (8, 71, 96-98). The specific Nup phosphorylation mechanism catalyzed by kinases in the ERK1/2 and p38 pathways is poorly understood, though it is clear that the triggering event requires only the presence of the viral Leader (L) protein (8, 99). *In vitro* or *in vivo*, L alone, in the context of cytoplasm and NPC targets, has been shown to irreversibly induce the inhibition of nucleocytoplasmic transport, including cellular mRNAs and nuclear-targeted reporter proteins (8, 100, 101).

L is a small protein (67 amino acids) with a novel N-terminal CHCC zinc-finger motif and a highly acidic (pI 3.8) β-hairpin motif at the C-terminus (62, 102). Despite being sufficient to shut down NCT, L itself has no predicted or observable enzymatic activity; therefore, L must act by binding or abrogating cellular and/or viral cofactors to bring about such significant cellular responses. Indeed, one of the proteins L has been shown to bind directly is Ran GTPase, a central component of all active NCT processes (9).

Ran, a member of the Ras superfamily of small GTPases, regulates the transport of practically all cargo through the NPC and also participates in mitotic spindle formation by binding and sequestering required karyopherins (103, 104). The normal function of Ran is to bind and hydrolyze GTP into GDP. The nucleotide-bound forms each have different cellular localizations as well as distinct structures (103), which facilitate the formation or dissociation of cargo:karyopherin complexes. During nuclear export, a complex of RanGTP, karyopherin, and cargo (e.g. mRNA) is formed in the nucleus near the NE. After traversing the NPC, cytoplasmic auxiliary proteins, RanGAP and RanBP1, accelerate Ran's intrinsically slow hydrolysis of GTP and the consequent structure change dissociates the complex, releasing the cargo in the cytoplasm. The free RanGDP is cycled back into the nucleus by its own unique karyopherin, NTF2. RanGDP then binds RCC1, a chromatin-tethered guanine-nucleotide exchange factor (GEF) to facilitate Ran nucleotide exchange (105). Since there is a higher concentration of GTP in the nucleus than GDP, most of the Ran converts to the GTP, as catalyzed by RCC1, and is ready for another round of transport, binding and dissociating any karyopherin:cargo dimers from the cytoplasm that have newly traversed the NPC during

the import process. Ran cycling back and forth across the NPC is therefore a critical process both for nuclear import and nuclear export.

Previous studies have shown that not only does EMCV L bind Ran, but that it also inhibits critical Ran functions. The addition of recombinant L to *Xenopus* oocyte extracts prevents mitotic spindle formation in a dose-dependent manner (9). In digitonin-treated cells, virus infections or cDNA transfections, Nup hyperphosphorylation, catalyzed by host kinases, and subsequent NCT inhibition is induced whenever the native, but not mutant L, is present (60). Since mAbs to L or Ran will immunoprecipitate L:Ran complexes under these conditions, this interaction must be critical to NCT function, presumably acting through hydrolysis interference or sequestering of Ran, and consequent activation of the requisite kinases (8). The mechanism by which L binds Ran and inhibits Ran's normal NCT cycling is of great interest, not only to the field of virus-host interactions, but also to the fields of mitotic molecular biology in which Ran plays a central role. Described here are biochemical methods exploring the importance of guanine-nucleotides on the interaction of L with Ran, measurement of the L:Ran binding constants, and the requirement of the Ran guanine-nucleotide exchange factor, RCC1, for efficient L:Ran binding.

Materials and Methods

Bacterial expression and purification of recombinant proteins:

The pGST-L (9) plasmid was transformed into *E. coli*, BL21 (OD_{600} of 0.6 at 37°C in 2xYT with 20 μM $ZnCl_2$). Cells were induced (30°C, 1 mM IPTG, ~5 hrs), collected

(6,000 x g, 15 min), resuspended in GST buffer (50 mM Tris, 125 mM NaCl, 2 mM DTT, 1 mM PMSF, pH 7.4), then lysed with hen egg white lysozyme followed by sonication. The lysate was spun (20,000 x g, 45 min), clarified (0.22 um filter) then loaded onto a GSTrap column (GE Healthcare) using an Akta Prime Plus FPLC (GE Healthcare). After elution (10 mM glutathione, 50 mM Tris, pH 7.4), the protein fraction was dialyzed overnight (10 mM Bis-Tris Propane, 50 mM NaCl, 2 mM DTT, pH 7.4), loaded onto a HiQ ion exchange cartridge (Biorad) and GST-L was eluted with an increasing salt gradient (50 to 500 mM NaCl over twenty column volumes). Recombinant GST was purified as above in the absence of $ZnCl_2$ from an empty pGEX plasmid.

His-Ran, produced from the p-RSETA-Ran plasmid (106) in transformed BL21 cells used similar procedures for growth, IPTG induction (~3.5 hrs) and lysate preparation. But after clarification and filtration, the lysate was loaded onto a HisTrap column (GE Healthcare) and eluted (325 mM Imidazole, 25 mM Na_2PO_4, 500 mM NaCl, pH 7.4). His-containing proteins were dialyzed overnight (20 mM HEPES, 100 mM KCl, 2 mM $MgCl_2$, pH 7.4), loaded onto a HiPrep S-100 Sephacryl gel filtration column (GE Healthcare), and fractionated by size exclusion.

The plasmid containing GST-RCC1 was a kind gift from Chris Wiese. Protein-containing lysates induced by this plasmid (as above) were loaded onto a GSTrap column, eluted (10 mM glutathione, 50 mM Tris, pH7.4), dialyzed (30 mM K_2PHO_4, 5 mM $MgCl_2$, 2 mM DTT, pH 7.4, 12 hrs) then fractionated by size exclusion (HiPrep S-100 Sephacryl gel filtration). After purification, all recombinant proteins were concentrated, snap-frozen by liquid nitrogen, and stored at -80°C. The proteins used in this study were >95% pure as verified by SDS-PAGE Coomassie staining. Protein

concentration was determined using a Nanodrop ND-1000 (Thermo Scientific, Wilmington, DE) with absorbance at 280 nm.

GST binding assays:

Glutathione-sepharose beads (GE Life Sciences) were washed in binding buffer (3X, 50 mM HEPES, 150 mM NaCl, 0.5% NP40, pH 7.4) then incubated with GST-L (50 nM, 1 hr, 25°C with agitation). His-Ran (50 nM) was added and the incubation continued (1 hr) in the presence or absence of GDP or GTP (2.5 μM) and/or GST-RCC1 (1 nM). The samples were clarified (500 x g, 5 min) and the supernatant transferred to separate tubes. These proteins were precipitated (30% trichloroacetic acid, TCA) on ice (1 hr), washed with acetone (3x) and resuspended in 1x alkaline SDS buffer. The collected beads were washed (3x) with binding buffer followed by addition of SDS buffer. Protein/SDS solutions were boiled for 10 minutes prior to SDS-PAGE fractionation. Gel bands were transferred to PVDF membranes and analyzed by Western blot using anti-Ran (mAb-Ran, Santa Cruz Biotech, Product #SC-1156) or anti-GST (mAb-GST, Novagen, Product #71097) antibodies. Relative protein quantities were determined by ImageQuant (GE Life Sciences) scanning of the membranes.

Nucleotide spectrofluorimetry:

Described methods using fluorescently labeled mant-GDP (N-methyl-anthraniloyl, λ_{ex}=355 nm, λ_{em}=420-460 nm) bound to His-Ran, were adapted (107) to confirm the activity of GST-RCC1 on His-Ran prior to collection of kinetic data. Samples were diluted in phosphate buffer (30 mM KP_i, 5 mM $MgCl_2$, 1 mM DTT, pH 7.4) in a 1

mL cuvette. Spectra were collected after incubation of His-Ran (1.5 μM, 15 min) and mant-GDP (75 μM) in the presence or absence of GST-RCC1 (30 nM), GST-L (1.5 μM), or GST (1.5 μM). Data collection used a QuantaMaster Model C-60/2000 Spectrofluorimeter (Photon Technologies International) with a 1 mm x 1 mm slit size. Analysis used Felix32 software (Siemens PTI) with the spectrum for mant-GDP (75 μM) subtracted from data.

Surface plasmon resonance:

Equilibrium binding studies were performed on a BIAcore 2000 instrument (BIAcore AB, Uppsala, Sweden) loaded with CM5 research grade sensor chips (GE Healthcare). Monoclonal antibodies specific to GST (Novagen, Product #71097) were covalently attached to the chips with amine-coupling. Purified recombinant GST-L (5 μg/mL, 120 nM) diluted in SPR buffer (10 mM bis-tris propane, 100 mM NaCl, 0.005% Tween-20, pH 7.4) was flowed over individual chip cells at a rate of 10 μL/min (75 μg total, 25°C). His-Ran (5 μg/mL, 200 nM) was then injected over the same cells (10 μL/min) in the presence or absence of GST-RCC1 (0.5 μg/mL, 10 nM). The total injection time was 1200 seconds (200 μL total) with a dissociation time of 300 seconds. For nucleotide inhibition experiments, GTP or GDP (10 μM) was added to the His-Ran/GST-RCC1 solutions, representing a 50x molar excess over His-Ran/GST-L. Chip surfaces were regenerated using tris-HCl (pH 1.7), stripping GST-L from the antibody. Controls used cells that only contained GST or cells with GST-RCC1 (i.e. lacking His-Ran) in series. Automatic, parallel reference subtractions were performed with an antibody-only lane to account for non-specific and bulk interactions. These values were

recorded then removed from the data (BIA evaluation software, version 4.1) to provide the normalized binding constants specific to Leader and Ran. A single analyte (Ran) concentration was used for kinetic measurements as a technical compromise to allow comparisons among different conditions (e.g., ±RCC1, GDP/GTP). Association and dissociation rate values were determined independently from best-fit curves, using Langmuir calculations at steady-state levels. The K_D was determined computationally by dividing the off-rate (k_d) by the on-rate (k_a). The uncertainty in the K_D is the standard deviation of triplicate measurements.

Results

GST-L interaction with His-Ran:

GST-L will pull-down native Ran from HeLa cell lysates even in the presence of 300 mM NaCl, suggesting a tight interaction (9). From such lysates, however, the captured samples sometimes display a number of Ran cofactors, including karyopherins and Nups, in a nucleotide-dependent manner (108), lending confusion as to whether L reacts directly with Ran, or Ran complexes. Recombinant GST-L and His-Ran were incubated at a 1:1 ratio, reacted with glutathione-sepharose beads, and then assayed for bound and unbound fractions. After one hour, ~32% of His-Ran was bound to GST-L (Fig. 2-1), indicating L and Ran do interact, but not efficiently in this context. The addition of 50x molar excess of GTP or GDP inhibited binding, reducing the pull-down efficacy by 28% for GDP compared to no nucleotide, with undetectable GST-L:His-Ran binding in the presence of GTP. When recombinant GST-RCC1 was added, virtually all

of the His-Ran was recovered from the beads, even in the presence of GTP. Since GST-L (50 nM) and Ran (50 nM) are in 50-fold excess to GST-RCC1 (1 nM), the enhanced pull-down cannot be due solely to the GST-RCC1 moiety. Indeed, GST-RCC1 alone pulled down practically undetectable amounts of His-Ran. While Ran and RCC1 do indeed bind *in vivo,* the off-rate is very high (107) and any formed complexes may not survive the wash conditions. Rather, these data were a strong indicator that RCC1 might be catalyzing required Ran structural shifts, making it more amenable to L binding. That GST-RCC1 also relieved the free nucleotide inhibition observed when only L-GST and His-Ran were present, further suggests that heightened flexibility in the Ran nucleotide-binding pocket, presumably increasing GTP/GDP turnover (i.e. the effect of RCC1), was important to the rate or stability of L:Ran interactions.

Nucleotide-spectrofluorimetry of complexes:

In cells, RCC1 localizes to the inner NE rim, accelerating by about 200,000 fold the exchange rate of GDP for GTP on Ran before it cycles through the NPC (107). Nucleotide-spectrofluorimetry was used to evaluate the nucleotide exchange activity of His-Ran in solution. The small mant (N-methyl-anthraniloyl) tag, on the 2’ or 3’ OH of GDP is quenched in solution (Fig 2-2), but fluoresces strongly when trapped in a hydrophobic environment, a method commonly used to evaluate the activity of small GTPases (107). In the absence of GST-RCC1, His-Ran showed a low level of mant-GDP fluorescence relative to background, indicating the expected slow exchange of the tag with co-isolated native nucleotides, or with proteins having initially empty nucleotide pockets from the isolation procedures (Fig. 2-3). The addition of GST-RCC1 increased

the fluorescence during the 15 min. time period by ~2.5 fold relative His-Ran alone. Therefore, the GST-RCC1 was catalytically active and could facilitate exchange of solution mant-GDP for native nucleotides, and/or accelerate the filling of empty binding pockets in recombinant His-Ran.

Excess free-nucleotides are inhibitory to L:Ran binding (Fig 2-1), presumably acting as competitive inhibitors for the same binding region. It was therefore expected that GST-L might lead to L-dependent exclusion of mant-GDP, and subsequent decreased fluorescence. Instead, GST-L when combined with GST-RCC1 more than doubled the fluorescence. Under these conditions, virtually all of the His-Ran is bound to GST-L (Fig 2-1). Such increased fluorescence could happen if both the mant-GDP and the GST-L bind the same His-Ran protein, and moreover requires that both binding sites be very near each other. Alternatively, GST-L binding to His-Ran could induce a conformational change that further buries the mant moiety. In these cases, the enhanced hydrophobic interactions provided by GST-L, directly or indirectly, could strengthen the fluorescence of mant-GDP.

Equilibrium constants by surface plasmon resonance:

Although GST-L and His-Ran do not by themselves reach binding equilibrium under typical experimental conditions (e.g. 32% in Fig 2-1), the presence of GST-RCC1 was sufficient to accelerate interactions so that virtually all of the His-Ran was complexed with GST-L in less than 1 hr. This is an important criterion for determining measurable and accurate dissociation constants. In pull-down reactions similar to Fig 2-1, in the absence of guanine nucleotides, GST-RCC1 facilitated ~79% GST-L:His-Ran

binding within ten minutes, and ~92% within 30 minutes (Fig 2-4). Once GST-L is attached to Ran (native or recombinant), the binding is very tight, and cannot be disrupted even with high salt (9). Nonetheless, previous attempts to determine a precise K_D using surface plasmon resonance (SPR) failed because in the absence of RCC1, the initial reaction was too slow and non-saturating (unpublished).

In new SPR experiments, the addition of GST-RCC1 significantly increased the rate and degree of surface binding over a 20 minute period, even after accounting for the slight additive binding of the GST-RCC1 tag moiety to residual anti-GST antibodies (Fig 2-5A). Small amounts of Ran also bound non-specifically to the chip surface containing antibody or antibody plus GST alone. This was likely due to the positive charge on the 6x-His tag interacting with the negative charge of the dextran matrix, and this correction was automatically removed as a reference subtraction from all other Ran data. When His-Ran and GST-RCC1 were flowed over the GST-L surface together, the normalized sensorgram approached equilibrium (Fig 2-5B), ensuring that the resulting binding data would be accurate and was that of the RCC1-catalyzed binding. Interestingly, GST-L:His-Ran binding was slightly delayed and sigmoidal, though this may be due to the requirement of a third protein in the complex, RCC1. Calculations using the BIAevaluation software determined the K_D of GST-L:His-Ran binding in the presence of GST-RCC1 to be ~3 nM (Table 2-1). This very tight interaction is consistent with previous findings that GST-L:Ran (native) complexes could withstand high salt without dissociation (9).

GDP or GTP was then added to equivalent chip eluents in the presence of His-Ran and GST-RCC1. The SPR experiments, with all required controls (as in Fig 2-5A),

were then repeated (all data not shown). As summarized in Table 2-1, the addition of excess GDP and GTP increased the determined K_D of GST-L:His-Ran interactions by 7-fold (to ~22 nM) and 15-fold (to ~49 nM), respectively, relative to the nucleotide-free samples. Further kinetic data extrapolated from the slopes of the normalized curves (e.g. Fig 2-5B) showed the presence of GDP or GTP decreased both on-rate constants by ~10-fold (relative to the absence of GDP/GTP) for this concentration of proteins. The off-rates correspondingly increased, with GDP at about 1.5-fold and GTP at about 2.5-fold. These changes translate into inhibitory constants of around 1 μM for either nucleotide, values far below the measured ~1 mM (109) cellular concentrations. The IC_{50} concentrations, which account for the concentration of analyte in the cell, were calculated using the Cheng-Prusoff equation (110). These values were 1 mM and 2.5 mM for GDP and GTP, respectively (Table 2-1), values much closer to the biologically relevant intracellular concentrations. Therefore, within EMCV-infected cells, native L:Ran interactions are expected to occur readily, very tightly, and be practically non-dissociable, despite high local concentrations of NTPs. This, however, will happen preferentially only if the initial interactions are localized to NE sites where RCC1 is prevalent.

Discussion

The data presented here demonstrate nanomolar dissociation constants between L and Ran. But the *in vitro* reactions reached measurable equilibrium only when the Ran-specific guanine-nucleotide exchange factor, RCC1, was present. Cellular

transfections with flag-tagged L cDNAs have shown this viral protein to localize in punctate markings lining the rim of the NE (9). The apparent *in vitro* requirement for RCC1, a protein normally found on the inner NE by virtue of its ability to bind both nucleosomes and DNA (111), is consistent with these locales. However, it is not yet clear whether L localization during virus infections is due to Ran-mediated NPC interactions, an L-dependent preference for RCC1 sites, or some yet-unknown interaction.

The full kinetic mechanism of GDP/GTP exchange on Ran catalyzed by RCC1 has been studied thoroughly (107). The basic intermediate of exchange is proposed to be a stable RCC1:Ran complex devoid of nucleotide, without significant preference for GDP or GTP. The solved co-crystal structure of RCC1:Ran supports this hypothesis, detailing a stabilized complex devoid of nucleotide (112). In this configuration, the Ran nucleotide-binding pocket is solvent-exposed, providing a large surface for new GTP entry, and where conceivably a small protein such as L could interact. These kinetic and structural data support a mechanism whereby the original nucleotide is released from such complexes, after insertion into Ran of an RCC1 β-wedge, destabilizing the configuration of key hydrophobic GNP pocket residues in the P-loop (108, 113). The studies also suggest that related, less stable pocket intermediates are likely to occur transiently throughout the process of nucleotide dissociation and association (107).

The pull-down experiments and SPR described here are consistent with the idea that RCC1-catalyzed structure changes, and in particular, a nucleotide-free Ran or related flexible intermediate, are favorable to L binding. Demonstration of this premise required that recombinant GST-RCC1 could accelerate His-Ran nucleotide exchange,

similar to the native proteins, a point proven by the rapid mant-GDP exchange. Le Chatelier's Principle would dictate that the addition of high concentrations of free GDP and GTP should force any Ran proteins, native or recombinant, into a stable, nucleotide-bound state. The fact that GST-L:His-Ran binding in the presence of high concentrations of GDP/GTP occurred readily only when in the presence of RCC1 strongly suggests that one of the key determinants of L:Ran binding was the structural stability (or rather, instability) of Ran. That is to say, L can bind most effectively when Ran has an RCC1-facilitated-labile structure around the nucleotide-binding pocket, presumably involving the phosphate-binding P-loop.

Since an increase in mant-GDP fluorescence requires the addition of hydrophobic residues proximal to mant-GDP, as was observed when GST-L was present, it is probable that not only can L bind Ran with a nucleotide in its pocket, but also that L does indeed interact at or near the pocket. HPLC studies conducted in our lab by Valjean Bacot-Davis suggest that approximately 30% of Ran proteins reacted by L have a nucleotides in their pocket. The nucleotide is more likely to be GDP than GTP when simultaneously bound to L (unpublished). This steric dependence is another indication that L may bind Ran at or near the nucleotide-binding site. It is plausible that L could bind elsewhere on Ran and induce a significant conformational change in the nucleotide pocket. Recently, the NMR solution structures of L and Ran bound to one another were solved (63). Further docking studies suggested that the C-terminal tail of Ran wraps around L, effectively pinning it to Ran. These models suggest that L does not make direct contact with the nucleotide-binding pocket of Ran, but does indeed induce a conformational shift in the protein.

During infections, however, L cannot shut down NCT solely by titrating Ran. There are approximately 10^6 copies of Ran per HeLa cell (109) and at most, ~10^3 copies of L during the early stages of infection when Nup phosphorylation occurs. More likely, L uses Ran as a means of translocation to or anchoring near the nuclear pore. Several Nups with zinc finger domains will bind Ran directly (114). These domains, however, do not resemble the zinc-finger of L either by sequence or structure. Other F/G-containing Nups react indirectly with Ran through various karyopherin-mediated interactions (115). Although L itself does not encode a demonstrable nuclear localization signal (NLS), the 2A protein of EMCV, which also binds weakly to L, does have an NLS for localization to nucleoli (without L) where 2A helps shut off cap-dependent translation by an unknown mechanism (80, 83, 116). One scenario being explored later in this thesis is that L may bind 2A in the cytoplasm, and is consequently ferried to the NPC. Given the low K_D of L:Ran complexes, it is likely that 2A is then efficiently displaced by Ran somewhere in the NPC environment, and especially in locales where RCC1 is present. The nuclear 2A would then be free to continue into nucleoli, having released its L cargo at the NE, while L:Ran complexes could remain associated with the NPC and direct Nup phosphorylation.

Cardiovirus L proteins are absolutely unique in sequence, structure and function. No other viruses yet identified attack NCT by a Ran-binding or Nup-hyperphosphorylation mechanism. Moreover, no other protein, viral or cellular, has been described which binds Ran directly, virtually irreversibly, and inhibits Ran GNP cycling. These potent activities of L can explain why L-mutant viruses or other cardioviruses

which posses additional domains within the L protein (i.e. the *Theiloviruses*) have such dramatically different phenotypes and outcomes of infection (72, 117, 118).

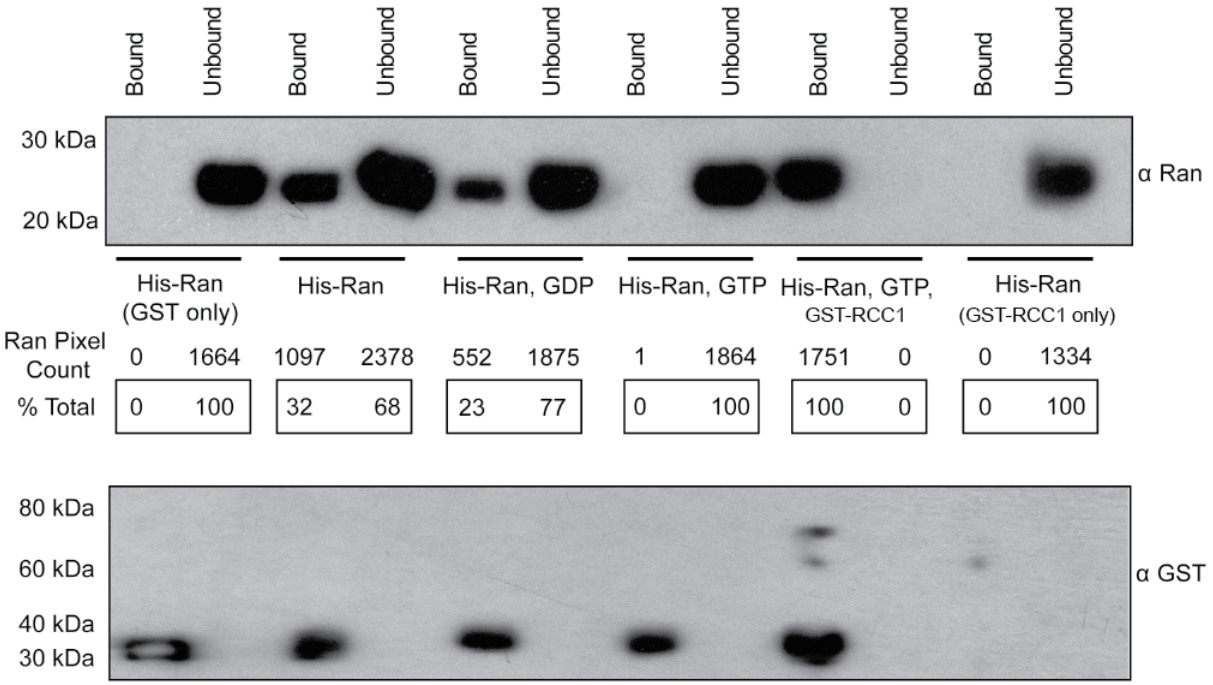

Figure 2-1: GST-L:His-Ran binding. GST-L linked to glutathione-sepharose beads (50 nM) was reacted (1 hr, 25 ^{0}C) with His-Ran (50 nM) in the presence or absence of GDP or GTP (2.5 μM) and/or GST-RCC1 (1 nM). The clarified supernatant (unbound) and bead-bound proteins (bound) were precipitated, solubilized (alkaline SDS), fractionated by PAGE, and then transferred to PVDF membranes. Western analyses used anti-Ran or anti-GST antibodies. Secondary antibodies were HRP-conjugated α-goat or α-mouse. Relative pixel counts (% total) were determined by ImageQuant (GE Life Sciences) scanning of the membranes.

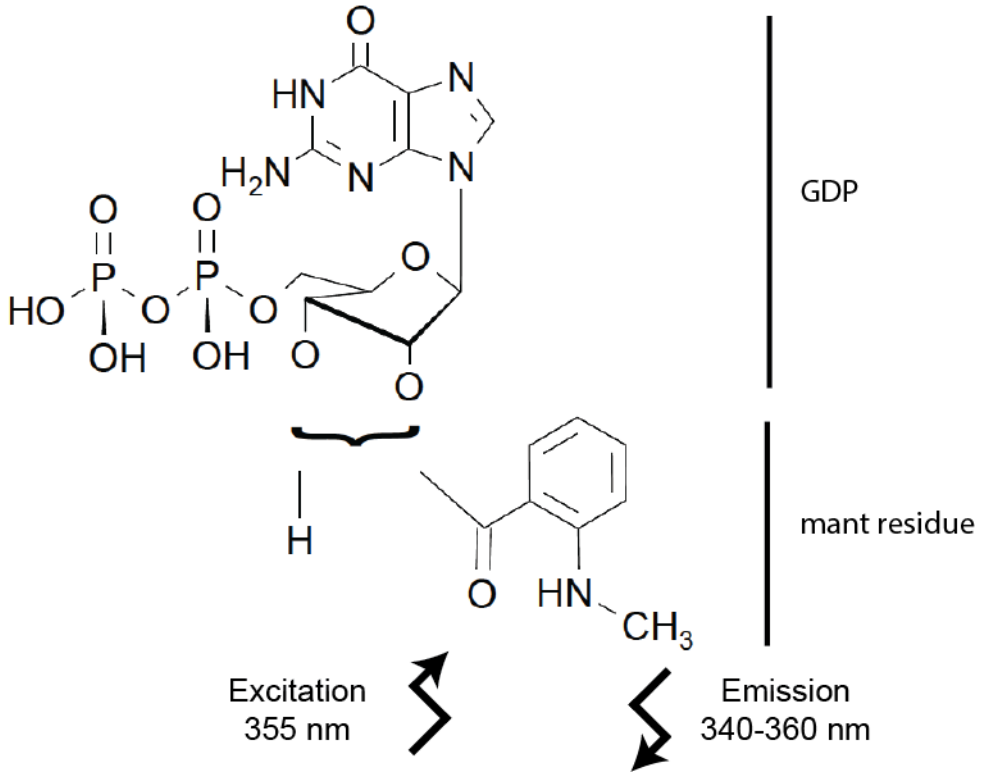

Figure 2-2: Structure and properties of mant-GDP. The structure of fluorescent probe 2'/3'-O-N-methylanthraniloyl-guanosine-diphosphate (mant-GDP/mGDP) is shown. The mant residue has an excitation wavelength of 355 nm and emission range of 340-360 nm. The mant residue is quenched in hydrophilic environments (i.e. in solution) and emits in hydrophobic (i.e. protein-bound) environments.

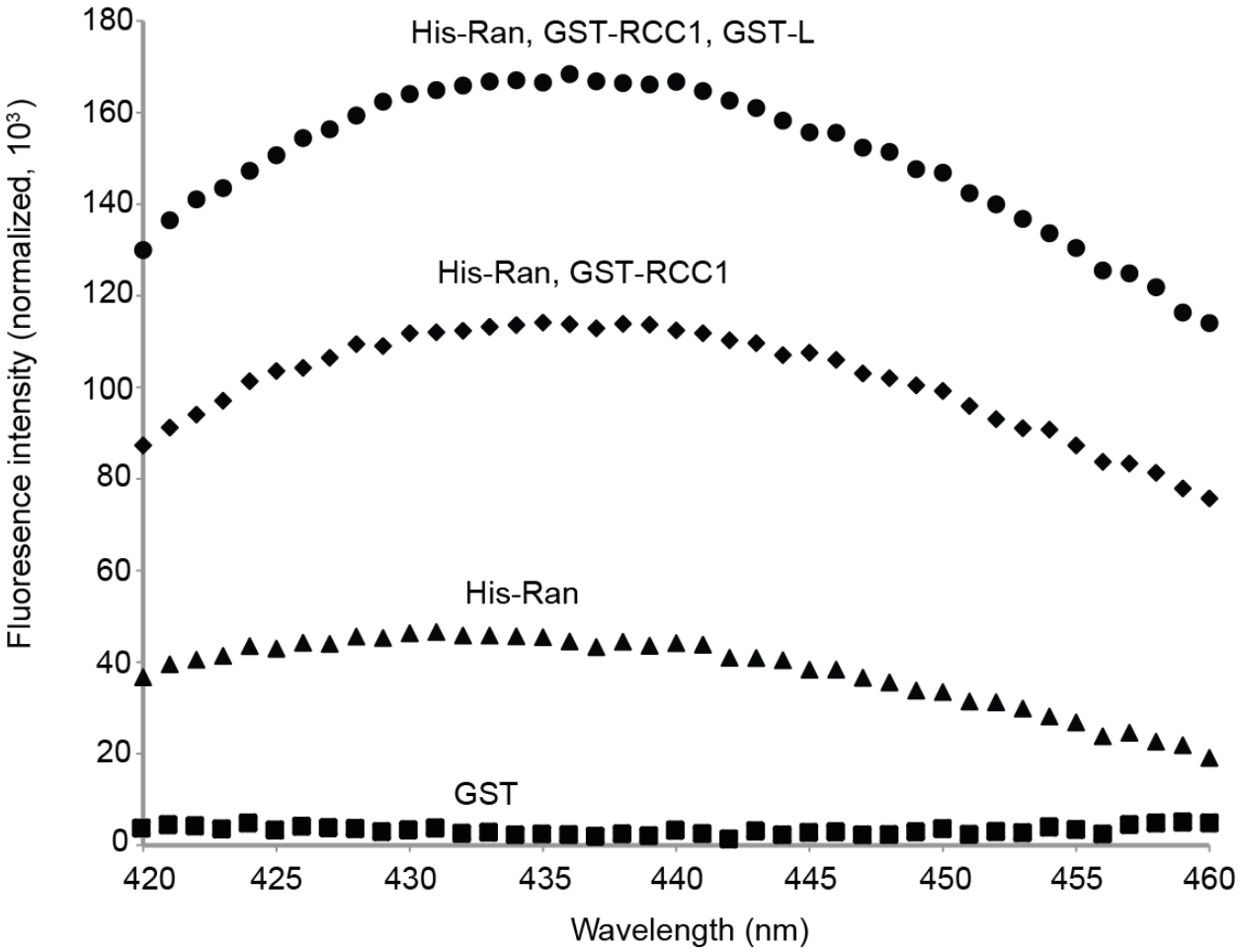

Figure 2-3: GST-RCC1 is catalytically active. The fluorescence of nucleotide analog mant-GDP (λ_{ex}=355 nm, λ_{em}=420-460 nm) was measured by spectrofluorimetry after 15 min. reactions at 25°C with His-Ran, GST, or GST-L (1.5 μm each). The analogue was at 50x molar excess (75 μm). The reactions were repeated in the presence of GST-RCC1 (30 nM) or a combination of GST-RCC1 (30 nM) and GST-L (1.5 μm).

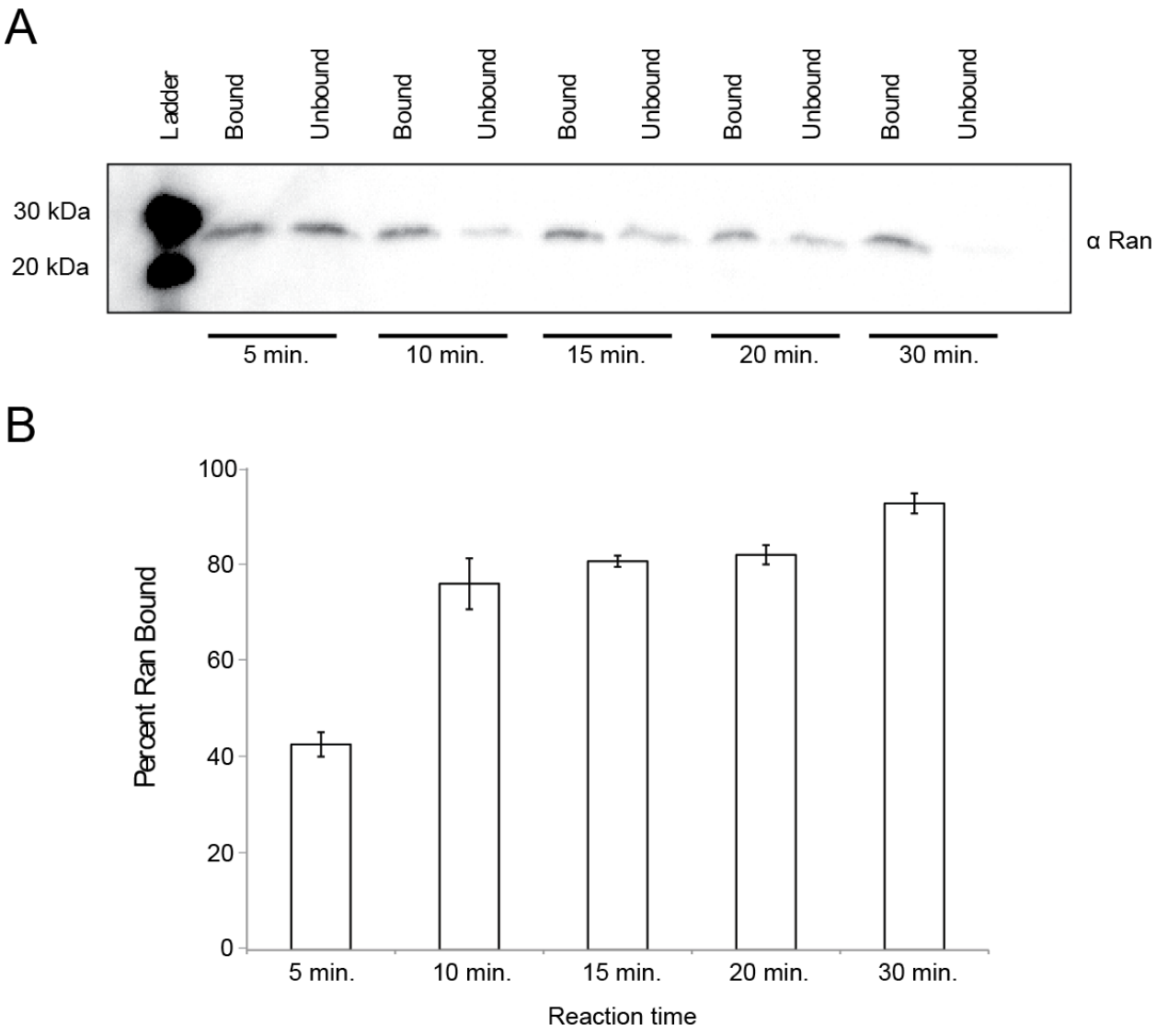

Figure 2-4: GST-RCC1 facilitates rapid GST-L:His-Ran binding. GST-L was reacted with recombinant His-Ran in the presence of GST-RCC1 and absence of nucleotide as in Figure 2-1. Parallel reactions were halted by clarification at the indicated time points. Quantitation of Ran signals (pixel count, % total) used scanned images of this membrane (n=3).

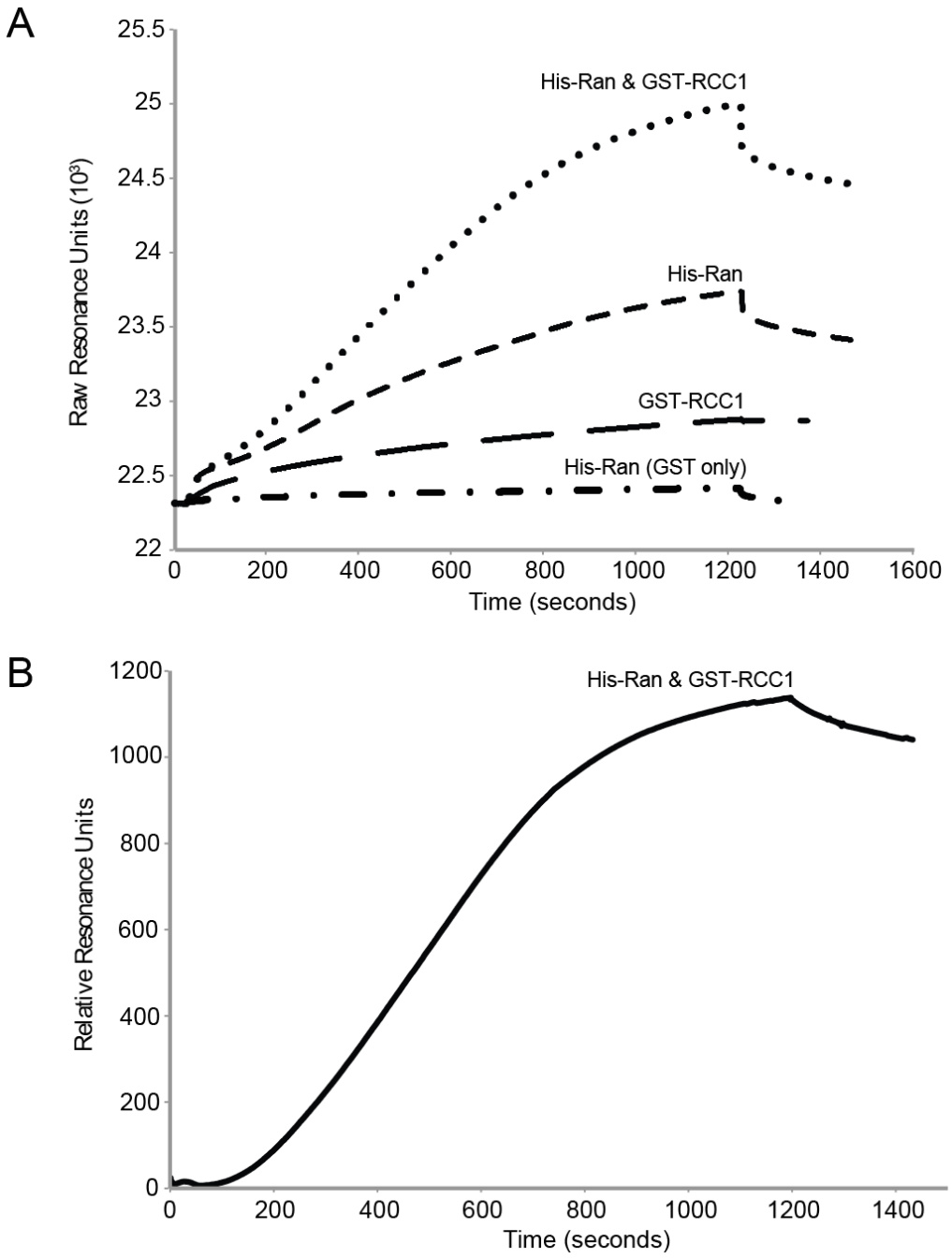

Figure 2-5: Measurement of GST-L:His-Ran affinity by SPR. A) Representative SPR sensorgram curves for His-Ran, GST-RCC1, and combined binding to GST-L using mAb α-GST surfaces. B) His-Ran (with GST-RCC1) binding to the GST-L surface is shown as normalized values, after subtracting binding controls. Triplicate SPR determinations like this, with and without added GDP/GTP (10 μM) gave similar processed curves and were used for the K_D calculations in Table 1.

Inhibitor	k_{on} ($M^{-1}s^{-1}$)	k_{off} (s^{-1})	K_D (nM)	K_i (μM)	IC_{50} (mM)
None	1.01 (± 0.01) x 10^5	3.39 (± 0.54) x 10^{-4}	3.25 (± 0.63)	NA	NA
GDP, 10 μM	2.33 (± 0.06) x 10^4	4.98 (± 0.36) x 10^{-4}	22.0 (± 1.4)	1.73 (± 0.11)	1.0 (±0.2)
GTP, 10 μM	1.79 (± 0.01) x 10^4	8.81 (± 0.07) x 10^{-4}	48.8 (± 0.2)	0.714 (± 0.003)	2.5 (± 0.1)

Table 2-1: Equilibrium constants for GST-L:His-Ran binding. On and off rates were determined through Langmuir fitting of normalized sensorgrams. K_D was determined as the ratio of k_{off}/k_{on} when adjusted for the concentration of His-Ran in solution. Uncertainty was determined as the standard deviation of triplicate measurements. Significant figures were limited by the precision of protein concentrations. K_i was calculated using the equation $K_i = [GXP]/[(K_D^{GXP}/K_D) - 1]$, where GXP represents either GDP or GTP. IC_{50} was calculated using the equation $IC_{50} = K_i(1 + [Ran^{cell}]/K_D)$. NA, not applicable.

Chapter 3

Binding interactions between the encephalomyocarditis virus Leader and protein 2A

Published in: The Journal of Virology, Volume 88, Pages 13503-13509 (2014)

The studies described in Figure 3-5 were performed by Holly Basta (Palmenberg Lab); those shown in Figure 3-7 were performed by Valjean Bacot-Davis (Palmenberg Lab)

Abstract

The Leader (L) and 2A proteins of cardioviruses are the primary anti-host agents produced during infection. For encephalomyocarditis virus (EMCV), the prototype of this genus, these proteins interact independently with key cellular partners to bring about inhibition of active nucleocytoplasmic trafficking and cap-dependent translation, respectively. L and 2A also bind each other and require this cooperation to achieve their effects during infection. Recombinant L and 2A interact with 1:1 stoichiometry at a K_D of 1.5 μM. The mapped contact domains include the amino-proximal third of 2A (first 50 amino acids) and the central hinge region of L. This contact partially overlaps the L segment that makes subsequent contact with RanGTPase in the nucleus, and Ran can displace 2A from L. The equivalent proteins from TMEV (BeAn) and Saffold virus, interact similarly in any subtype combination, with varying affinities. The data suggest a

mechanism whereby L takes advantage of the nuclear localization signal in the COOH-region of 2A to enhance its trafficking to the nucleus. Once there, it exchanges partners in favor of Ran. This required cooperation during infection explains many observed co-dependent phenotypes of L and 2A mutations.

Introduction

The *Cardiovirus* genus of the *Picornaviridae* family is divided into several species and subtypes. Among the important members are encephalomyocarditis virus (EMCV), Theiler's murine encephalomyelitis virus (TMEV) and Saffold virus (119, 120). All have single-stranded, positive-sense RNA genomes encoding single, open reading frames. The polyproteins are cleaved co- and post-translationally by an endogenous 3C protease (121). Unique to this genus, the polyprotein begins with an amino-terminal Leader protein (L) and a centrally located 2A protein that are without homolog or analog in other viruses or cells. Together, they are primarily responsible for almost all cardiovirus anti-host activities (8, 68-70, 116).

For EMCV, the L_E protein is 67 amino acids (aa). Saffold (L_S, 71 aa) and TMEV proteins (L_T, 76 aa) are slightly longer. The solution structure of Mengo L_M (an EMCV strain) has been determined in free form and as bound to RanGTPase, a key cellular participant in L-dependent activities (63). The conformation is primarily coiled-coil, except for an amino-proximal CHCC zinc-finger motif (aa 10-22). The structure of the remainder relies on induced-fit contacts dependent upon specific binding partner(s). The

mapped functional units, in addition to the zinc finger, include a central “hinge” region (aa 35-44), essential to Ran interactions, and an “acidic domain” (aa 37-52), that confers an overall pI of 3.8 to the protein (62). The L_S and L_T homologs are similar, with equivalent low pIs, except they also have short, characteristic “Theilo domain” (13 aa) and “Ser/Thr domain” (12 aa) insertions, configured putatively as linked helices, near their respective C-termini (67).

For any L_X to function in cells, it must be phosphorylated. The required sites include Tyr_{41} and Thr_{47} for L_E, Ser_{57} for L_T, and Thr_{58} for L_S. Kinases CK2, SYK and AMPK participate in these modifications, but the precise timing of the reactions and stepwise requirements during infection are not yet clearly understood (66, 67). It is clear, however, that during infection or in recombinant form, the introduction of phosphorylation-competent L_E, L_S or L_T into cells induces a rapid inhibition of active nucleocytoplasmic trafficking (NCT) (8, 66). The mechanism requires, in addition to L phosphorylation, specific L interactions with RanGTPase, a key cellular trafficking regulator. When aided by catalytic amounts of nuclear Ran guanine-nucleotide exchange factor (RCC1), L_M binds tightly to Ran (K_D of 3 nM), diverting its normal activities into anti-host events (122). The consequence is induced hyperphosphorylation of Phe/Gly-containing nuclear pore proteins (Nup) by cellular kinases in the p38 and Erk1/2 pathways (8, 9, 60) and subsequent cessation of active NCT. It has been proposed that L_M:Ran complexes achieve this by trapping exportin-bound activated kinases within the nuclear pores (NPC) (63). Since Ran-dependent NCT is essentially shut down, the movement of cellular proteins and RNA through the NPC is reduced to that permitted by diffusion alone. Recombinant L_M, L_E, L_T or L_S alone are necessary and

sufficient for observing these effects when their genes are transfected into cells (9, 67). During infection, however, cardiovirus L proteins are not the exclusive anti-host activators.

The functions of protein 2A are not as well characterized. EMCV 2A (143 aa) is translated between the P1 (capsid) and P2/3 (replication) regions of the polyprotein. The protein has a distinctive C-terminal 13-16 aa “scission cassette” (Fig 3-1) ending with an Asn-Pro-Gly-Pro motif (NPG/P). The unit functions in viral or exogenous contexts, through a co-translational ribosome-skipping mechanism, separating otherwise co-joined proteins between the Gly and Pro residues (6). The NPG/P event provides primary scission of cardiovirus polyproteins. The N-terminal release, as with the C-terminal release of L, from an L-P1-2A precursor, is subsequently catalyzed by viral $3C^{pro}$. Antibodies specific to EMCV 2A track the dominant cellular localization to nucleoli during infection, although there is also significant cytoplasmic accumulation (116). The protein has a very basic pI of 9.67, which presumably allows it to remain nucleolar through rRNA binding contacts. Mutagenic mapping has identified a ribosome protein-like nuclear localization signal (NLS) and a C-proximal eIF4E binding site, which partially overlaps the scission cassette sequences, and are common to all known cardioviruses (80). Similar mutations, tested during infection, link the activities of 2A (EMCV) to virus-induced shut-down of cap-dependent translation (61, 116). The protein influences 4EBP1 pathways in certain cell types, and moreover, 2A-deficient viruses can be rescued by chemical inhibitors of mTOR and PI3K, elements required for cap-dependent but not virus-dependent translation (123). During infection, a portion of 2A is

found in association with 40S, but not 60S or 80S ribosomal subunits, though no determined mechanism yet links these observations (61).

Cardiovirus L and 2A interactions with various cellular partners have been the subject of much study and speculation (9, 61, 80, 122). As part of this process, we employed yeast two-hybrid systems to fish out unknown, potential reaction candidates (unpublished). Given their reciprocal pIs, perhaps it should not have been a surprise that both came back as preferred partners of each other. The specificity and required elements for these reactions have now been documented by mutagenesis and biochemistry. Within the virus lifecycle, including the Theilo and Saffold viruses, the mutual L:2A pathways may explain why these proteins' anti-host activities should probably not be considered independently. Phenotypes attributed to one protein are, in some steps, co-dependent upon the other.

Materials and Methods

Recombinant Constructions:

The N-terminal His-tagged GB1 gene for parental plasmid pT-hGB1 originated from a pET30-GBFusion1 vector (a kind gift from John Markley), as excised by PCR using appropriate primers. After digestion with Nco I and Hind III, the amplicon was gel purified, then ligated into pTri-Ex 1.1 (Novagen) using the same restriction sequences. The EMCV 2A gene from pEC9 (124) was amplified in parallel, and then digested with Hind III and Xho I. Plasmid pT-hGB1-2A substituted this fragment into the corresponding sites of parental pT-hGB1. Bacterial expression produces an in-frame

His-tagged GB1-2A fusion protein (hGB1-2A). Derivative plasmids, using different primer sets were equivalent, but included only those EMCV 2A sequences encoding amino acids 1-50, 51-100, or 101-143. Expression plasmids for Saffold (SafV-2) and TMEV (BeAn) 2A, were of similar configuration and founded on amplicons generated from infectious cDNAs (generous gifts from Dr. Howard Lipton). Leader-GST fusion plasmids for EMCV (L_E-GST), Saf-2, (L_S-GST) and BeAn (L_T-GST) have been described (66), as have GST-L_E proteins with substitution mutations, GST-L_{K35Q}, GST-L_{D37A}, and GST-L_{W40A} (65). The sequences of all materials were verified by restriction mapping and Sanger sequencing.

Protein Purification:

For hGB1-2A synthesis, plasmids were transformed into Rosetta BL21(DE3) pLac I cells (Novagen). Single colonies were picked then grown overnight in 2XYT (1% glucose, 34µg/mL chloramphenicol, 50µg/mL ampicillin) at 30ºC. The stocks primed larger cultures, which at an OD_{600} of 0.6, were treated with isopropyl ß-D-1-thiogalactopyranoside (1 mM, IPTG). Growth continued (30^{o}C) until harvest at an OD_{600} of 2.4-3.2. The cells were collected (6,000 x g, 15 min, 4ºC) and frozen at -80ºC. Expressed proteins were extracted after resuspending the pellets in His-2A buffer (50 mM NaH_2PO_4, 300 mM NaCl, 10 mM imidazole and 25% v/v glycerol) containing phenyl-methane-sulfonylfluoride (1 mM, PMSF). After incubation with lysozyme (1mg/ml, 30 min, 4^{o}C) the DNA was sheared by sonication. The soluble fraction (20,000 x g, 45 min, 4ºC) was filtered (0.2µM filter, GE Healthcare) then loaded onto a HisTrap HP column (GE Healthcare). Bound proteins were eluted with an imidazole step

gradient (20, 60, 120, 250, 500 mM). Relevant fractions were pooled and concentrated, then applied to Sephacryl S-100 columns (GE Healthcare). Separation was by size exclusion (50 mM NaH_2PO_4, 300 mM NaCl, 25% v/v glycerol, pH 7.4). The proteins were collected, dialyzed (same buffer), concentrated, and then stored at -80ºC. The expression and purification of C-terminal GST-tagged Leader proteins, L_E-GST, L_T-GST and L_S-GST have been described (67), as have protocols for human RanGTPase (N-terminal His-tagged), and (N-terminal GST-tagged) human guanine-nucleotide exchange factor, RCC1 (122).

Recombinant Protein Interactions:

Protein interaction assays took advantage of the respective GST and hGB1 tags on the L_X and 2A recombinant panels. When GST proteins were the baits, they (50 nmol) were bound to glutathione-sepharose 4B beads (GE Life Sciences) in 10 ml reaction volumes (50 mM HEPES, 125 mM NaCl, 0.5% NP40, pH 7.4, 4°C, overnight). The beads were collected (500 x g) washed with the same buffer (2x), then incubated (1 hr, 25°C) with increasing amounts of prey protein (e.g. hGB1-2A, 5-100 nmol/sample). For competition experiments between 2A and Ran (50 nmol), the bait protein (GST-L_E or mutated variants) was prebound to beads as above, before the incubation (2 hrs) with various prey combinations. Reactions with Ran also included catalytic amounts of RCC1 (1 nmol). Reciprocal experiments used hGB1 protein baits (50 nmol) bound to Ni^{+2} charged chelating-sepharose beads in buffer (50 mM HEPES, 400 mM NaCl, 50 mM imidazole, pH 7.4) for the capture of GST-L_E preys (5-100 nmol/sample). Binding affinity reactions were similar except for the variable salt concentrations (125-500 mM

NaCl). Interspecies L_x-GST (on beads) and hGB1-2A reactions were performed as above. For all reactions, after extensive washing (3x) to reduce background signals, the bead-bound proteins were released by boiling in SDS buffer, fractionated by SDS-PAGE, detected by Coomassie staining and quantitated (ImageQuant software). Alternatively, after transfer to PVDF membranes, the proteins were detected by Western analyses. The antibodies included: murine aGST (Novagen, Product #71097), goat aRan (Santa Cruz Biotechnologies, Product sc-1156); anti-murine secondary (Sigma-Aldrich, Product A2554), and anti-goat secondary (Sigma, Product A5420). The GB1 tag is a derivative of the IgG binding B1 domain of the streptococcal protein G (125). As such, assays to detect this protein (αGB1) need only the murine secondary antibody.

GST-L_E Phosphorylation:

Bait (10 mmol, GST-L_E) and prey (hGB1-2A) complexes bound to glutathione sepharose 4B beads were established and collected as above, except during the protein capture (1 hr, 20^{o}C) the prey concentration varied (2.5, 10 or 40 nmol). Once the beads were collected, they were resuspended into (manufacturers') buffers supplemented with 5.0 µCi [γ-^{32}P] ATP (3,000Ci/mmol, 10mCi/ml), 10 units of CK2 (New England Biolabs), 10.3 units of SYK (SignalChem), or 10 units of both CK2 and SYK. After reaction (37°C, 60 min) the beads were washed (3x) with PBS buffer (plus 500mM NaCl, 0.02% Triton X-100), then boiled in SDS, before protein fractionation by SDS-PAGE. Detection was by silver stain, or phosphorscreen, as visualized with a Typhoon scanner (GE Healthcare).

Surface Plasmon Resonance:

Equilibrium binding studies used a BIAcore 2000 instrument (BIAcore AB, Uppsala, Sweden) loaded with CM5 research grade sensor chips (GE Healthcare). aGST (above) was covalently attached to the chips with amine-coupling chemistry. GST-L_E (5 µg/ml, 120 nM) diluted in SPR buffer (10 mM bis-tris propane, 100 mM NaCl, 0.005% Tween-20, pH 7.4) was flowed over individual chip cells at a rate of 10 ml/min (75 mg total, 25°C). The buffer was then changed to include hGB1-2A (or iterations) in varying concentrations (10, 20, 50 µg/ml, 20 ml/min). The total injection time was 450/600 seconds (120/150 ml total) with a dissociation time of 120 seconds. Chip surfaces were regenerated using 20 mM piperazine (pH 9.0) with 2 M KCl. Automatic, parallel reference subtractions were performed with an antibody-only lane to account for non-specific and bulk interactions. BIA evaluation software, (version 4.1) calculated the normalized binding constants specific to L_E and 2A. Association and dissociation rates were determined independently from best-fit curves, using Langmuir calculations at steady-state levels. The slope and y-intercept values, plotted in Excel, recording the concentration of analyte (hGB1-2A) against the k_{obs}, were used to determine the final K_D.

Results

L_E:2A Interactions:

The small size and high charge of cardiovirus L_X proteins makes them difficult to work with in experiments involving Western assays unless they are fused to tags like

GST (220 aa). These tags, whether C-linked or N-linked, do not affect the structure or biological activity of L_E constructs (9). Likewise, the cardiovirus 2A proteins are relatively insoluble, unless they too are coupled to tags like hGB1 (56 aa) or maltose-binding protein (396 aa, MBP) (unpublished). The combined tags make protein purification easier, and binding studies can take advantage of high specificity commercial reagents. Recombinant GST-L_E and hGB1-2A were tested in reciprocal pull down assays, dependent upon their respective tags, and shown to interact with each other. In multiple experiments, the “bait” protein captured “prey” in approximate proportion to its solution concentration, reaching saturation at about a 1:2 molar ratio (100 nmol/reaction of prey), regardless of the bead-bound protein. The interactions were not due to either protein’s tag, as these alone were unable to capture cognates. An example experiment is in Fig 3-2A (all data not shown). Formation of such complexes withstood the presence of 250-500 mM salt (Fig 3-2B), indicating a reasonably specific affinity between the L_E and 2A proteins with a strength that could not be due to simple charge:charge interactions (i.e. pI 3.8 verses pI 9.7).

As a better assessment of this complex, the binding constant was determined by surface plasmon resonance. SPR is essentially a pull down assay using a mass-sensitive chip. In this case, three concentrations of hGB1-2A analyte were reacted over an antibody-fixed GST-L_E surface, and the increased mass over 450 or 600 seconds of exposure was recorded in a sensorgram. A plot series is shown in Fig 3-3A. From these curves, including the decay phase after the analyte is flushed, normalized values for k_{obs} can be calculated for each concentration (Fig 3-3B). These in turn extrapolate to absolute on/off rates [k_{on}=1.4(±0.1)x10^{-3} $M^{-1}s^{-1}$, k_{off} =2.1(±0.1)x10^{-6} s^{-1}] and a K_D for the

L_E:2A reaction, determined here as 1.5±0.1 μM. The shape(s) of the sensogram curves are consistent with 1:1 stoichiometry. Higher order cooperative interactions would have different plots (Fig 3-3A), and non-linear extrapolated slopes (Fig 3-3B).

Homolog Interactions:

Among L_E, L_S and L_T sequences (67-71 amino acids, aa) for which there are cDNAs, there is about 29% shared aa identity, and 42% aa similarity (67). The equivalent 2A proteins vary in length from 133-143 aa, and share 14% identity (Fig 3-1) with 39% similarity. If properly controlled, capture experiments can provide a measure of relative affinity for panels of similar proteins. In this case, a C-terminal tagged L_X-GST panel was chosen as baits because Saffold and Theilo Leader proteins become biologically inactive if the tag is attached N-terminal (67). These and cognate hGB1-2A proteins were isolated, quantitated, then reacted in matched samples (Fig 3-4). In repeated experiments (all data not shown) there was cross-reactivity with every combination, but surprisingly, the 2A from EMCV was always the most reactive with each of the Leaders regardless of species. L_S-GST and L_T-GST bound nearly twice as much of this protein, as they did their homologous counterparts. The EMCV 2A was clearly the preferred binding partner.

Required 2A Elements:

No 2A structure is available for any cardiovirus. For all these sequences though, the C-terminal third of the protein, maintains characteristics of an extended alpha helix (80). The first and second portions are not responsive to structure predictions. These

regions are more variable in sequence between species. Most of the basic residues contributing to the pI map in these upstream regions, imparting the clearest pI differential to the first two thirds of the protein (Fig 3-1). Among 2As, this portion of the EMCV protein is the most basic. The EMCV 2A binding segments making contact with L_E were approximated by dividing the gene into fragments encoding residues 1-50, 51-100 and 101-143. The peptides were then expressed with hGB1 tags for solubility. In turn these served as prey in GST-L_E capture experiments (Fig 3-2C). GST-L_E was able to pull down a significant portion of fragment 1-50 (73% compared to input), but neither of the other fragments was reactive in this context. Therefore, fragment 1-50 probably contains the dominant 2A determinants for L_E interactions, at least as measured in the absence of an intact 2A conformation. Follow up SPR experiments with the hGB1-$2A_{1-50}$ fragment and GST-L_E were inconclusive because the much smaller mass change of the prey did not give reproducible signals, especially at low concentrations.

L_E Partner Competition:

In the presence of catalytic amounts (1 nmol/reaction) of RCC1, L_E binds RanGTPase at 1:1 stoichiometry with a K_D of 3 nM (122). The K_D for L_E:2A, as determined above by SPR, is much higher (1.5 μM), so in theory, Ran should be able to outcompete 2A if the preferred L_E binding sites overlap. Ran interacts with the central hinge region of the L_E protein (63) within which mutations at K_{35}, D_{37}, and W_{40} mark the most significant sites (65). 2A (50 nmol), Ran (50 nmol) or a mixture of both preys (50 nmol each) were added GST-L_E bait, allowed to reach equilibrium (2 hrs), and then assessed for relative 2A binding. A typical gel series is shown in Fig 5A. The indicated

values (Fig 3-6B) were averaged from multiple (n=4) identical experiments. They show that hGB1-2A binding was reduced by 16-26% when the bait GST-L_E had any of the key mutations in the hinge region (74-84% relative binding). Nonetheless, Ran, when present, bound simultaneously to the same GST-L_E beads with essentially 1:1 stoichiometry (122). The combined preys reduced hGB1-2A binding to the wild-type GST-L_E by 22%, and clearly, that binding was further weakened with mutant L_E sequences because Ran then displaced even more hGB1-2A (40-71% relative affinity). Still, that Ran did not entirely displace hGB1-2A from the bound GST-L_E suggests these proteins have partially overlapping, but not mutually exclusive preferences for L_E sites.

2A Impedes L_E Phosphorylation:

During infection, L_E is sequentially phosphorylated at T_{47} and Y_{41} by CK2 and SYK enzymes, respectively (66). The sequence, even with recombinant proteins, is obligatory, because mutations which block the CK2 reaction (e.g. T_{47}A) also prevent the SYK reaction at Y_{41} unless the substitution is a phosphomimetic (e.g. T_{47}E) (66). When added to GST-L_E, neither hGB1 nor hGB1-2A prevented the incorporation of ^{32}P, as long as the bait protein had a wild-type CK2 site at T_{47}. But when treated with CK2 and then SYK, the Y_{41} site became masked in the presence of hGB1-2A (Fig 3-7). The control hGB1 alone did not allow this masking, either on the wild-type GST-L_E, or with the phosphomimetic bait, T_{47}E. Therefore, Y_{41}, which lies to the C-terminal side of the L_E hinge domain is among the likely contact sites for 2A binding. This site and T_{47} are found solvent-exposed when L_E binds Ran (63).

Discussion

At the earliest stages of a cardiovirus infection, viral proteins are in low abundance. And yet the virus must take swift action to combat innate host antiviral defenses. The L_E protein of EMCV achieves this by leveraging a cell kinase-based phosphorylation cascade directed against Phe/Gly-containing nuclear pore proteins (60). The effect is a rapid shutdown of active transport of macromolecules across the NPC (8). Addition of L_E to permeabilized cells, or transfection of L_E-encoding cDNA into intact cells, can readily demonstrate this effect (8, 60). But in both cases, the viral protein concentrations are effectively much higher than the scant few molecules initially translated from an infecting genome. We previously hypothesized that the viral protein 2A, which encodes an active nuclear localization signal, may help shuttle L_E to the nuclear rim, thereby placing it directly into contact with RanGTPase, the required L_E activation partner (122). This would, however, require a physical interaction between L_E and 2A, either directly or indirectly.

These proteins, encoded at opposite ends of the L-P1-2A precursor, are released sequentially by tandem cleavages with $3C^{pro}$ almost as soon as the protease is available (82, 126, 127). Their respective pIs as the most basic (2A) and acidic (L_X) proteins in the polyprotein should make obvious the potential for interaction. Indeed, we demonstrated here that L_X and 2A from three different cardioviruses can bind directly *in vitro* and in any combination, from any virus (Fig 3-4). The binding is stoichiometric. For EMCV 2A, it can be almost entirely recapitulated with a shorter fragment containing only the first 50 amino acids (Fig 3-2C). Theilo and Saffold L_X cognates reacted with all

homologous 2A proteins, but preferred the sequence from EMCV, presumably because that particular 1-50 segment is almost 2 logs more basic than their normal partners (Fig 1). When measured by SPR, the EMCV proteins had a K_D of 1.5 μM that was partially responsive to salt but the majority of complexes were still able to form at concentrations up to 500 mM. Therefore, these proteins must have a degree of specificity in addition to simple charge:charge interactions.

The preferred partner for L_E, Ran, binds with a much lower K_D (3 nM). Competitions between 2A and Ran for bead-bound L_E, however, suggest that both proteins can be accommodated simultaneously, implying only partially overlapping binding sites. Mutated L_E sequences with weaker binding affinities for 2A (e.g. $W_{40}A$) were more readily displaced by Ran (Fig 3-6A). Interestingly, L_E:2A interactions also clearly masked L_E residue Y_{41}, one of two crucial phosphorylation sites for the activity of L_E. Phosphorylation is not required for L_E interactions with Ran, but without these modifications, the subsequent complex cannot proceed to ternary or quaternary reactions required to trigger the Nup phosphorylation cascade (63). Therefore, logically, 2A cannot remain perpetually bound to L_E, during the normal course of events during infection. For complete L_E phosphorylation after it is bound to Ran, the 2A must be released. Since L_E:Ran interactions are facilitated by the conformational morphing of Ran, as catalyzed by RCC1 tethered to chromatin just inside the nuclear rim, the results are entirely consistent with a 2A-dependent trafficking pathway of L_E to nuclear RCC1 sites, where it is displaced by Ran. Subsequently, L_E, bound to Ran can be dual phosphorylated, and primed for Nup inhibition activities. The freed 2A then presumably proceeds to nucleoli and initiates its independent cellular translation inhibition activities.

If this scenario is true, it can explain some previously observed experimental anomalies in 2A and L_E mutational studies. For example, deletions in L_E (102), 2A (80) or chimeric viruses exchanging EMCV and Theilo L_X or their 2A (82) typically have incomplete or improperly processed L-P1-2A regions. Presumably, the L-2A interaction, even in this precursor stage, could act to facilitate proper P1 folding, creating the requisite conformational substrates for sequential reactions with $3C^{pro}$. Without this interaction, disrupted by the deletion or mutation of either protein, $3C^{pro}$ would not efficiently process protomers into functional assembly intermediates. The L_X:2A binding reactions we tested with EMCV, Saffold and Theilo proteins showed that some chimeric combinations had poorer affinities. For example (Fig 3-5), L_E and Theilo 2A bind to only 10% saturation compared to L_E and EMCV 2A. When tested in a virus context it has been reported these same homologous swaps have, as expected here, concordant processing and replication defects (82, 118). The results also imply that studies aimed at mutagenesis of L_T domains (71, 72), with regard to its assigning nuclear pore activities or effects on cytokine trafficking, could easily cause unintended disruption of 2A-dependent trafficking, or reduced L_T:2A affinities, that would manifest as phenotypes with impeded L_T localization to the nuclear pore and subsequent shutoff of NCT. All told, our findings show that the anti-host activities of cardiovirus L_X and 2A proteins should not be considered independent of one another. Some phenomena previously ascribed solely to 2A or to L_X, may result from their affinity for each other.

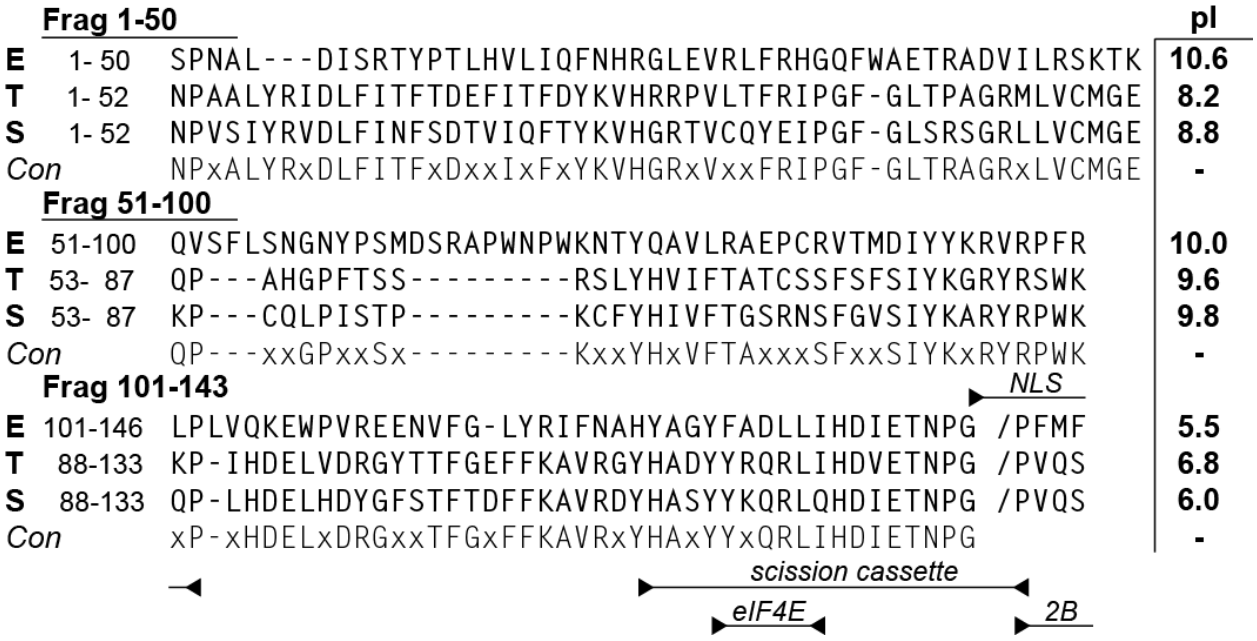

Figure 3-1: 2A Protein Sequences. EMCV-R (Genbank ABC25550), TMEV BeAn (Swiss-Prot P08544), and Saffold-2 (Genbank AFP86294) were aligned with (Lasergene 9) MegAlign software using the Jotun Hein method. The consensus (Con) required 2 or more identities. Tested protein fragments (L_E), their pI values, and functional motifs are indicated.

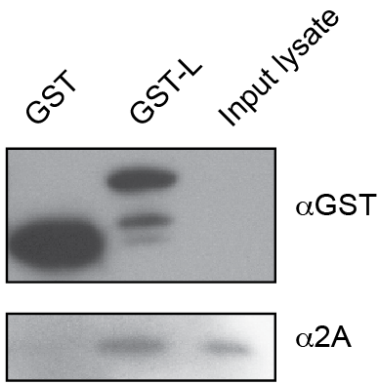

Figure 3-2: Native 2A pull-down. EMCV-infected HeLa lysates (100 µL) were incubated with either GST or GST-L_E (10 µg/reaction). Beads were washed, boiled, and analyzed by Western blot (αGST and α2A).

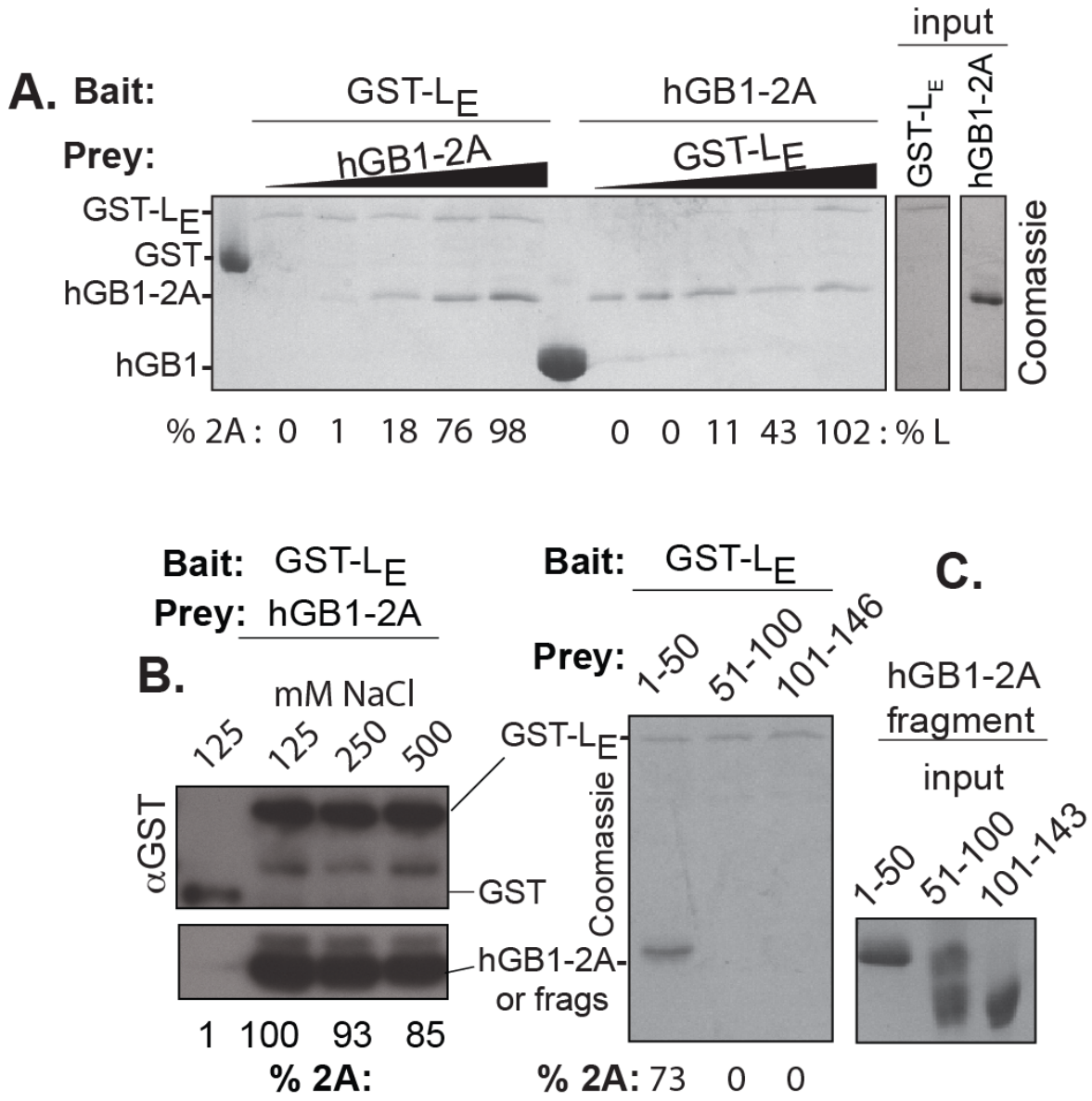

Figure 3-3: Pull-down Assays. A) The indicated recombinant "baits" and "preys" were used in reciprocal pull-down assays. The baits were held at 50 nM/reaction, while the prey concentrations varied (5-100 nM/reaction) as described in Methods. Band quantitation is relative to input (50 nM). B) Similar to A, the association reactions and wash reactions used the indicated salt concentrations. Band detection was by Western analyses (αGST). hGB1(-2A) is recognized by the secondary α-mouse antibody. C) Similar to A, EMCV 2A fragments were reacted with bead-bound GST-L_E. Captured prey was detected with Coomassie-staining. The right hand marker panel shows the input 2A fragments.

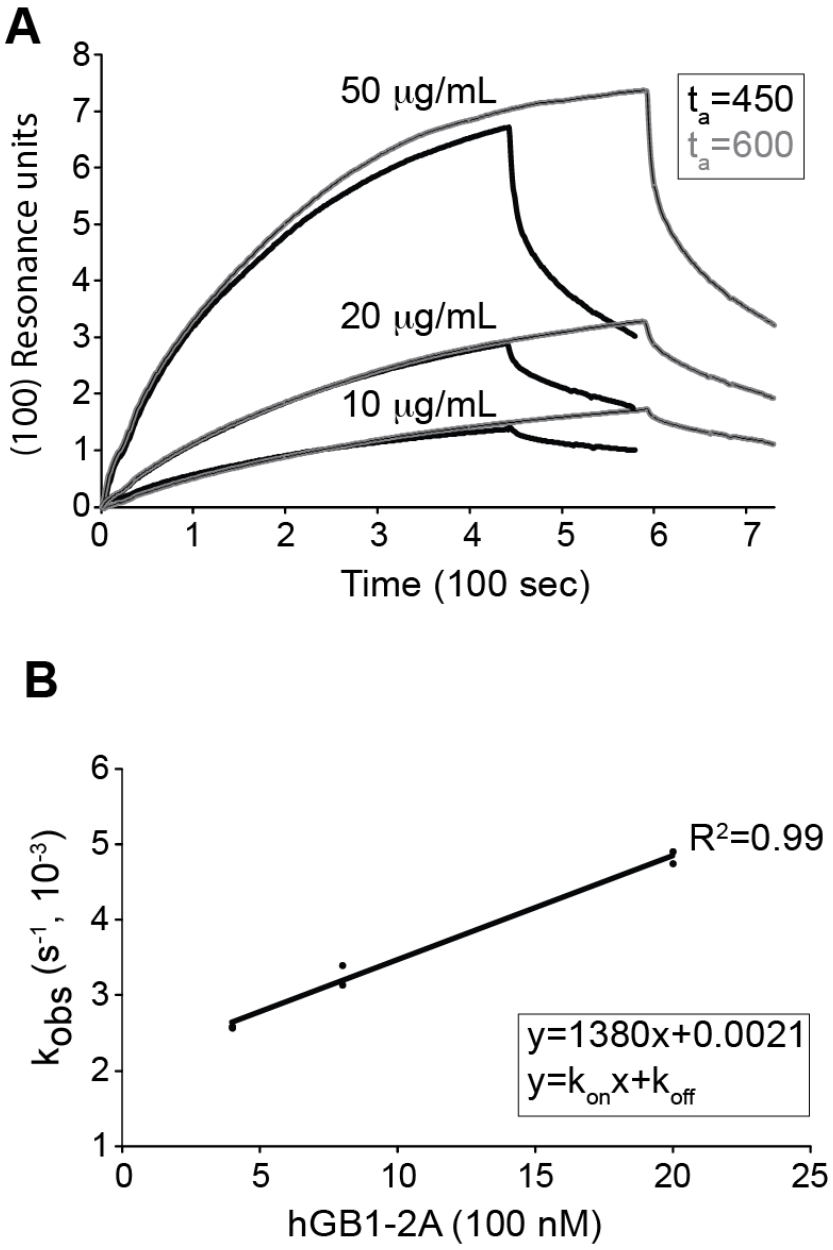

Figure 3-4: SPR of L_E:2A Binding. A) SPR sensorgram curves for hGB1-2A flowed over GST-L_E-bound αGST surfaces on CM5 chips at the indicated concentrations. Association phase was either 450 or 600 seconds with a dissociation phase of 120 seconds. Reference subtraction used a lane containing only αGST (not shown). B) BIAevaluation software calculated association and dissociation rates based on sensorgram curves in A, using Langmuir fitting. The k_{obs} was plotted against the concentration of hGB1-2A to extract the normalized K_D using a best-fit line in Excel.

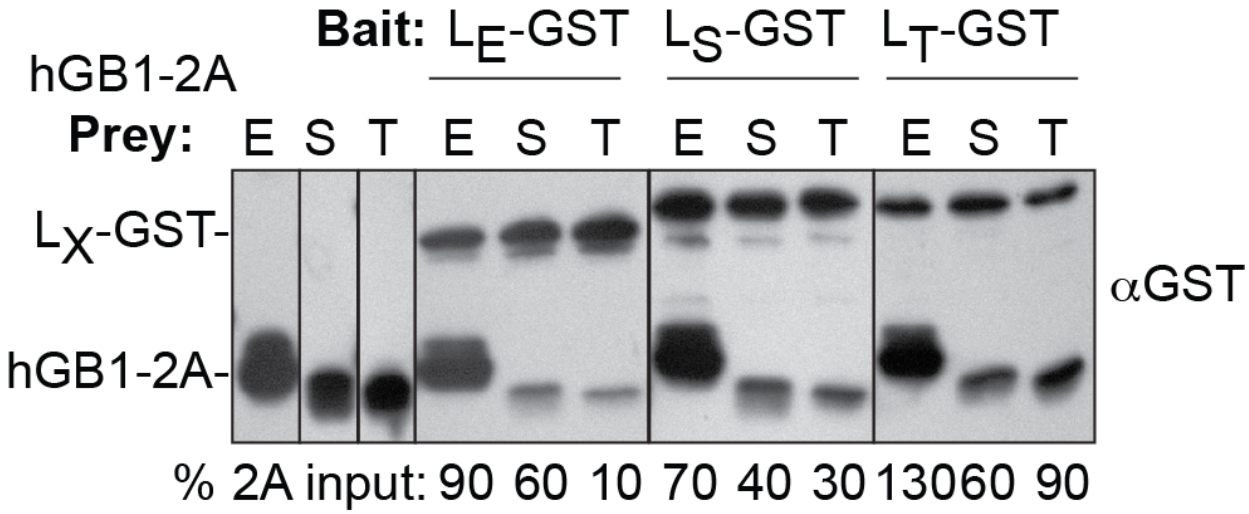

Figure 3-5: Intra- and Interspecies Reactions. L_E-GST, L_S-GST and L_T-GST baits were reacted with hGB1-2A prey from EMCV (E), SafV (S) or TMEV (T). Bead-bound protein was fractionated then detected by Western analyses with αGST. The secondary (anti-murine) mAb is also reactive with GB1 sequences. Band intensity values (hGB1-2A, ImageQuant) were normalized to each respective input lane.

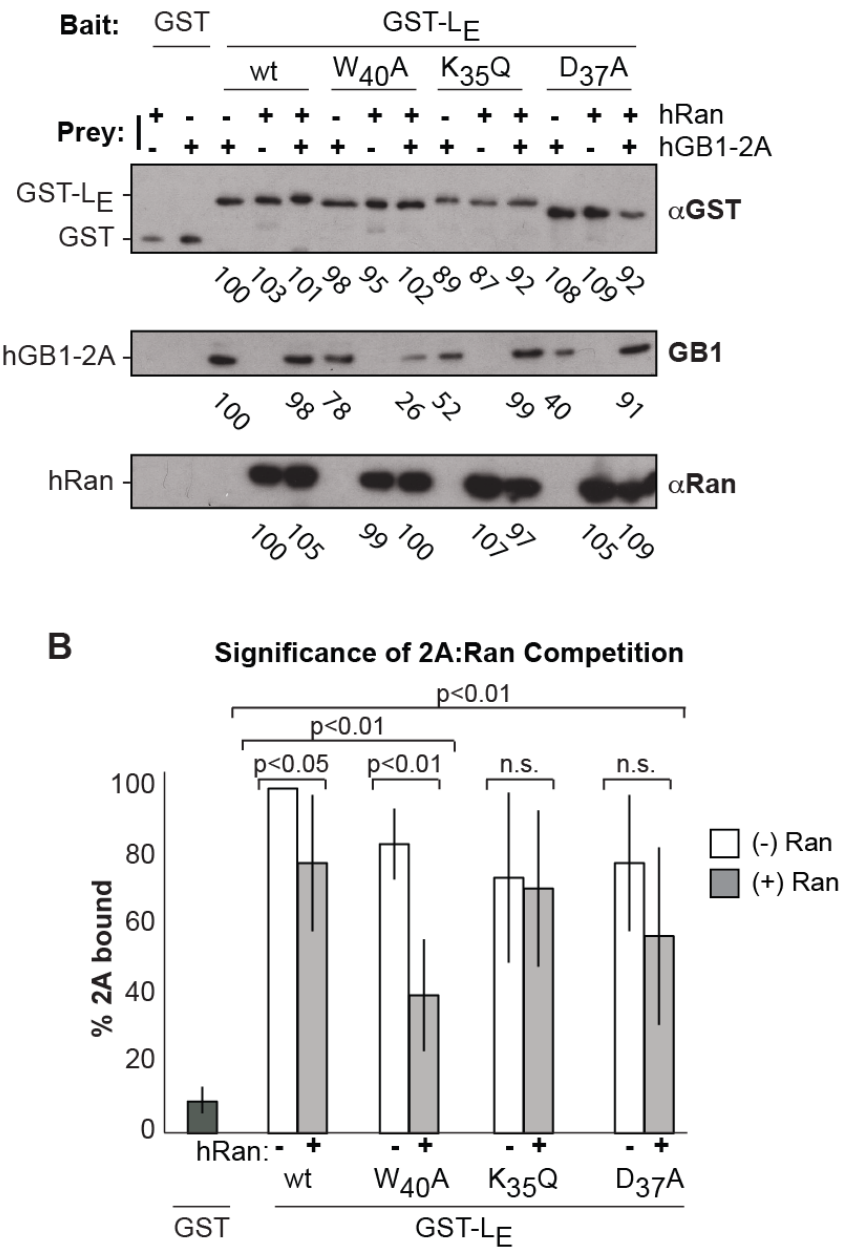

Figure 3-6: Ran and 2A Competitions. A) Recombinant GST or GST-L_E with substitution mutations K35Q, D37A or W40A were pre-bound to beads as baits, then reacted with equimolar hGB1-2A, hRan (with GST-RCC1), or a combination of hGB1-2A plus hRan. The proteins were detected by Western analyses. Bands (ImageQuant) were normalized to levels of hGB1-2A pulled down by wild-type L_E. B) The experiment in A was repeated (n=4), values were averaged over all experiments, and plotted to show the variance. Standard T-test significance for plus or minus Ran, are indicated ("n.s." not significant).

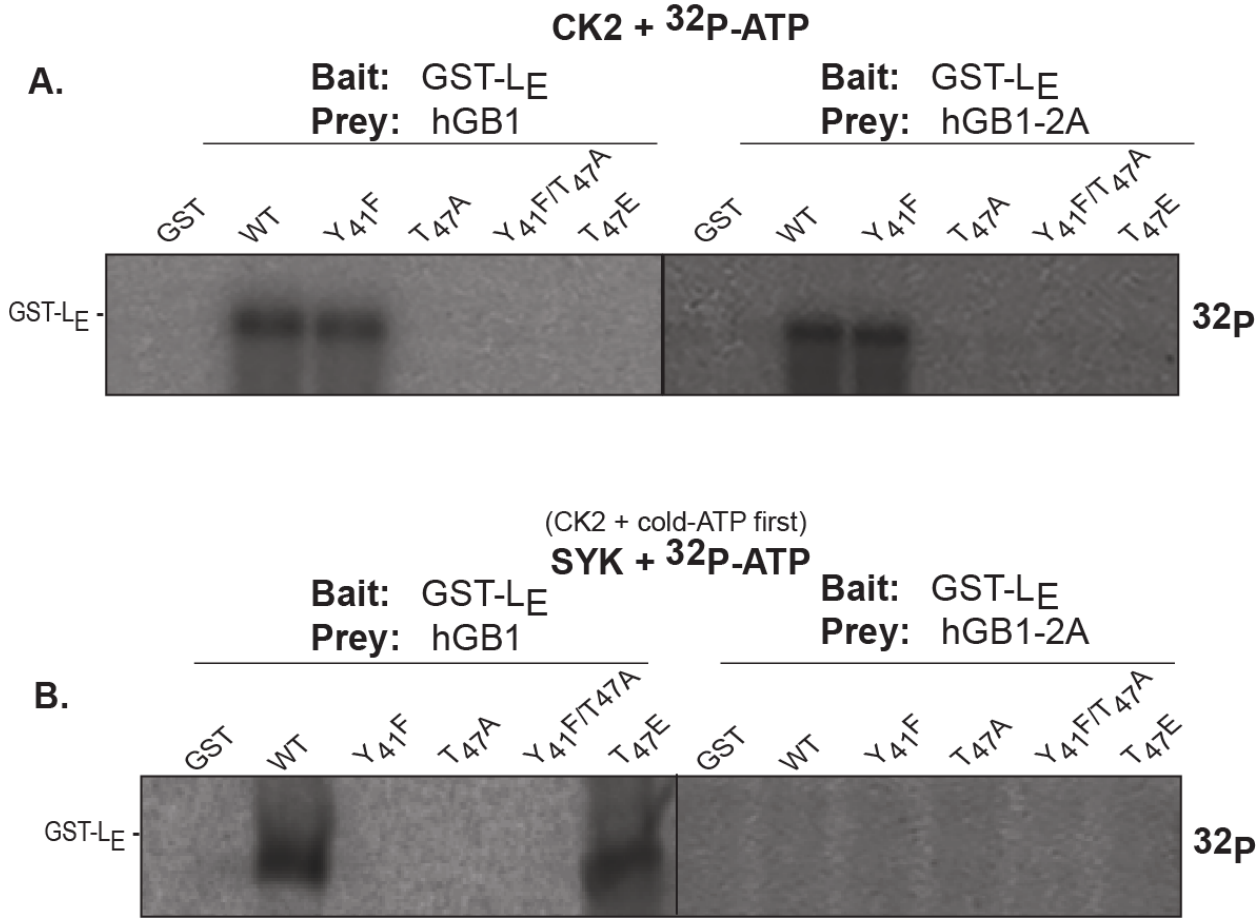

Figure 3-7: Phosphorylation of L_E:2A Complexes. A) GST-L_E and mutant derivatives (bait) and hGB1-2A or hGB1-2A (prey) bead-bound complexes were reacted with CK2 in the presence of ^{32}P-ATP. B) Similar to A, the SYK plus ^{32}P-ATP reactions were preceded by incubation with CK2 and cold ATP as in (12). Fractionated proteins were detected by phosphorimaging.

Chapter 4

2A alters translational complexes to promote IRES-driven translation

Abstract

The mechanism by which Cardioviruses shut down cellular translation is poorly understood. Mutagenesis and biochemical studies have implicated the 2A protein as a significant viral determinant in host cell translation control. Here, we examined the cellular pathways, proteins, and regions of 2A responsible for this translation shutdown. Both deletion and point mutation of the nuclear localization signal (NLS) of 2A reduced virus production and gene expression relative to wild type. We confirmed previous studies that showed that Rapamycin (Rap), an mTOR inhibitor, promotes virus translation and titers. We found, however, that PI3K inhibitors LY294002 (LY) and Wortmannin (Wort) both repressed 2A NLS mutant virus translation and infectious titers. LY directly prevented CK2 phosphorylation of L as an off-target effect, while 2A mutant viruses were mildly inhibited by Wort. We then showed that recombinant 2A could both directly reduce translation and promote IRES over cap-dependent translation in rabbit reticulocyte extracts. The first 50 amino acids of 2A were sufficient to induce the IRES:cap change, but were insufficient to broadly reduce translation. Removal of eIF4G:4E interactions recapitulated this effect. Finally, we observed that 2A directly induces the formation salt-sensitive 80S ribosomes. These studies further define the

ability of 2A to induce a shutdown of host translation during infection to promote viral translation.

Introduction

Translation is one of the most heavily regulated processes in the eukaryotic cell (84, 128). Unsurprisingly, it is also one of the most heavily targeted processes by picornaviruses during infection (85, 129-132). Picornaviruses have evolved diverse mechanisms with which to shut down host cap-dependent translation, thereby favoring translation of their own IRES. Enteroviruses and Aphthoviruses directly cleave eIF4G, removing the domain that binds eIF4E, the cap-binding factor (7, 42, 133). Cardioviruses have evolved a seemingly less direct method, one that is still poorly understood.

L has been shown to affect translation (68), though this may be indirectly due to its detailed activity of shutting down NCT, thus preventing transcribed RNAs from exiting the nucleus and transcription factors from entering (8). Left then to compete are the cellular mRNAs that are still in the cytoplasm at the time of virus entry and initial genome translation. eIF4G is not cleaved during Cardiovirus infection (11), yet cellular translation is still shut down in favor of the virus. Previous data has implicated protein 2A in this modulation of the host translational environment (61, 80, 116).

Inhibitors of the mTOR (mammalian target of rapamycin) and PI3K (phosphoinositide-3 kinase) pathway enhance translation of both wild type and 2A deletion EMCV in BHK cells (123). During normal cell growth, external growth factors

stimulate cell-surface receptors, which in turn activate PI3K to phosphorylate phosphatidylinositols (PIs). These molecules then activate further downstream kinases, of which a dominant one is mTOR (for overview, see Fig 4-1). Two well-defined substrates of mTOR are 4EBP1 (eIF4E-binding protein) and p70S6K, which directly phosphorylates and activates ribosomal protein S6 (134, 135). While phosphorylation of S6K and S6 activate them, stimulating translation, phosphorylation of 4EBP1 actually inactivates it, preventing it from carrying out its normal cellular role of binding and sequestering eIF4E. Once 4EBP1 is inactive, eIF4E is free to bind cellular mRNA caps and further promote translation (136).

As many cancers often contain aberrant, constitutively active growth factor kinase cascades, these proteins have been of significant interest and many inhibitors have been discovered or developed around them. Rapamycin (for which mTOR is named) is one such inhibitor. PI3K inhibitors include wortmannin, an irreversible inhibitor, and LY294002, a reversible, competitive inhibitor.

An initial hypothesis to EMCV 2A activity was that when localized to nucleoli, 2A incorporated into ribosomes and actively formed complexes that preferred IRES translation over caps; however, when ribosomes were analyzed, it was discovered that fully assembled 80S ribosomes were devoid of 2A, though 2A did incorporate into 40S (and pre-40S) subunits (61). In addition, were 2A to assemble virus-oriented ribosomes at the sites of ribosome biogenesis in the nucleolus, it would ultimately be difficult for these massive complexes to export through the NPCs, which have been shut down by L. We therefore studied the effect of 2A both *in vitro* and *in vivo*; finding that 2A directly impacts translation initiation to promote translation instead by the viral IRES.

Materials and Methods

vEC9 and 2A mutant virus production:

vEC9 and 2A mutant viruses Δ7 and AAA were generated as previously described (80). Briefly, pEC9 or 2A mutant cDNAs were linearized with SalI and transcribed with T7 RNA polymerase (New England Biolabs). DNA was removed (RQ1 DNAse, Promega), vRNAs were purified with an RNeasy kit (Qiagen) and transfected into HeLa cells (Lipofectamine 2000, Invitrogen). After 28 hrs (48 hrs for 2A mutants), plaques were picked and incubated overnight in Medium A to release virus. Virus was then amplified on HeLa cells for 28 hrs (48 hrs for 2A mutants), freeze-thawed (3x) and stored at -20°C.

Virus infection and comparison:

To compare the infectivity, translation, and virus production of vEC9 and 2A mutant viruses, HeLa cells were infected (30 min. attachment) at MOI=30 for 3.5 hrs in 1x P5. After infection, cells were washed with PBS (3x), scraped, and boiled in SDS buffer. Virus translation was monitored by western blot using primary mAbs against EMCV 2A (1:3,000), 3D (1:10,000), and capsid (1:2,500) followed by α-mouse secondary (1:10,000) (83). Phosphorylation of Nups as an upward mobility shift on western blots was measured using mAb414 (1:5,000), which targets F/G repeat-containing Nups. Nup62 was used for phosphorylation comparisons. All protein band intensities were measured using ImageQuant software (GE Healthcare). For time-

course experiments, parallel infections began simultaneously and were ceased by washing/boiling at the indicated time point.

PI3K and mTOR inhibitor effects on virus translation/production:

Rapamycin (10 nM), LY294002 (50 μM), and Wortmannin (10 μM) (Cell Signaling Technologies) were resuspended in DMSO and used at the manufacturer's suggested concentration unless otherwise indicated. For plaque assays, cells were pre-treated for one hour in medium containing the indicated drug. Cells were then infected with the indicated virus (30 min. attachment, MOI=10) with drug-supplemented media. After six hours, cells were freeze-thawed (3x) and spun (10,000 x g, 10 minutes) to remove cellular debris. Clarified viral lysates were tested for infectivity by plaque assay (28 hrs for wild-type, 48 hours for 2A mutants). For western blots, infections proceeded for 3.5 hours (MOI=30), were washed, boiled in SDS buffer, and probed via western blot using α3D (1:10,000) and mAb414 (1:5,000) primary mAbs followed by HRP-linked α-murine secondary mAbs.

GST-L phosphorylation inhibition and 2A-binding assay:

Recombinant GST-L (5 μg/reaction) was incubated in the presence of 0.5 units recombinant CK2 (New England Biolabs), pretreated with LY (50 μM), 4,5,6,7-Tetrabromo-2-azabenzimidizole (TBB, 50 μM) or DMSO, or HeLa cytosol pretreated with LY or DMSO for 1hr at 37°C followed by addition of 2 μL 20 mM ATP and 1 μL (10 μCuries) gamma-labeled ^{32}P in 80 μL 1x CK2 buffer for 45 minutes at 37°C. Reactions were incubated with 10 μL glutathione sepharose beads and washed 5x in PBS.

Samples were then boiled in SDS buffer and fractionated by SDS-PAGE followed by silver staining, exposure to a phosphor screen (GE Life Sciences, 24 hrs), and imaging by a Typhoon scanner (GE Life Sciences).

For 2A binding studies, GST-L was incubated in the above reaction without hot ATP, but with SYK (0.5 units, New England Biolabs). Single (CK2) and double (CK2 and SYK) phosphorylated GST-L was incubated with hGB1-2A and analyzed as in Fig 3-5.

pF/R dual luciferase assays:

The pF/R construct has been previously described (137). Briefly, the pF/R construct is a bicistronic plasmid encoding a single T7-driven RNA that expresses firefly luciferase from a 5' cap and *Renilla* luciferase from an EMCV IRES (Fig 4-10). The pF/R plasmid was linearized with HpaI followed by transcription with the T7 RiboMAX Transcription Kit (Promega) in the presence of 5' cap analog (Promega). The capped RNA was purified by RNeasy kit (Qiagen).

For *in vitro* translation of pF/R, rabbit reticulocyte (RR) lysates were used (Promega). pF/R RNA (1 µg, supplemented with 0.5 µL RNasin) was incubated in the presence or absence of recombinant proteins GST, GST-L, hGB1, hGB1-2A, and truncations (5 µg unless indicated otherwise) for one hour at 37°C. Alternatively, RRs (17.5 µL) were incubated with the same indicated proteins for one hour at 37°C. After incubation, reactions were combined to produce the full 25 µL translation mixture, supplemented with amino acids and 0.5 µL RNasin (Promega). Translation proceeded for 90 minutes followed by the addition of Dual Luciferase Assay substrates (50 µL

each, Promega), and luciferase production was measured on a Veritas luminometer (Promega).

Recombinant RV-A16 $2A^{pro}$ was a generous gift from Dr. Kelly Watters (purification previously described (11)). $2A^{pro}$ (2 µg) was pre-incubated with RRs (17.5 µL) for one hour at 37°C, while RNA (1 µg) was simultaneously incubated with hGB1 or hGB1-2A (5 µg). Reactions were combined and supplemented with amino acids. After 90 minutes, luciferase expression was measured with the Dual-Glo Luciferase Assay (Promega, 50 µL each, 10 min. incubation) on a Veritas luminometer. This assay corrects for the inherent advantage of the IRES over cap translation and results in lower RLU readings for *Renilla* luciferase. Uncertainty in all pF/R data was the standard deviation of triplicate experiments.

Ribosome profiling:

hGB1 or hGB1-2A (100 µg) was incubated with 1mL HeLa cytosol supplemented with 500 mM KCl at 37°C for 1 hr. Ribosome populations were profiled as previously described (61). Briefly, samples were loaded onto a 15-45% linear sucrose gradient (Gradient Mate, time=1:53, angle=81.5°, speed=17) and run on an SW-41 rotor (34,000 rpm, 4°C, 210 minutes). Fractions were collected by peristaltic pump from the bottom of the tube (~0.5 mL/min) and absorbance was measured (280 nm) on an AktaPrime. Fractions were precipitated with 20% TCA, washed with acetone, and suspended in alkaline SDS buffer. Fractions were analyzed by SDS-PAGE and western blot using α-His (Abcam, 1:2,000) and αS6 (CST, 1:1,000) primary mAbs with α-mouse and α-rabbit HRP-linked secondary mAbs.

Results

2A NLS mutants are deficient in virus translation:

2A mutant viruses Δ7 and AAA have been generated and studied previously (80) (Fig 4-2) and contain a deletion (Δ7) or point mutation (KRR>AAA) of the NLS of 2A. These viruses replicate slower than vEC9 and produce smaller plaque sizes (Fig 4-5, top series). At the molecular level, Δ7 cannot properly process its L-P1-2A precursor (80), which results in low levels of fully processed 2A and capsid during infection (Fig 4-3). While the P2 and P3 regions are properly processed, they are in very low abundance relative to wild type (Fig 4-3). The AAA mutant does not have the aberrant 3C processing phenotype that Δ7 does, but still produces its proteins in low abundance relative to vEC9 (Fig 4-3). As may be expected, this decrease in viral protein production similarly results in decreased phosphorylation of Nups.

When observed over a time course, it becomes clear that these defects are merely setbacks, at least in cell culture. At 6 hours post-infection, all three viruses have initiated translation and induced hyperphosphorylation of Nups (Fig 4-4). At the initial stages of infection, vEC9 is the most effective at viral translation and cellular shutdown, with Δ7 being the weakest and AAA an intermediate phenotype.

mTOR/PI3K inhibitors impact virus production:

Previous studies on 2A deletion mutant viruses observed that the mTOR and PI3K inhibitors rapamycin (Rap) and wortmannin (Wort), respectively, were able to enhance replication of the wild type virus and rescue deletion of the central third (Δ58)

of 2A (123). It is important to note, though, that these studies took place in BHK cell lines. We sought to test whether these drugs produced similar effects for our mutant viruses in HeLa cells.

We grew PFU-equivalent viruses in the presence of drug pre-treated cells for six hours and determined infectious virus production by plaque assay (Fig 4-5). Rap produced modest increases in virus production for vEC9 and Δ7 (2 fold increase) while AAA appeared unaffected (Table 4-1). With LY, a PI3K inhibitor, vEC9 production was moderately inhibited, as was AAA virus production (80-90% decrease). The Δ7 virus was strongly inhibited, with virus yield dropping nearly three logs. This led us to test the effects of an alternate PI3K inhibitor, wortmannin. Wort did not substantially affect vEC9 production, but did inhibit Δ7 and AAA by ~50-70%.

This disparity in effects for two different inhibitors of the same kinase led us to investigate if LY was targeting more than just PI3K activity in the cell. We first tested if there was a substantial dose-dependent effect of LY on virus translation, as measured by $3D^{pol}$ expression. At the manufacturer's suggested concentration (50 μM), $3D^{pol}$ translation was reduced over 90% for vEC9 at 3.5 hrs post-infection, similar to the decrease observed in virus yield (Fig 4-6). Reducing the concentration of LY by half, though still nearly 20x the IC_{50} of 1.4 μM, dramatically alleviated the translation inhibition observed previously. Successive reductions in concentration produced a negligible affect on $3D^{pol}$ production relative to the control. Interestingly, the addition of Rap in the presence of LY was able to partially restore $3D^{pol}$ expression from 4% up to 67% of untreated virus (Fig 4-6, fourth lane).

LY directly inhibits CK2 phosphorylation of GST-L:

We discovered that LY had been previously observed to target CK2 at a concentration similar to the IC_{50} of LY towards PI3K (138). We tested recombinant CK2 and GST-L to see if LY could have a direct inhibitory effect on this critical phosphorylation event. While the CK2-specific inhibitor TBB reduced GST-L phosphorylation by over 90%, LY inhibited GST-L phosphorylation with both recombinant CK2 (75% inhibition) and HeLa cytosol (50% inhibition) at the concentrations used in previous cell culture experiments (50 μM) (Fig 4-7).

Phosphorylation of L does not impact 2A binding:

Phosphorylation of L by CK2 is a required step for Nup hyperphosphorylation and NCT shutdown (66). Given that 2A binding blocks the phosphorylation of Y_{41} on L (Fig 3-7), we tested to see if the phosphorylation state of L affected its ability to bind 2A. We found that non-phosphorylated, singly (CK2 on T_{47}), and doubly (CK2 on T_{47} and SYK on Y_{41}) phosphorylated L all bound 2A to saturation in pull-down assays (Fig 4-8), suggesting that L:2A binding is unaffected by the phosphorylation state of L.

Wortmannin reduces Δ7 translation and Nup phosphorylation:

Given that LY inhibition on virus gene expression appeared targeted at L, we wanted to verify if PI3K inhibition by Wort still impacted virus translation. For vEC9, inhibition of PI3K by Wort reduced $3D^{pol}$ translation by 76% and marginally impacted Nup phosphorylation (Fig 4-9). It is interesting that translation appears inhibited at 3.5

hrs post-infection, whereas virus production is relatively unaffected at 6 hrs post-infection (Table 4-1).

For Δ7, Wort reduced $3D^{pol}$ expression 90%, which corresponded to a ~50% decrease in Nup phosphorylation (Fig 4-9). $3D^{pol}$ expression is reduced to similar levels between vEC9 and Δ7 virus with LY while the ultimate outcome of infectious virus production is dramatically different between the two, though Nup hyperphosphorylation is similarly impacted at 3.5 hrs post-infection in the presence of LY. Surprisingly, Rap inhibits Δ7 3D expression ~50% at 3.5 hrs while virus production appears enhanced at 6 hrs post-infection.

2A impacts on cap and IRES translation:

Observing that kinases involved in the mTOR/PI3K pathway, which ultimately regulate numerous translation factors, impact vEC9 and 2A mutant viruses, we sought to test if recombinant 2A had a direct impact on translation itself. It has been shown that 2A contains both eIF4E and RNA-binding capabilities (80, 139). To test potential 2A-directed effects, we used a bicistronic reporter consisting of firefly luciferase under the control of a 5' cap and *Renilla* luciferase under the control of an internal EMCV IRES (Fig 4-9).

Recombinant hGB1-2A was pre-incubated with rabbit reticulocyte (RR) extracts or RNA at 1 µg/25 µL reaction. This produced no statistically significant change in expression of either luciferase (Fig 4-10A) and the ratio of IRES:cap (i.e. *Renilla*:firefly) was unchanged. When the concentration of hGB1-2A increased to 5 µg/reaction, translation as a whole was reduced by ~10 fold for 2A that was pre-incubated with RNA

or the RRs. In addition, pre-incubating hGB1-2A with RNA inhibited cap-dependent translation to nearly undetectable levels (Fig 4-10B). The IRES:cap ratio also increased ~10 fold, but only when hGB1-2A was pre-mixed with the RNA, *not* with the RRs (Fig 4-11).

We then sought to test if the individual truncations of 2A could recapitulate any, if not all, of this activity. Neither hGB1-2A$_{51-100}$ nor hGB1-2A$_{101-143}$ could impact the level of translation or IRES:cap ratio, despite hGB1-2A$_{101-143}$ containing the eIF4E-binding site. We also tested if hGB1-2A$_{1-50}$, which contains the RNA-binding site, could impact translation. While hGB1-2A$_{1-50}$ cannot generally suppress translation like the full-length protein, it nevertheless shifted translation from cap to IRES to a nearly identical level (Fig 4-11).

L does not directly impact cap- or IRES-driven translation

Given that L has been linked to translational effects previously (68, 102), we tested if recombinant GST-L could directly impact either cap or IRES translation. Neither GST nor GST-L had a significant impact on translation (Fig 4-12A) or the IRES:cap ratio (Fig 4-12B).

eIF4G cleavage enhances 2A-associated EMCV IRES translation:

To further dissect the effects of 2A association with RNA and translation components, we tested whether eIF4E/4G availability altered cap or IRES translation. We used a recombinant 2A^{pro} from RV-A16, which selectively cleaves the domain of eIF4G that recruits eIF4E to generate a cap-binding-deficient translation extract. In the

absence of EMCV 2A, RV $2A^{pro}$ simultaneously reduced cap-dependent translation and enhanced EMCV IRES-driven translation (Fig 4-13A, first and second bars). This resulted in an IRES:cap ratio similar to that induced by hGB1-2A alone (Fig 4-3 B, third bar). The combination of EMCV 2A and RV $2A^{pro}$ produced the most dramatic effect, increasing the IRES:cap ratio ~100x (compared to ~15x for EMCV or RV 2As individually).

2A generates unstable 80S ribosomes:

2A appeared to directly affect the initiation complex, so we then tested if 2A had an impact on the population of ribosomes in the cell. Previous studies using full-length virus showed that EMCV infection generated salt-sensitive 80S ribosomes, devoid of mRNA (61). We followed these tests using recombinant proteins to see if 2A was indeed the virus element responsible for this effect. In the presence of hGB1 alone, the 80S to 60S and 40S (combined) ratio of KCl-supplemented HeLa cytosolic extracts was 0.6 (Fig 4-15); however, the addition of hGB1-2A shifted populations away from fully formed 80S into 60S and 40S subunits in a, ~35% drop (ratio 0.38). However, this drop is substantially less than the shift previously observed with full virus during infection (61). When tested for the presence of recombinant protein in these fractions, we found that hGB1 was completely excluded from ribosomes, whereas hGB1-2A was incorporated into 40S subunit and polysomes, but not the 60S subunit or 80S ribosome.

Discussion

2A, like L, is a dispensable protein in tissue culture, but is absolutely required for causing pathogenesis in animals (82, 140). We sought to detail the mechanism by which 2A facilitates host cell shutdown for the virus. The interaction of L and 2A (detailed in Chapter 3) led us to investigate 2A's NLS to see if mutations impacted L activity. We used a deletion mutant (Δ7) and a point mutant (AAA), both of which have been shown to eliminate or strongly reduce the nuclear localization of 2A (80). We first found that capsid, 3D, and 2A expression were all well below vEC9 levels (Fig 4-3), and the phosphorylation of Nups was similarly reduced. As native L travels directly through blotting membranes, it is difficult to examine the levels of L produced by these mutant viruses, though it should be equivalent to those of other EMCV proteins made at similar time points. Were we able to detect levels of L, we may be able to differentiate between a hypothesized 2A-dependent localization requirement and a simple dose-dependent effect.

By 6 hours post-infection, the AAA mutant has been able to catch up with vEC9, producing similar levels of all viral proteins tested and phosphorylating Nups to equivalent levels (Fig 4-4). Even the Δ7 mutant had begun to produce substantial levels of viral proteins at this time point. Despite this, both 2A mutants form smaller plaques, produce fewer infectious particles and require longer to do so (28 vs. 48 hrs) than the non-mutant virus (Fig 4-5, top row). While a few hours lag behind wild type may not seem much at first, in an animal where these proteins have evolved (i.e. in the presence of an immune system including interferon, to which EMCV is highly sensitive), hours

could mean the difference between complete pathogenesis/viremia, and a controlled/cleared infection by the host.

Given that 2A appeared to have significant anti-host effects independent of L, we wanted to examine the cellular pathways in which 2A may be involved. It was previously reported that both rapamycin and wortmannin, inhibitors of mTOR and PI3K, respectively, were able to both promote wild-type virus growth and rescue a 2A deletion virus (123). We found that Rap did enhance virus translation and protein production, but found that both Wort and LY inhibited 2A mutant viruses (Fig 4-5, Table 4-2). LY had the most dramatic, reducing viral titers of Δ7 nearly 3 logs. This effect was dose-dependent and was capable of being partially rescued by Rap. It was previously reported that LY is able to inhibit CK2 at similar concentrations (138). CK2 is a required kinase for the phosphorylation of L residue T_{47} (66). This phosphorylation is critical to the function of L, and mutation of this site to alanine significantly reduces L-induced Nup hyperphosphorylation (66). Very recently, it was shown that knockdown or deletion of PI3Kβ (a predominantly nuclear PI3K isoform) was able to inhibit RCC1 localization to chromatin, thus preventing RCC1:Ran interactions (141). This could theoretically prevent L:Ran interactions as well; however, inhibition of kinase activity with the PI3Kβ-selective inhibitor TGX-221 was unable to reduce Ran cycling.

We examined if LY was able to directly inhibit phosphorylation of L by CK2 and found that pre-incubation of LY with recombinant CK2 substantially reduces phosphorylation of L (Fig 4-7). HeLa cytosol, pretreated with LY, produced a similar, albeit lesser, inhibition of L phosphorylation, down to 50% of control. Even a 50%

reduction may substantially hamper the virus when it relies upon very low initial numbers of L molecules to shut down host trafficking and antiviral defenses.

To eliminate the possibility that LY inhibition was not also impacting L:2A binding, we produced both singly (T_{47}) and doubly phosphorylated (T_{47}/Y_{41}) L and found that phosphorylation did not noticeably impact binding of 2A (Fig 4-8). This requirement of phosphorylation for L activity is then likely due to an additional cellular factor involved in either anchoring L to the pore or recruiting/activating the kinases responsible for Nup hyperphosphorylation during infection.

The involvement of the mTOR/PI3K pathway led us to test 2A's direct effects on translation, specifically the difference between 5' cap (host) and IRES (virus). While L itself was unable to directly affect translation (Fig 4-13), we found that full-length hGB1-2A was able to strongly repress both cap and IRES-driven translation (Fig 4-11), though cap was repressed ten-fold more (Fig 4-12). Surprisingly, the RNA-binding region of 2A (hGB1-$2A_{1-50}$) was sufficient to repress cap-dependent translation, but did not negatively impact IRES-driven translation. Given that viruses with mutations in the eIF4E-binding region of 2A have severely reduced replication and that removal of 4E both by 4G cleavage (Fig 4-14) or recombinant proteins (4EBP1) enhances IRES translation, we suspected that 2A's ability to repress translation is most likely occurring at the initiation stage (1, 80). It is interesting to note that 4E-binding-deficient 2A mutant viruses, while poorly replicating, can still moderately shutoff host translation (80). These 2A mutants, however, still contain a fully functional NLS and L-binding domain (Chapter 3). L may then be fully functional in these infections, subsequently shutting down NCT. At the 7

hour time point tested for 4E-binding-deficient viruses, inhibition of mRNA export due to active L could theoretically manifest itself as host translation shutdown (80).

An initial hypothesis regarding 2A's activity was that it could incorporate into ribosomes and create complexes that preferentially translated vRNAs. This proved to be incorrect as 2A can only be found in the 40S ribosome particle and not the full translation-competent 80S (61). Similarly it was observed that EMCV infection caused a dramatic shift from polysomes to monosomes and that 80S ribosomes were devoid of most cellular mRNAs (61). These previous studies were all performed in an infection with the full complement of viral proteins. We tested if purified, recombinant 2A was sufficient for observing these effects as well. While 2A did not demonstrably impact the ratio of polysomes to monosomes (Fig 4-15), it did induce a shift from fully formed 80S ribosomes to the individual 60S and 40S subunits, though the changes were much less pronounced than observed previously with EMCV infected cells (61). These profiles were conducted in the presence of 500 mM KCl, which destabilizes mRNA-devoid 80S particles (61). This would indicate that 2A can either prevent the initial formation of 80S ribosomes or can induce formation of "zombie" 80S particles, devoid of mRNA. Further experiments can differentiate these possibilities by digesting endogenous cellular mRNAs prior to addition of 2A and conducting similar ribosome profiles. If the former is true and 2A inhibits the formation of 80S complexes, the addition of translation-competent RNAs should still not allow formation of 80S complexes in the presence of 2A. If the latter is true, extracts devoid of mRNA should still be able to form translation-incompetent 80S ribosomes in the presence of 2A.

Taken together, our data suggest that instead of directly producing IRES-preferential ribosomes, 2A may instead be creating a “trap” on the mRNA/eIF4E cap complex, thus selectively inhibiting cap-dependent translation, as EMCV RNAs require neither caps nor eIF4E. Alternatively, 2A may be forming translation-incompetent “zombie” ribosomes, which could function as an additional step (along with L-induced mRNA export shutdown) to inhibit cellular mRNA translation.

While the nucleolar lifecycle of 2A remains a mystery, these data form a greater understanding of the mechanisms by which cytoplasmic EMCV 2A is able to induce a broad shutdown of translation, namely by modulation of host initiation complexes.

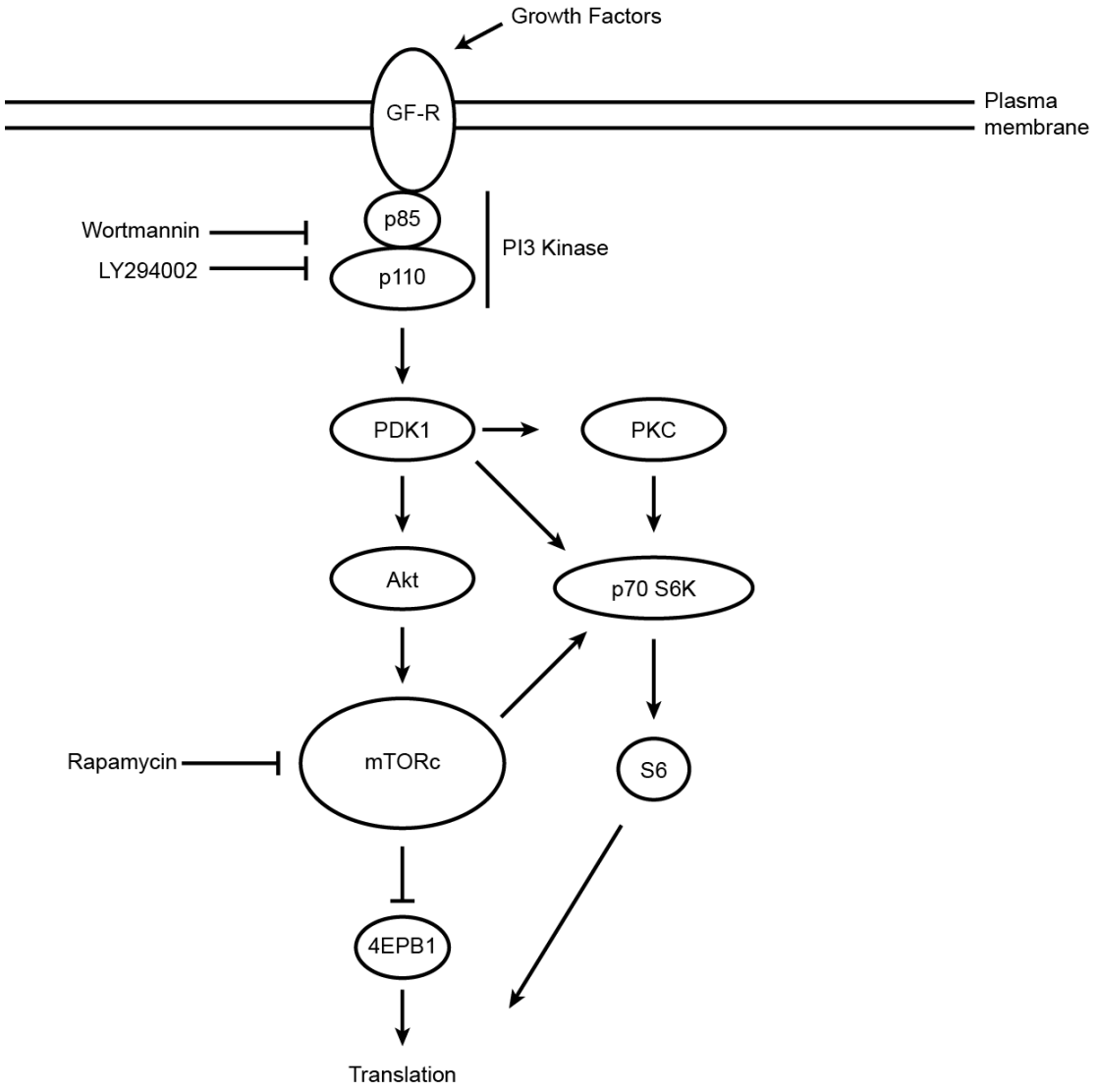

Figure 4-1: Overview of PI3K/mTOR pathway and drug inhibition. The general PI3K/mTOR pathway is shown. Drugs used in these studies include Rapamycin (mTOR inhibitor), LY294002 (PI3K), and Wortmannin (PI3K). Growth factors (GF) stimulate Growth Factor Receptors (GF-R), which stimulate PI3K to convert phosphatidylinositol (PIP) to phosphatidylinositol-3-phosphate (PI3P). This stimulates a cascade, which activates p70 S6 Kinase (S6K) and mammalian target of rapamycin complex (mTORc). mTORc inactivates 4EBP1 and S6K activates S6, both resulting in a stimulation of translation.

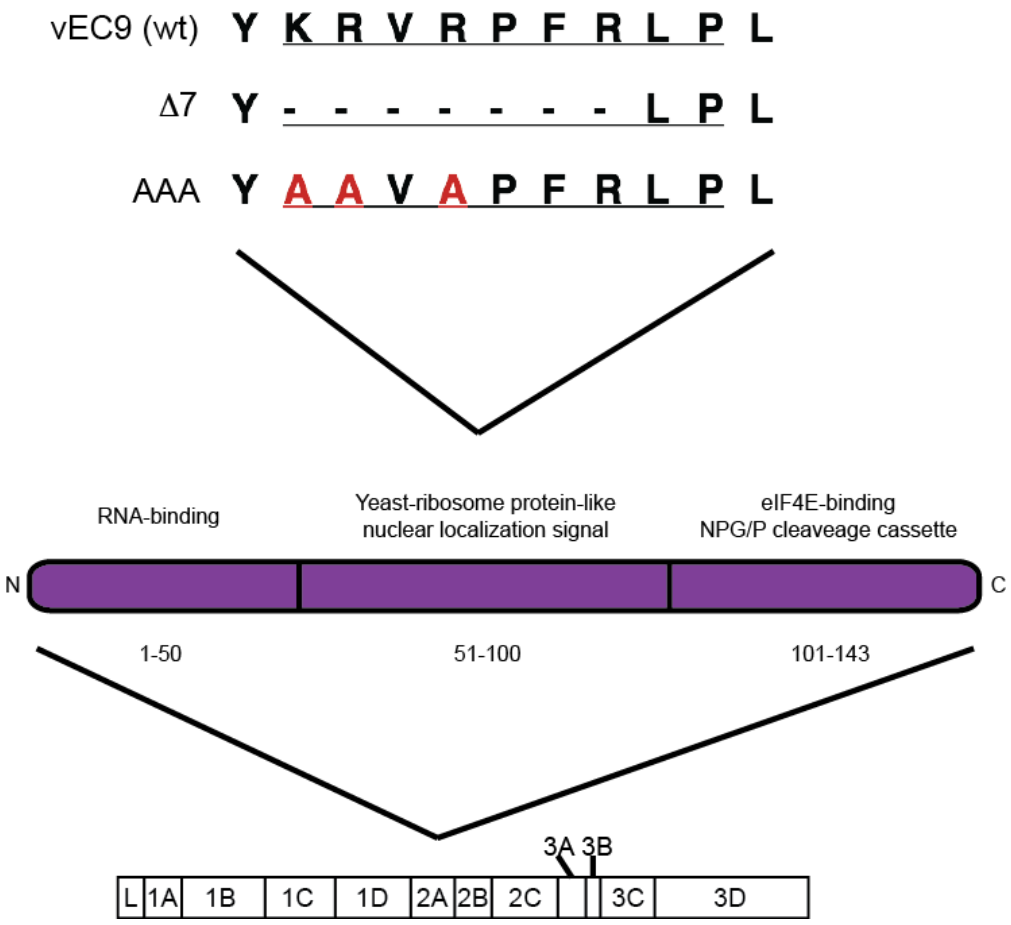

Figure 4-2: Schematic of 2A mutant viruses. 2A mutant viruses contain either a seven amino acid deletion (Δ7) or three amino acid alanine point mutation (AAA) in the NLS of 2A. Viruses were grown from plaque purified RNA transfections.

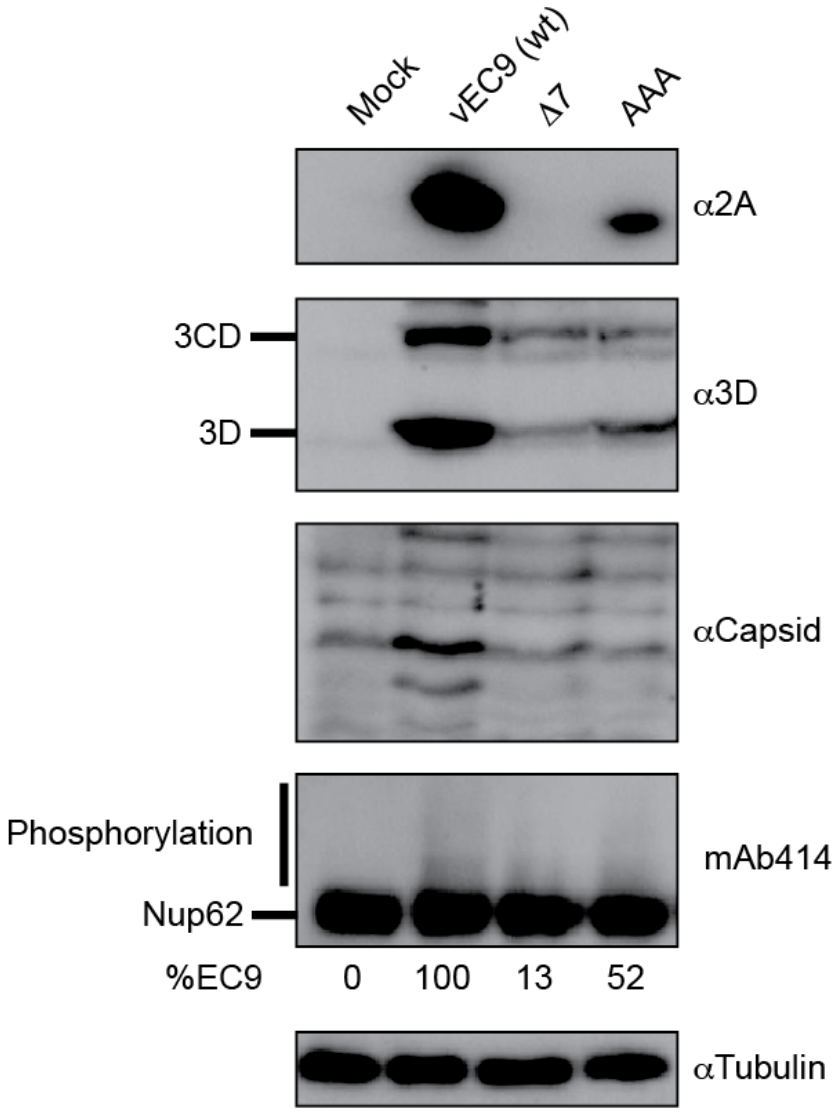

Figure 4-3: Comparison of 2A mutant viruses. HeLa cells were infected with vEC9, Δ7, or AAA at MOI=30 for 3.5 hrs. Lysates were probed using western blot against tubulin, F/G repeat Nups (mAb414), EMCV 2A, 3D, and capsid. Phosphorylation of Nup62 was measured by upwards mobility using ImageQuant and normalized to vEC9.

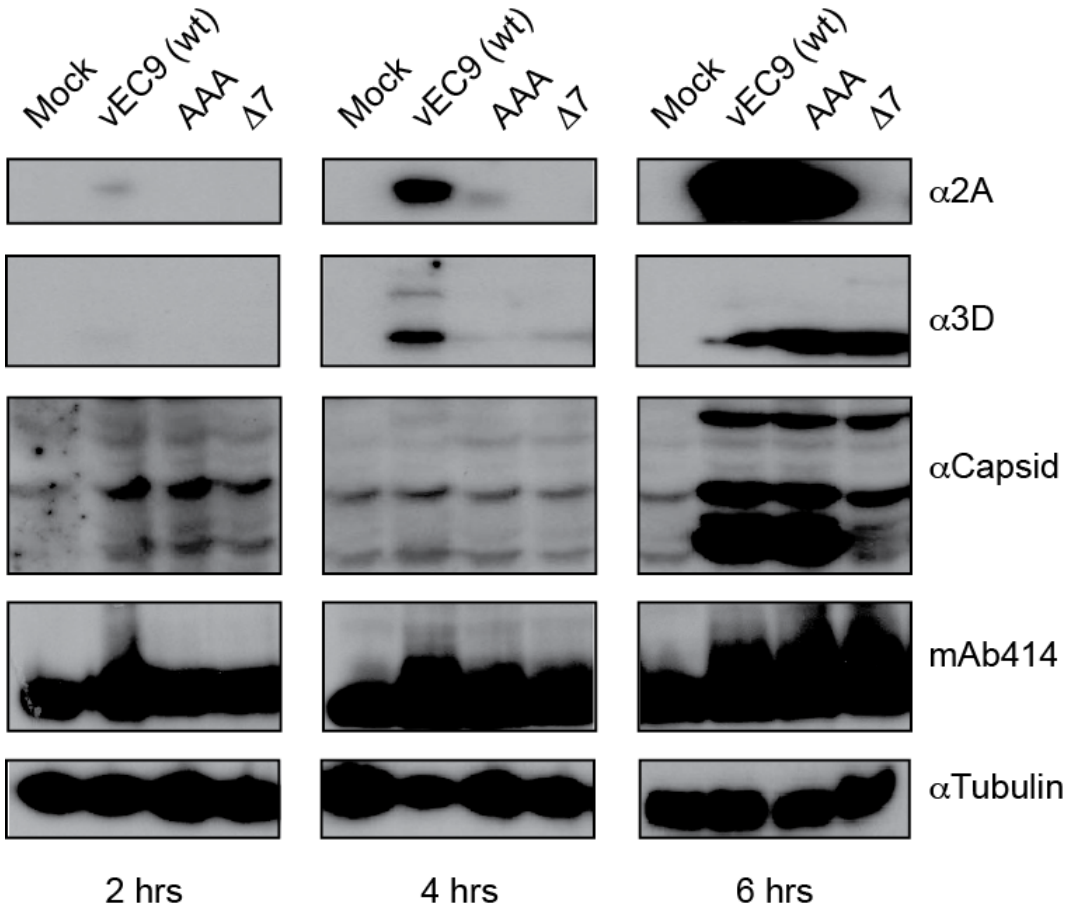

Figure 4-4: Time course of 2A mutant viruses. HeLa cells were infected with vEC9, Δ7, or AAA at MOI=30 for 2, 4, or 6 hrs. Lysates were probed using western blot against tubulin, F/G repeat Nups (mAb414), EMCV 2A, 3D, and capsid.

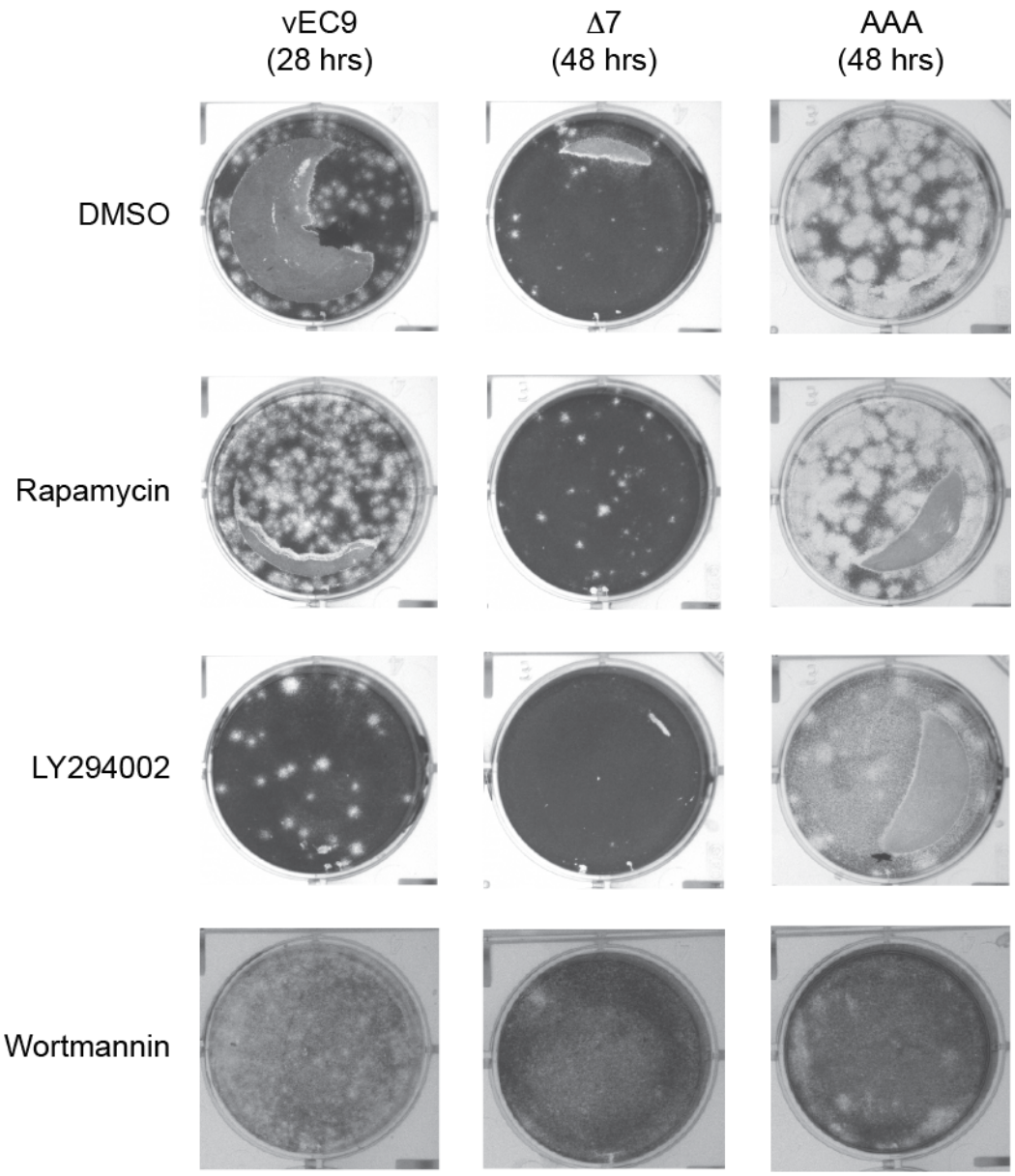

Figure 4-5: Kinase inhibitor effects on viral infectivity and titers. HeLa cells were pre-treated with rapamycin (10 nM), LY294002 (50 mM), or wortmannin (1 mM) for one hour. Cells were then infected with vEC9, Δ7, or AAA (MOI=10) for 6 hours, followed by freeze-thaw (3x). Lysates were used to determine viral titer by plaque assay (28 hrs. for vEC9, 48 hrs. for Δ7/AAA), detailed in Table 4-1. Representative plaque assays shown are all at 10^{-6} dilution.

Drug	Virus titer (PFU/mL)		
	vEC9	Δ7	AAA
DMSO	1.1×10^9	1.0×10^8	4.0×10^8
Rapamycin	6.9×10^9	2.1×10^8	4.0×10^8
LY294002	1.9×10^8	2.1×10^5	2.4×10^7
Wortmannin	1.3×10^9	6.3×10^7	1.2×10^8

Table 4-1: Drug effects on viral titers. Virus titers for drug treatments (PFU/mL) from experiment in Figure 4-5. Titers were determined from a weighted average of dilutions containing between 10-100 plaques.

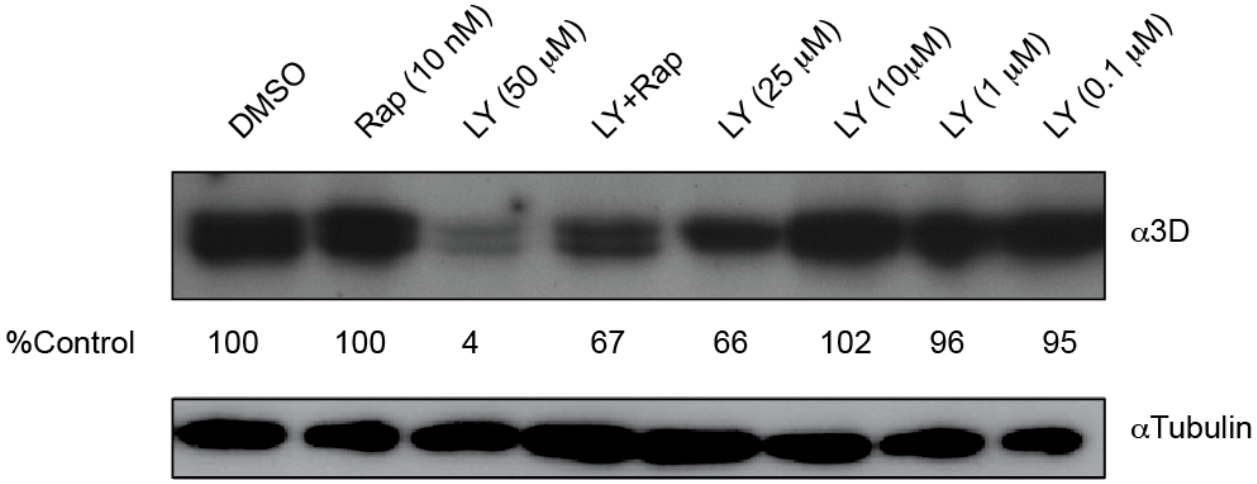

Figure 4-6: Dose dependence of LY294002 on EMCV translation and rescue by rapamycin. HeLa cells were pre-treated with rapamycin (Rap) or LY294002 (LY) at indicated concentrations for 1 hr. Cells were then infected with vEC9 for 3.5 hours, followed by analysis with western blot against EMCV 3D and tubulin. Band intensity was measured in ImageQuant and normalized to tubulin and DMSO control.

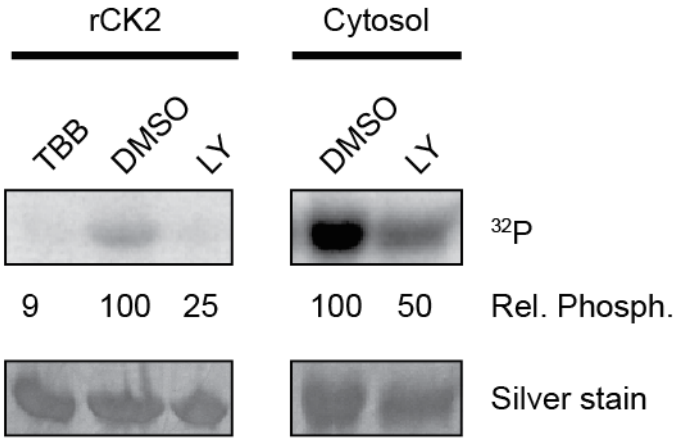

Figure 4-7: LY inhibition of L phosphorylation. GST-L was incubated either with recombinant CK2 (New England Biolabs, left panel) or HeLa cytosol (right panel) pre-treated for 1 hr with TBB (CK2-specific inhibitor), LY, or DMSO control. Gamma-labeled ^{32}P ATP was added and reactions were incubated for 45 minutes. GST-L was concentrated by glutathione-sepharose bead pull-down and analyzed by SDS-PAGE followed by silver stain and phosphorscreen. Band intensity was measured in ImageQuant and normalized to protein input.

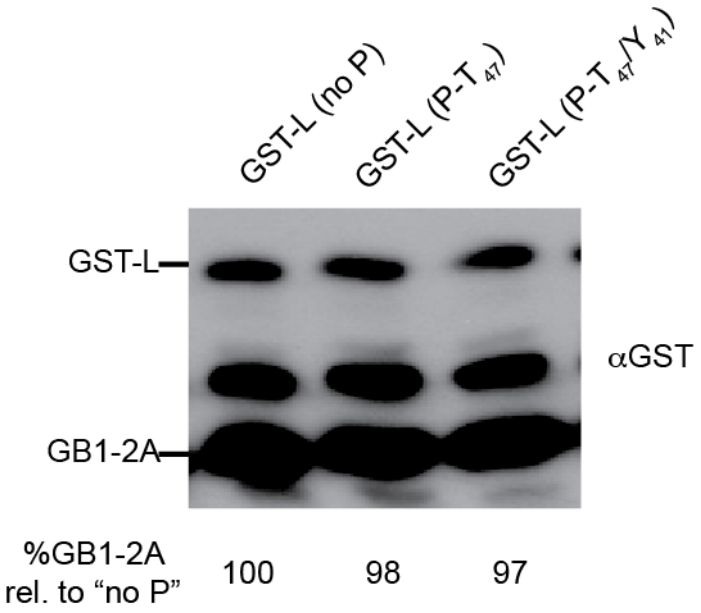

Figure 4-8: Phosphorylation of L does not affect 2A binding. GST-L was pre-incubated with either no kinase, CK2, or CK2 and SYK with ATP to phosphorylate T47 and Y41 (respectively). GST-L (50 nM) were then incubated with hGB1-2A (50 nM) in GST binding buffer for 1 hour followed by incubation with glutathione sepharose beads. Beads were washed (5x) followed by SDS-PAGE and western blot using αGST primary and HRP-linked α-mouse secondary. Band intensity was measured by ImageQuant and compared to non-phosphorylated GST-L.

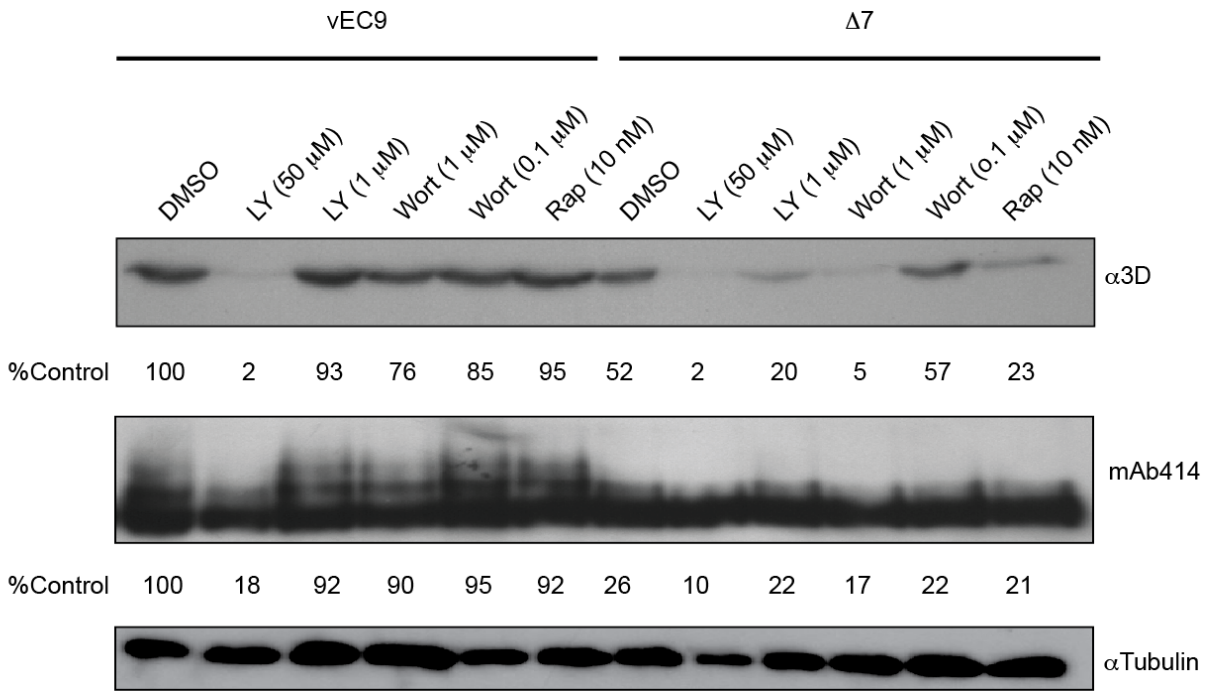

Figure 4-9: Wortmannin inhibits Δ7 mutant virus. HeLa cells were pre-treated with Rap, LY, or Wortmannin (Wort) at indicated concentrations for 1 hr. Cells were then infected with EC9 or Δ7 (MOI=30) for 3.5 hours, followed by analysis with western blot with EMCV 3D, mAb414, and tubulin primary mAbs and HRP-linked α-mouse secondary mAbs. Band intensity was measured in ImageQuant and normalized to tubulin and DMSO control.

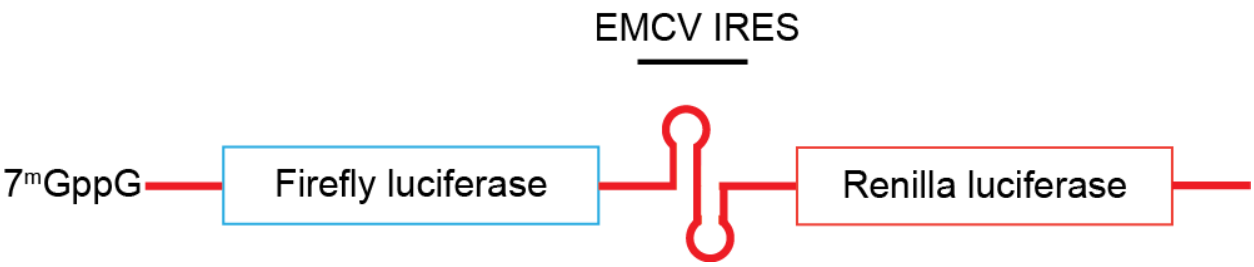

Figure 4-10: Schematic of pF/R construct. The pF/R RNA is shown. Firefly luciferase is expressed from a capped RNA and Renilla luciferase is expressed from an EMCV IRES on the same RNA.

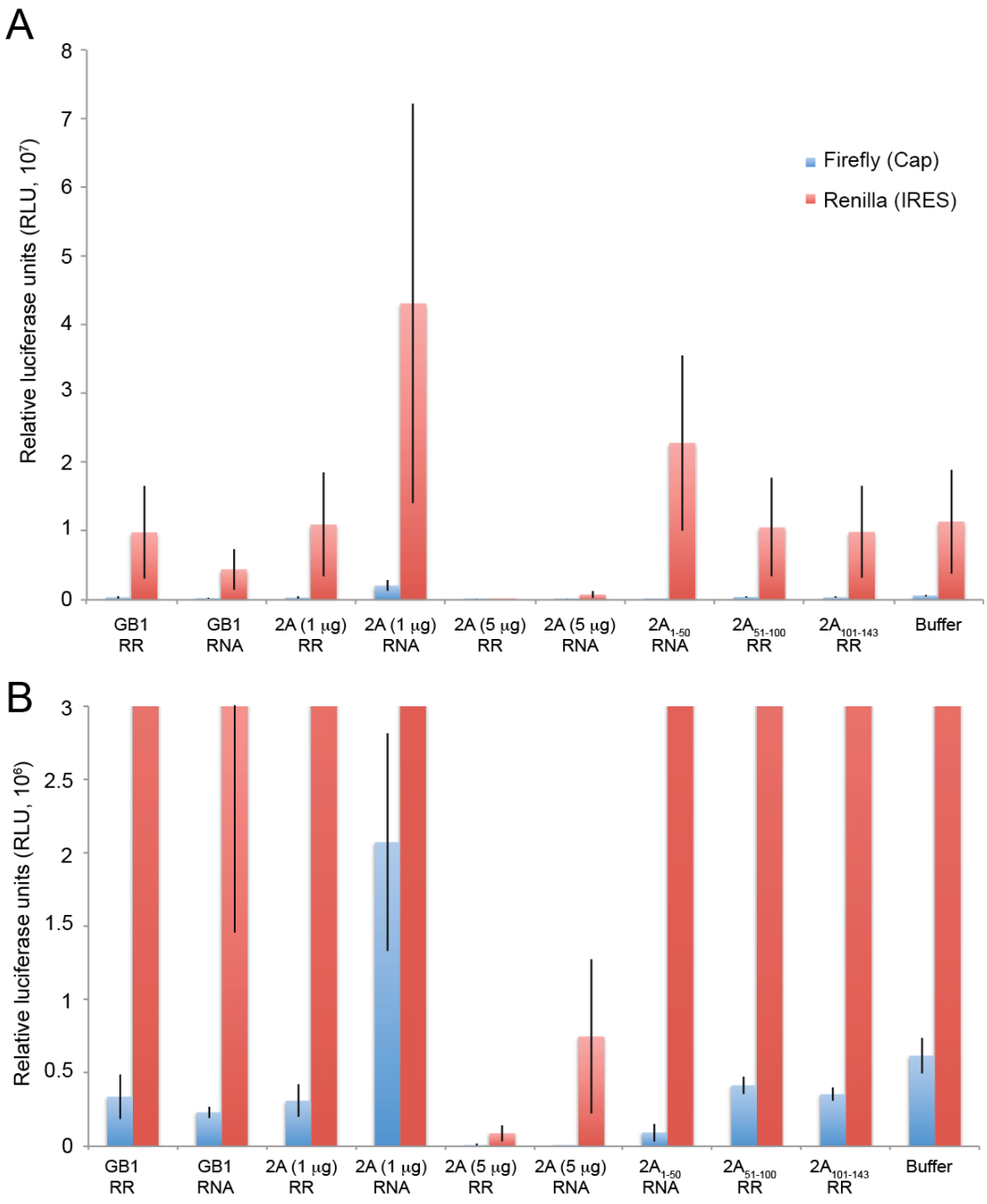

Figure 4-11: 2A induces shutdown of translation. A) Recombinant hGB1-2A and truncations (5 μg, unless indicated) were premixed with either pF/R RNA (RNA) or rabbit reticulocyte lysates (RR) for one hour at 37°C. RR or RNA (respectively) was then added, along with amino acids, and reaction was incubated for 90 minutes. Firefly and Renilla luciferase expression was then measured (Dual Luciferase Assay, Promega). Reactions were performed in triplicate with error bars shown. B) The bar graph in A has been resized to show the comparison of cap expression.

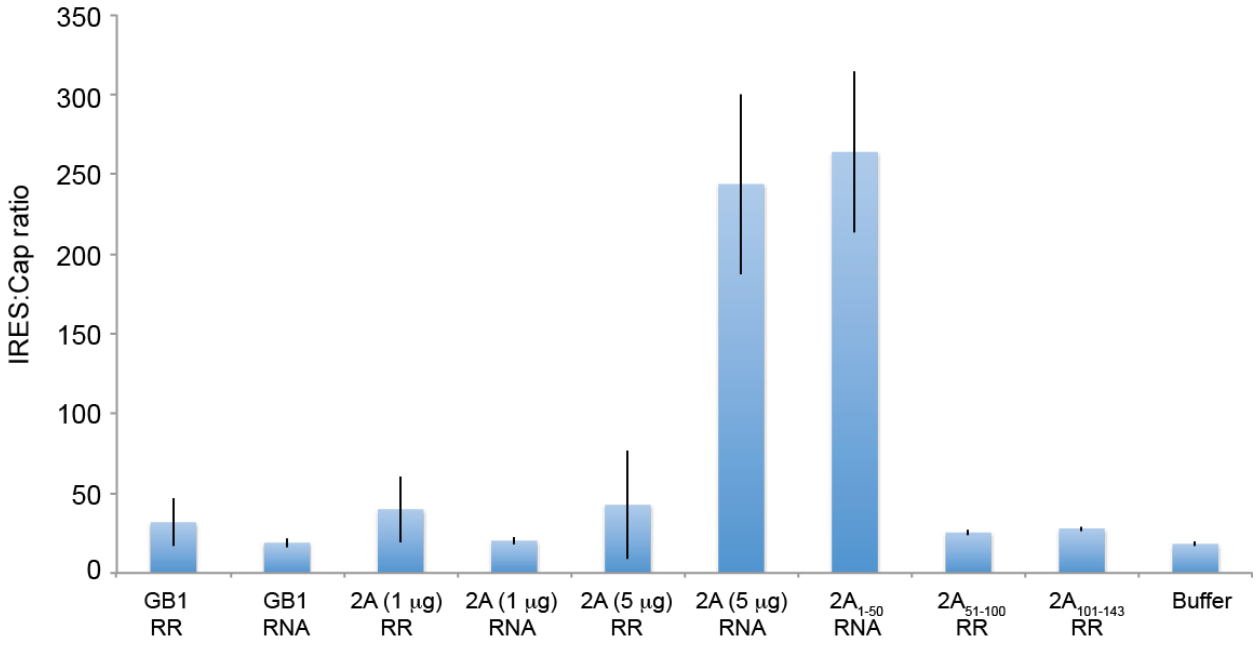

Figure 4-12: 2A enhances the IRES:Cap ratio of pF/R translation. Individual Renilla and Firefly RLU values from reactions in Fig. 4-10 were divided to produce a ratio of IRES:Cap translation.

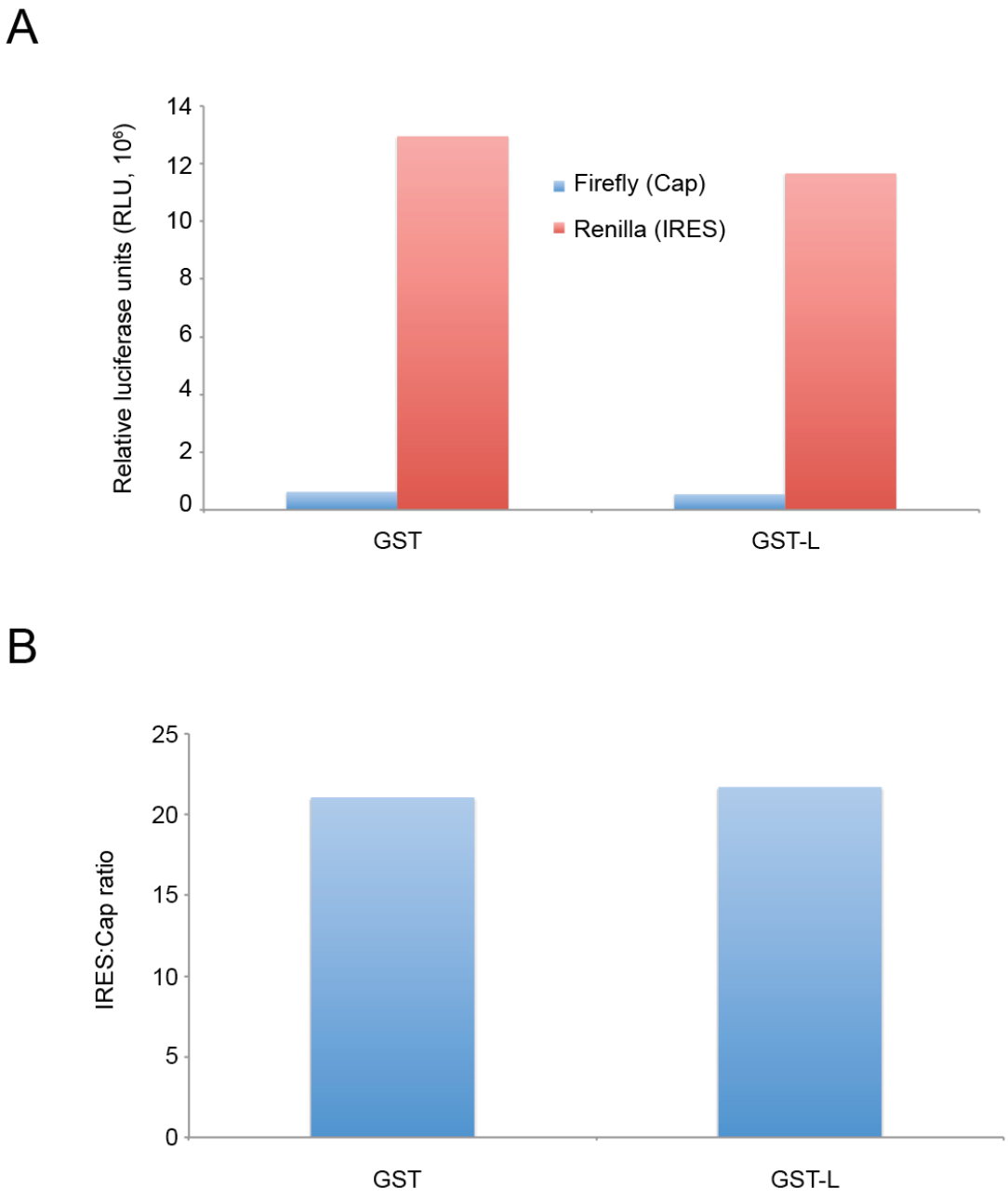

Figure 4-13: L does not directly affect translation. A) GST or GST-L (5 mg) was reacted in similar conditions to Figure 4-10. B) IRES:Cap ratios were determined as in Figure 4-11.

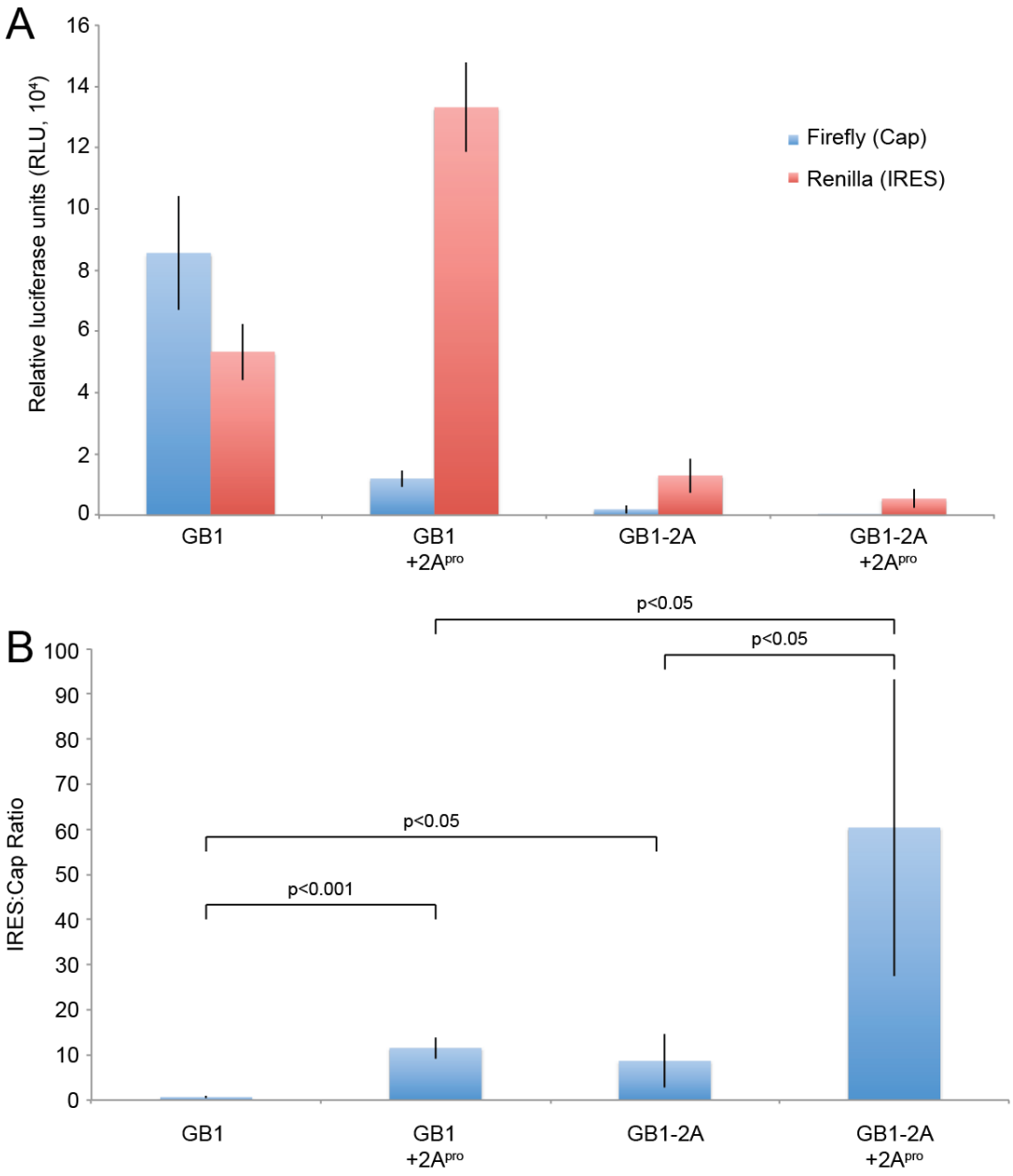

Figure 4-14: RV 2A^{pro} and eIF4G cleavage enhance EMCV IRES translation. A) hGB1 or hGB1-2A was incubated with RNA while RRs were incubated with or without RV-A16 2A^{pro} for one hour at 37°C. Samples were combined for 1.5 hrs and assayed (Dual-Glo Luciferase Assay, Promega) for Firefly and Renilla luciferase expression. This assay uses different substrates, which results in lower raw RLU values for Renilla luciferase compared to Figure 4-10. B) IRES:Cap ratios were determined as in Figure 4-11. Statistical analyses used the Student T-test for determining significance.

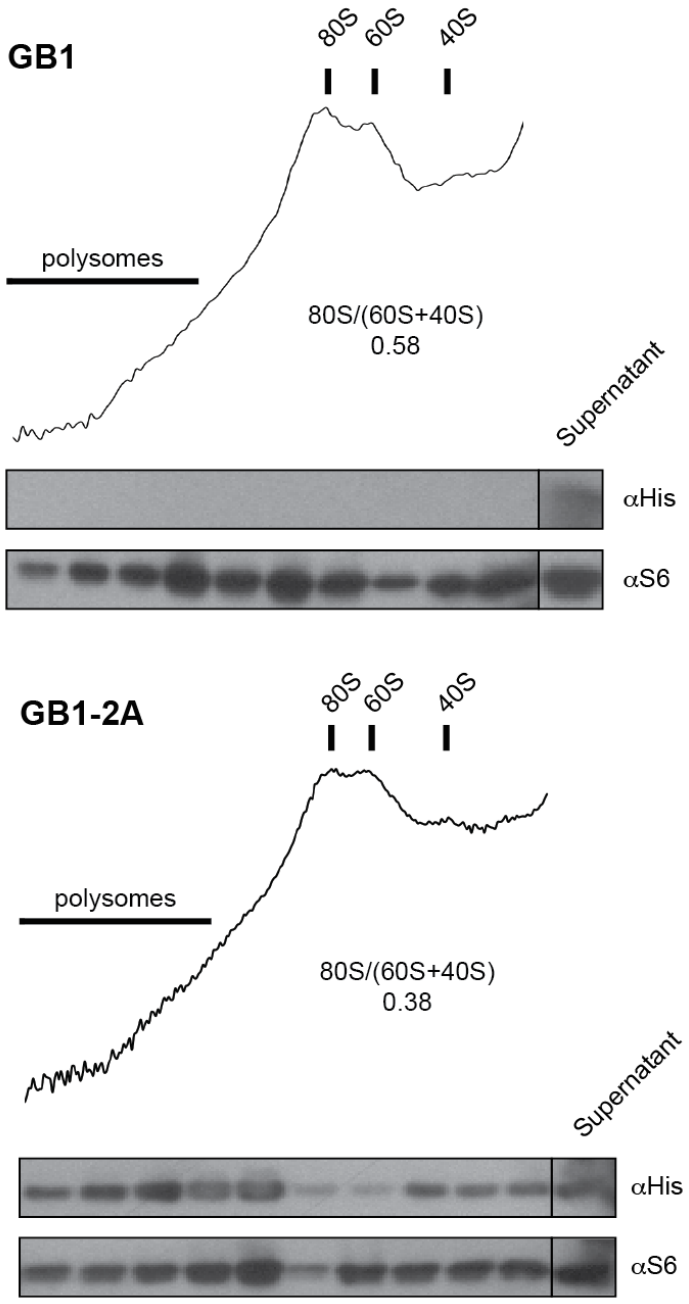

Figure 4-15: 2A impacts ribosome populations. hGB1 or hGB1-2A (100 µg) was incubated with HeLa cytosol (1 mL) supplemented with 500 mM KCl for 1hr at 37°C followed by centrifugation on a 15-45% sucrose gradient. Samples were fractionated from the bottom (left) and measured by absorbance (280 nm). Fractions were precipitated and analyzed by western blot using αHis (hGB1 tag) and αS6 primary mAbs. Peak ratios were determined by summation in Excel.

Chapter 5

Summary and future directions

Chapter 2: Guanine-nucleotide exchange factor RCC1 facilitates a tight binding between EMCV Leader and cellular Ran GTPase

- GDP and GTP inhibit L:Ran binding, RCC1 can rescue this inhibition
- L affects the nucleotide binding pocket of Ran
- RCC1 promotes rapid L:Ran binding
- L:Ran bind with a K_D of 3 nM

Chapter 3: Binding interactions between the encephalomyocarditis virus Leader and protein 2A

- L binds 2A, conserved among Cardioviruses
- First 50 amino acids of 2A is sufficient for binding L
- L:2A bind with a KD of 1.5 μM
- The central hinge region of L, including Y41 and W40A are important to 2A binding
- L, Ran, and 2A can all bind simultaneously
- 2A can block phosphorylation of L on residue Y41 by SYK

Chapter 4: 2A alters translational complexes to promote IRES-driven translation

- 2A mutant viruses show reduced viral translation and Nup phosphorylation
- Rapamycin enhances EMCV translation and virus production
- PI3K inhibitor LY294002 dramatically reduces mutant 2A translation and prevents CK2-dependent phosphorylation of L
- L phosphorylation does not affect L:2A binding
- PI3K inhibitor Wortmannin reduces mutant 2A translation
- 2A directly inhibits translation and shifts components towards IRES translation
- First 50 amino acids of 2A is sufficient for shifting towards IRES, but not inducing a general translation shutdown
- This shift towards IRES involves 2A binding of RNA
- Preventing eIF4E:4G interaction enhances 2A effects on translation
- 2A generates unstable 80S ribosomes

Cardioviruses modulate the host cell primarily through the L and 2A proteins (60, 61, 71, 73, 80). The ultimate activity of L appears to be the hyperphosphorylation of Nups which results in a rapid cessation of active nucleocytoplasmic trafficking (8). The removal of active NCT from the cell debilitates the antiviral response by both preventing pro-interferon transcription factors from localizing to the nucleus and preventing mRNAs for antiviral proteins from exiting the nucleus (69, 71, 93). L induces activation of kinases in the MAPK pathway, primarily p38 and ERK1/2 (60). The mechanism of this activation was poorly understood, but appeared to require the involvement of the small, NCT-regulatory GTPase Ran (9). Protein 2A has also been shown to be an important anti-host factor for cardioviruses (142). The mechanism by which 2A induces a general shutdown of translation in the cell, however, has been rather muddied, though it appears to involve 2A's ability to localize to the nucleolus, bind to eIF4E, and incorporate into nascent 40S ribosomes (61, 80). Here, we sought to further elucidate the mechanisms and host factors responsible for the potent anti-host activities of the Cardiovirus L and 2A proteins.

The study of L:Ran binding on the kinase-inducing activities of L required the efficient formation of a recombinant L:Ran complex for *in vitro* studies. Previous attempts were unable to saturate this reaction, possibly indicating the requirement of another factor. We showed that RCC1, the RanGEF, was required for this reaction, especially in a cellular context rich in guanosine nucleotides (Chapter 2). We then showed that L had an additional binding partner, the viral 2A protein. This binding was conserved across Cardiovirus species/strains and the required regions of L and 2A for this binding were mapped (Chapter 3). We then examined the role of 2A in host cell

control using 2A mutant viruses and kinase inhibitors, revealing an impact of the PI3K/mTOR pathway on virus translation and subsequent virion production. In addition we showed that 2A has a direct effect on translation, and that this activity likely involves eIF4E (Chapter 4).

A strong complement to the *in vitro* biochemical assays detailing L:Ran interactions would be to resolve the structure of L bound to Ran. As L:Ran bind to only ~30% saturation in solution alone, an additional chemical or biological factor was required to push this reaction to completion. We showed that recombinant RCC1 was able to efficiently fill this role. The use of RCC1 has several practical implications and applications. As RCC1 is exclusively a nuclear protein, this implied that L had a nuclear portion to its life cycle. Previous studies using Flag-tagged L revealed that L localized to punctate foci along the nuclear rim (9). These studies were unable to resolve if L was on the nuclear, cytoplasmic, or both sides of the nuclear envelope, or was specifically co-localized with the NPC. RCC1 is normally found in the nucleus bound to nucleosomes on chromatin, though these complexes are concentrated around the nuclear pores (143, 144). Importantly, the discovery that RCC1 efficiently promoted L:Ran binding helped to resolve the L:Ran structure by NMR (63). The structures for L bound to Ran and vice versa were solved and modeled onto one another (Fig 1-5). The low K_D with which L:Ran bind would have required substantial residue contacts between the two proteins, and indeed this was found to be true. The C-terminal tail of Ran wraps around and clamps the hinge domain of L into a locked position, however both the N and C-terminus of L are free to bind additional partners. When this conformation is modeled onto the solved structure of Ran and RCC1 (145), the interface upon which L binds is

wide open (Fig 5-2), supporting the *in vivo* prediction of RCC1 as a required cellular cofactor to L activity. One test for this would be to use the temperature sensitive RCC1 mutant BHK cell line, tsBN2 (146). At higher temperatures, the RCC1 protein is misfolded and degraded, which results in a cessation of Ran cycling and subsequent shutdown of active NCT. The shutdown of active Ran cycling may have additional consequences, however, which could make interpreting results difficult.

The implication of a nuclear lifecycle for L and the rapidity with which L shuts down NCT during infection implied active targeting of L to the nucleus. L lacks a NLS, though the 2A protein does contain one (80). We showed that these viral proteins do indeed bind one another using pull-downs. The first 50 amino acids of 2A were both necessary and sufficient for this binding. Likewise we mapped several residues in the hinge region of L that contributed to this binding through mutagenesis and phosphorylation assays. While 2A can be visualized in cells either through GFP labeling or immunofluorescence, L is very difficult to image, even when Flag-tagged (9, 80). Such co-localization, either by direct imaging (immunofluorescence or immuno-gold electron microscopy) or through fluorescence resonance energy transfer (FRET) would provide more definitive *in vivo* data detailing the L:2A interaction.

Finally, we examined the role of 2A in the shutdown of cap-dependent translation. We showed that the deletion of the NLS from 2A has dramatic effects on both viral translation and titers. It is curious that deletion of a small set of amino acids, far from the primary cleavage cassette, would disrupt cleavage by $3C^{pro}$ (80). When the NLS was mutated to alanines, no such abrogation of cleavage occurred, though translation was still reduced. One possible explanation is that the folding of the P1

region requires an L:2A interaction. It may not be coincidence that L and 2A are the first proteins cleaved from the L-P1-2A precursor, despite being on opposite ends of the polyprotein (25). It would be interesting to see if an unrelated dimer (such as a leucine zipper) situated on either end of the P1 region would be capable of restoring proper processing by $3C^{pro}$.

Ideally, a structure of 2A by either x-ray crystallography or NMR would reveal a plethora of information regarding its function and interaction partners. Previous attempts at generating a crystal structure have failed, as 2A is insoluble at the high concentrations required for crystallographic study. NMR may present a better solution to this problem, since the concentrations required are lower than that of crystallography and 2A is a relatively small protein (<25kDa is the ideal size for NMR). A modeled structure of L:2A generated similarly to L:Ran would be even more revealing (63). We submitted the amino acid sequence of EMCV 2A to I-TASSER, a structure prediction algorithm (147-149); however, due to the low sequence similarity of 2A with any protein for which a structure exists, the confidence in a *de novo* folding to generate a model was statistically low.

Next, we examined the role of the PI3K/mTOR pathway on EMCV 2A mutants. Rapamycin, an mTOR inhibitor, was able to both enhance viral translation and rescue the inhibition caused by the PI3K (and inadvertently, CK2) inhibitor, LY294002. mTOR has a handful of downstream targets including p70S6K and 4EBP1 which both modulate translation in the cell. There have been conflicting reports of 4EBP1 phosphorylation during EMCV infection (80, 123). Interestingly, both eIF4E and p70S6K are phosphorylated in an ERK-dependent manner during EMCV infection (unpublished,

FW Porter). While 2A may not have a direct effect on these kinases, as ERK is activated instead by L, 2A does indeed have a direct effect on translation (61). We observed that recombinant 2A induces a general shutdown of translation, but more heavily represses cap-dependent over IRES-driven translation, leading to an overall shift in favor of the IRES. The first 50 amino acids of 2A were sufficient to induce the shift towards the IRES but were insufficient for shutting down translation to the degree of full-length 2A. Removing active eIF4E (via 4G cleavage by RV-A16 $2A^{pro}$) was similarly able to replicate the shift towards IRES-driven translation and this effect was enhanced further in the presence of EMCV 2A. $2A_{1-50}$ contains the RNA-binding domain (unpublished) whereas the eIF4E-binding site is located in the C-terminal region of 2A (80). These data combined imply that both the RNA- and eIF4E-binding region may function in tandem to modulate host translation in a manner seen with the full-length protein.

While 2A predominantly localizes to the nucleolus during infection, there is also considerable 2A in the cytoplasm (61, 80). It may be that 2A specifically targets capped mRNAs in the cytoplasm (by binding eIF4E) and tightly binds them through the RNA-binding domain. This could have the net result of inhibiting 80S formation upon those mRNAs, stalling the complex at the 40S stage (Fig 5-3). The substantial decrease in IRES (though less so than cap) translation observed here and previously may be more due to the fact that these experiments are carried out in lysates, devoid of proper cellular localization. It would be beneficial to show that eIF4E and 2A can co-localize in cells and to see if this complex also co-localizes with factors of the 40S ribosome.

The role of 2A in the nucleolus remains a mystery. 2A has been shown to affect rRNA processing (unpublished, RR Groppo) and is implicated in the inhibition of Pol-II transcription (83). The nucleolar-localization of 2A may serve as a means of redundancy for the virus, targeting cellular mRNAs at the transcriptional (nucleolus) *and* translational (cytoplasm) level. While 2A has been shown to bind RNA in a seemingly non-specific manner (unpublished, BA Brown), it may still be useful to do a pull-down of recombinant 2A from uninfected and infected lysates and compare, through deep sequencing, the RNAs with which 2A dominantly interacts. Further examination of 2A may help to better resolve the structure and function of the nucleolus as well as dissect the complex and dynamic mechanism of translation initiation.

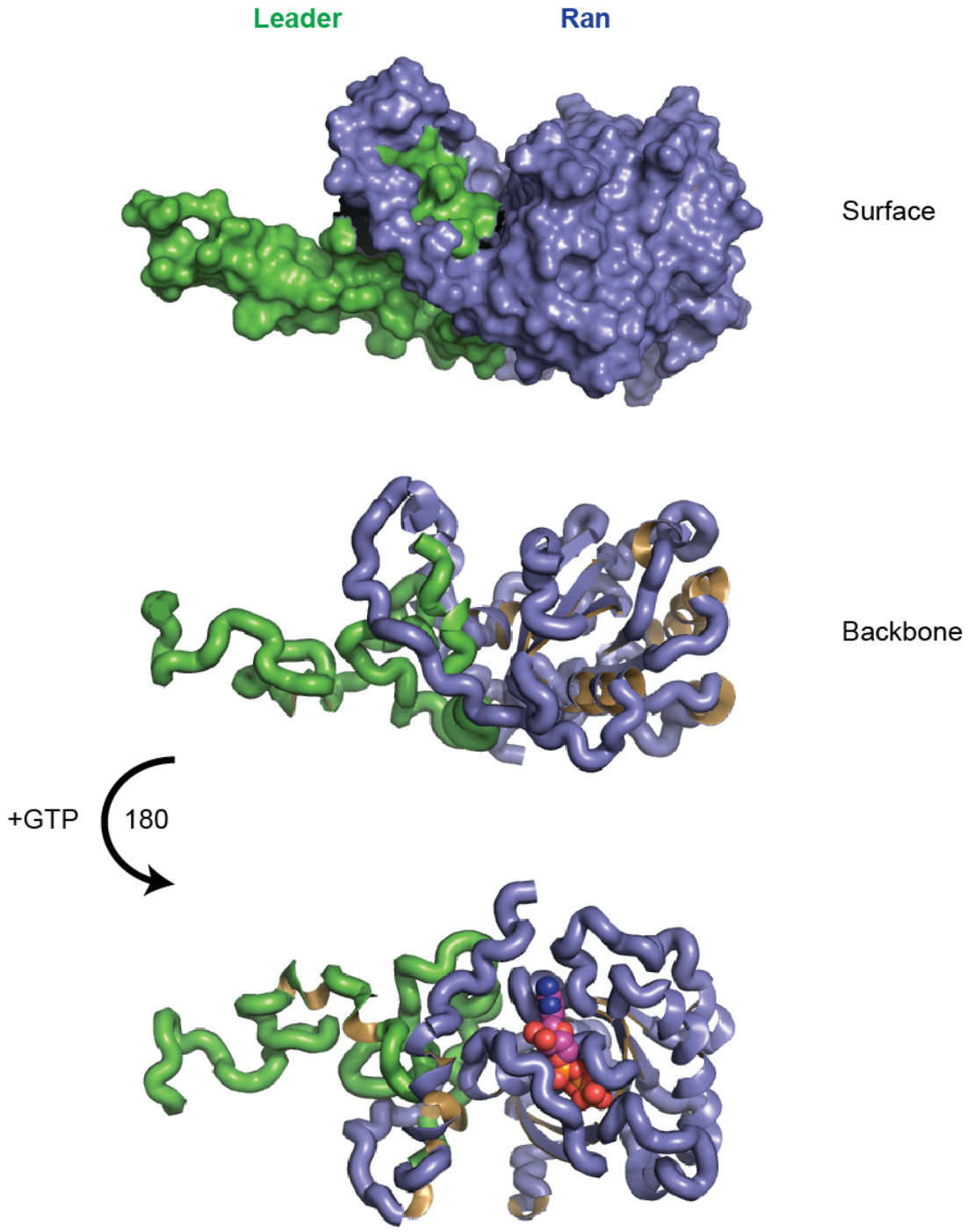

Figure 5-1: Model of L:Ran. The solution structures of L and Ran (PDB: 2MMH [green] and 2MMG [blue]) were docked using HADDOCK (performed by Ann Palmenberg) and displayed in Pymol. The C-terminal tail of Ran wraps around L in the surface (top) and backbone (middle) representation. The model is horizontally rotated 180° and GTP is modeled into the nucleotide-binding pocket (bottom).

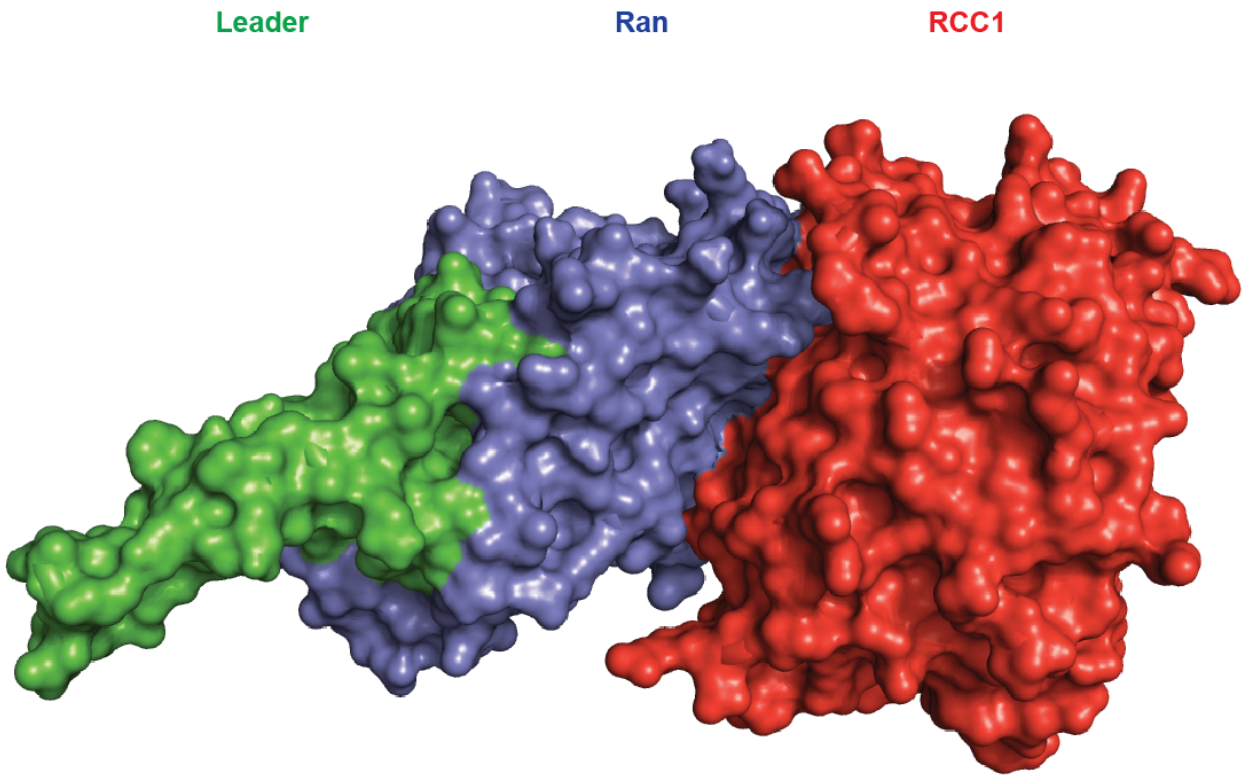

Figure 5-2: Model of L:Ran:RCC1. The model of L:Ran from Figure 5-1 was used to replace the Ran structure, as bound to RCC1 (red, PDB: 1I2M).

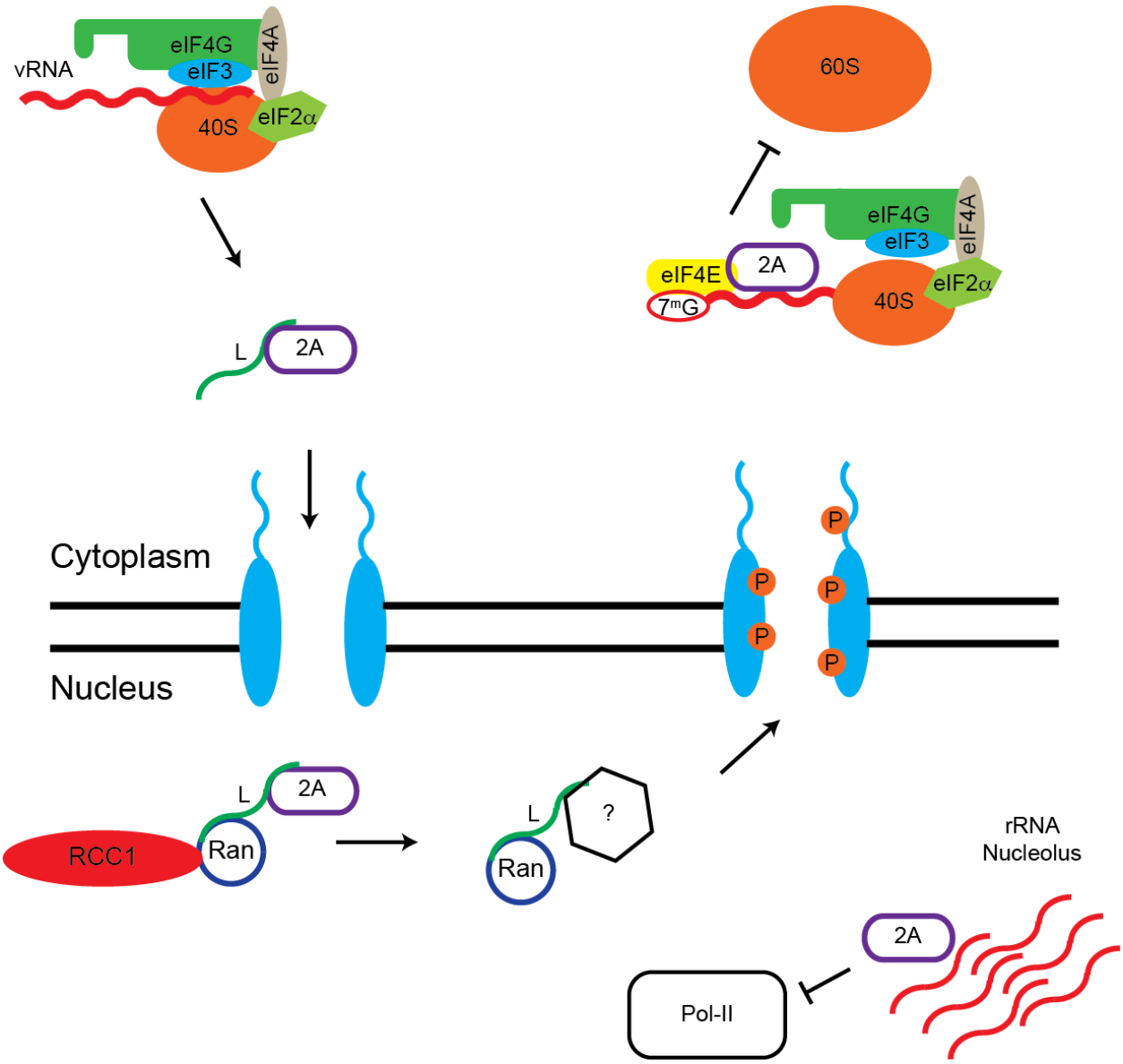

Figure 5-3: Proposed model of L:2A functions during infection. L and 2A are released from the polyprotein by $3C^{pro}$ and travel to the nucleus. In the nucleus, 2A is displaced from L by Ran or an additional factor. The L:Ran complex returns to the NPC and induces hyperphosphorylation of Nups via cellular kinases. 2A localizes to the nucleolus to inhibit rRNA processing and Pol-II transcription or egresses to the cytoplasm to inhibit cap-dependent translation.

Appendix

Comparison of ICAM-1 binding to major group rhinoviruses via modified ELISA

Experiments in Figure A1 were designed by Ryan Petty and Kazuyuki Nakagome and performed by Kazuyuki Nakagome and Rebecca Brockman-Schneider. Roadmaps in Figure A3 were developed by Jean-Yves Sgro.

Abstract

Viruses have evolved a variety of mechanisms to bind cell-surface receptors and enter host cells. This first step, entry, is one of the most highly targeted for anti-viral therapies. Rhinoviruses (RVs) are one of the most ubiquitous human pathogens as the causative agent of the common cold and have been linked to asthma exacerbations and pneumonia. Major group RVs use the receptor ICAM-1 for entry into epithelial cells of the upper and lower respiratory tract. With over 150 identified strains (and counting) of RVs, it is surprising that virus-receptor interactions have only been studied for a very small subset of RVs. We have developed a modified ELISA assay to determine the equilibrium dissociation constants (K_D) for six major-group RV strains (A7, A16, A36, B6, 52, and B72). The highest affinity virus, A16, had a K_D of 130 nM whereas the lowest affinity virus tested, A36, had a K_D of 760 nM. We then identified several key

ICAM-1 contact residues in A16 VP1, namely residues T_{153}, Y_{202}, and K_{203}, which sit at the periphery of the RV:ICAM-1 interface and may contribute to this variety in K_D. These substantial differences could influence pathogenicity among RV strains and species and/or the number of virions required to initiate an infection. Additionally, this new method can allow for high-throughput cell-free assays, measuring RV:ICAM-1 interactions under a variety of conditions.

Introduction

Rhinovirus (RV) infection is the primary cause of the common cold, and has been linked to more severe illnesses such as asthma exacerbation and pneumonia (150-152). RVs are positive-sense, single-stranded RNA Enteroviruses in the *Picornaviridae* family consisting of three distinct species, RV-A, -B, and -C, further divided into over 150 identified strains (153).

The first step in the RV lifecycle is viral attachment to the cell surface. RV-A and -B have two recognized cell surface receptors (RV-C receptor is yet unknown); “Major” group RVs bind Intracellular Adhesion Molecule-1 (ICAM-1) (154, 155), whereas “Minor” group RVs bind Low Density Lipoprotein (LDL) receptors (156). The binding of major group RVs to ICAM-1 has been detailed previously (157-159). While these studies are highly informative, the landscape of RV:ICAM-1 interactions and variations among RV types remains poorly understood. Surface plasmon resonance (SPR) can be used to examine virus association and dissociation rates; however, this method has two

limitations with respect to RVs. First, the initial attachment step that conjugates virus to the surface must occur in an acidic buffer (sodium acetate, pH ~5-6) to which RVs are highly sensitive. Second, the procedure is time-intensive and cannot easily test multiple conditions (e.g. pH, salt, drug) or RV species in parallel.

Given the wide variety of symptoms induced by different RV species (151), there are likely numerous viral and host determinants for pathogenicity of any specific RV. We sought to determine if major group RV species have differing affinities for ICAM-1 and if these differences correlate with species- or strain-specific differences in pathogenicity. We developed an ELISA-based assay adapted from similar experiments that measured the equilibrium affinities for antibodies targeting viruses or individual proteins (160, 161) and tested six rhinovirus strains (A7, A16, A36, B6, B52, and B72) for ICAM-1 affinities.

Materials and Methods

RV production:

RV-A16 is a clinical isolate that was cloned and provided by Dr. Wai-Ming Lee (Biological Mimetic Inc.). RV-B52, RV-B72 and RV-A36 are clinical isolates that were cloned previously (162), and the RV-A1 clone was kindly provided by Dr. William Kelly (Medical College of Wisconsin). All isolates were obtained from nasal secretion samples of infants participating in a birth cohort in 1998–2001 (151). Viruses were produced by transfecting viral RNA into WisL or Hela cells as previously described (162-164). After three freeze and thaw cycles, the cell lysate was treated with RNase A (10 μg/ml,

Qiagen, Valencia, CA) for 10 minutes at room temperature to remove free RNA (cellular, input, and unpackaged). The viruses were purified by pelleting through a 30% sucrose cushion (40,000 rpm, 16°C, 2 hours). Pelleted virus was resuspended in PBS and stored at −80°C. RV-A7 and RV-B6 are also clinical isolates that were produced by inoculating nasal secretions into WisL or Hela cells, as previously described (162, 165, 166) and purified using the same protocol used with the cloned viruses except for RNase A treatment.

RV RNA concentrations were determined by qRT-PCR as previously described (162-164). The University of Wisconsin Human Subjects Committee approved the protocol and informed consent was obtained from the patients' families.

Equilibrium measurements of ICAM-1 affinity:

96-well ELISA plates (Costar, Corning Inc., Corning, NY) were coated with 10^8 RNA-copies of virus in 50 µL reactions (Tris, pH 7.5) for 1 hr. Wells were washed three times (PBS with 0.05% v/v Tween-20, pH 7.4) then blocked with wash buffer supplemented with 3% (w/v) BSA for 1 hr. Wells were washed again three times in wash buffer. Human ICAM-1-Fc fusion protein (R&D Systems, Minneapolis, MN) was added to wells at a final concentration of 0, 1.25, 2.5, 5, 7.5, 10, 15, 20, and 40 µg/mL in 50 µL of wash buffer with 1% BSA for 4 hrs. Wells were washed 5 times in wash buffer followed by addition of HRP-linked anti-human IgG (Jackson ImmunoResearch Laboratories, West Grove, PA, 50 µL, 1/5,000 dilution) for 1 hr. Wells were washed 7 times in wash buffer then exposed to TMB substrate (SureBlue, KPL, Gaithersburg, MD,

100 uL) for 30 mins. Luminescence was measured at OD 450 nM on a Multiskan Ascent (Thermo Scientific).

Determination of RV:ICAM-1 affinity:

Data were plotted in Excel and normalized by subtracting the OD_{450} in the absence of sICAM-1-Fc for each virus. Analysis of the data was adapted from methods previously described (160, 161). In summary, fluorescence intensity at 40 µg/mL ICAM-1-Fc was selected as the saturation concentration (F_{max}) and the ratio of fluorescence intensity at each sICAM-1-Fc concentration (F_x) over F_{max} yielded "i" for each ICAM-1-F_c initial concentration (C_0). Data were linearized by plotting 1/(1-i) vs. C_0/i; for which the inverse of the slope of the best-fit line (determined by LINEST function in Excel) is the dissociation constant K_D. The second highest ICAM-1 concentration, 20 µg/mL, was not included in the data is it often approached the saturation value and heavily skewed the linearized data.

Sequence analysis of RV:ICAM contact residues:

Sequences for VP1 of selected viruses were aligned as described (153, 167) using all publicly available sequences. RV VP1 residues that make contact with ICAM-1 were selected (163). Roadmaps of RV:ICAM-1 contact residues were generated on the surface of RV A16 (PDB: 1AYM) and B14 (PDB: 4RHV) as previously described (168).

Results

Measurement of RV:ICAM-1 binding by modified ELISA:

Numerous methods exist for studying protein:protein interactions. We adapted a previously described ELISA assay (160, 161) which measures equilibrium binding of a surface-fixed RV virus to a ICAM-1-Fc fusion protein (Fig A1). We used both a blank surface as well as the minor group (LDL-binding) RV-A1 for controls and found both were below background levels (Table A1). Using RNA-copy equivalent virus and increasing concentrations of ICAM-1-Fc, we found that RV-A16 bound substantially more (~5x) ICAM-1 than did all other RVs tested (Fig A2A). When data were linearized (Fig 2B), we found that best fit lines encompassed the data well (R^2 0.85-0.99) and all fits (based upon F-ratio) were statistically significant ($p<0.01$). The slope of the best-fit line provides the association constant, K_A, that we inversed to provide the dissociation constant, K_D (Table 2).

RV-A16 had the lowest K_D (strongest affinity) at 130 nM while A36 had the highest K_D (weakest affinity) at 760 nM. Of the tested RV strains, RV-B species appeared to be more clustered with K_Ds ranging from 220-360 nM, whereas RV-As were more variable (see above).

Sequence analysis of RV:ICAM-1 contacts residues:

Next we sought to identify any key residues that may be influencing ICAM-1 affinity. We aligned all six RV VP1 sequences and selected only those residues that have been shown to make contact with ICAM-1 (163) (Tables A3 and A4). We

identified three residues in A16 that differed substantially from the consensus RV-A sequence. At position 153, both A7 and A36 contain a hydrophobic residue (isoleucine or valine, respectively) whereas A16 contains a hydrophilic threonine. Similarly, at position 202, both A7 and A36 contain an alanine, whereas A16 contains a tyrosine. Position 203 may reveal the subtleties of ICAM-1 binding though, in that A16 contains a lysine while the second highest affinity RV-A, A7, also contains a hydrophilic residue (serine), whereas the weakest affinity RV-A, A36, contains an alanine. Comparing RV-B species is a bit more difficult as their K_Ds were all relatively similar, and there is no standout virus with regards to sequence. B14, B52, and B72 all contain residues unique from the RV-B consensus sequence of viruses tested.

When these residues are mapped onto the surface of RV-B14 (PDB: 4RHV) or A16 (PDB: 1AYM), an interesting pattern arises. On the surface roadmap of A16 (Fig A3A), the three residues identified above (153, 202, 203) all map on the periphery of ICAM-1 contact, specifically on complete opposite ends of the contact site. The most well conserved residues all map to a central core region. While each tested RV-B strain had at least one residue that differed from the consensus, each one of these residues was invariably located on the periphery of the ICAM-1 contact site (Fig A3B).

Discussion

While much attention has been paid to the ability of neutralizing antibodies to prevent RV:ICAM-1 interactions (157, 169-171), little has been to the species and strain diversity of RV:ICAM-1 interactions. Here we sought to test this diversity and determine

if differences in affinities correlated with changes at the sequence level. We developed a modified ELISA assay to test equilibrium binding between six major-group RV strains, 3 RV-As and 3 RV-Bs.

We observed that RV-A16, one of the most well studied RVs (172-174), had the highest affinity of all six tested RVs (K_D=130 nM) whereas A36 had the lowest affinity (K_D=760 nM). The K_Ds measured agree well with K_Ds determined previously by methods such as SPR; RV-B3, not tested here, was previously found to bind to ICAM-1 with two distinct affinities, a weaker binding site at 12.5 μM and a stronger binding site at 690 nM (158). We did not observe secondary binding sites after linearization of data; however, this may be the result of measuring only the equilibrium binding, and not the individual on and off rates.

Next we analyzed the known VP1 residues that contact ICAM-1 to determine if certain residues correlated with increased affinity. For A16, residues 153, 202, and 203 all had chemical properties that differed from other RV-As tested (i.e. hydrophobic vs. hydrophilic). Interestingly, there was very little consensus among all RV-As sequenced to date in ICAM-1 contact residues as compared to RV-B. This may indicate not only a further diversity among ICAM-1 affinities, but also evolutionary race between the virus, host cell, and host adaptive immune response (as several of these residues are also immunogenic). For RV-B strains, all viruses had at least one residue that differed from the other tested RV-Bs and indeed the B viruses all had more highly clustered K_Ds ranging from 210 to 360 nM. We also observed that for all viruses tested, the residues that differed from the consensus were all localized to the periphery of the ICAM-1 footprint (Fig. A3). It is interesting to note that previously identified drug-resistant

compensatory RV-B14 VP1 mutations (N100S and N105S) (175) are also located on the periphery of the ICAM-1 footprint (see Fig 3B). It may be that natural selection has pushed RVs to conserve a set of residues located at the core of the ICAM-1 footprint to establish a basal level of affinity, whereas diversity exists in the periphery, which results in the differing affinities between RV strains observed here. Many of these periphery residues are located on the "walls" of the canyon into which ICAM-1 binds (176).

These differing affinities in virus:receptor interactions may help to explain the behavior of the virus during clinical infections. There is clinical and experimental evidence that RV species/strain affects viral replication, induction of chemokines, and severity of clinical illness; in each case, RV-Bs had lesser effects than did RV-C or RV-A (151, 162). Our data do not support that RV-B are less virulent because of reduced affinity for ICAM-1. Even so, type-specific differences in K_D could influence virulence within species, as well as variations in the number of virions required to initiate infection and the response to antivirals that block binding of the virus to cellular ICAM-1. Furthermore, this assay provides a simple technique that could be scaled up for high throughput, cell-free screening for compounds that interfere with RV:ICAM-1 binding.

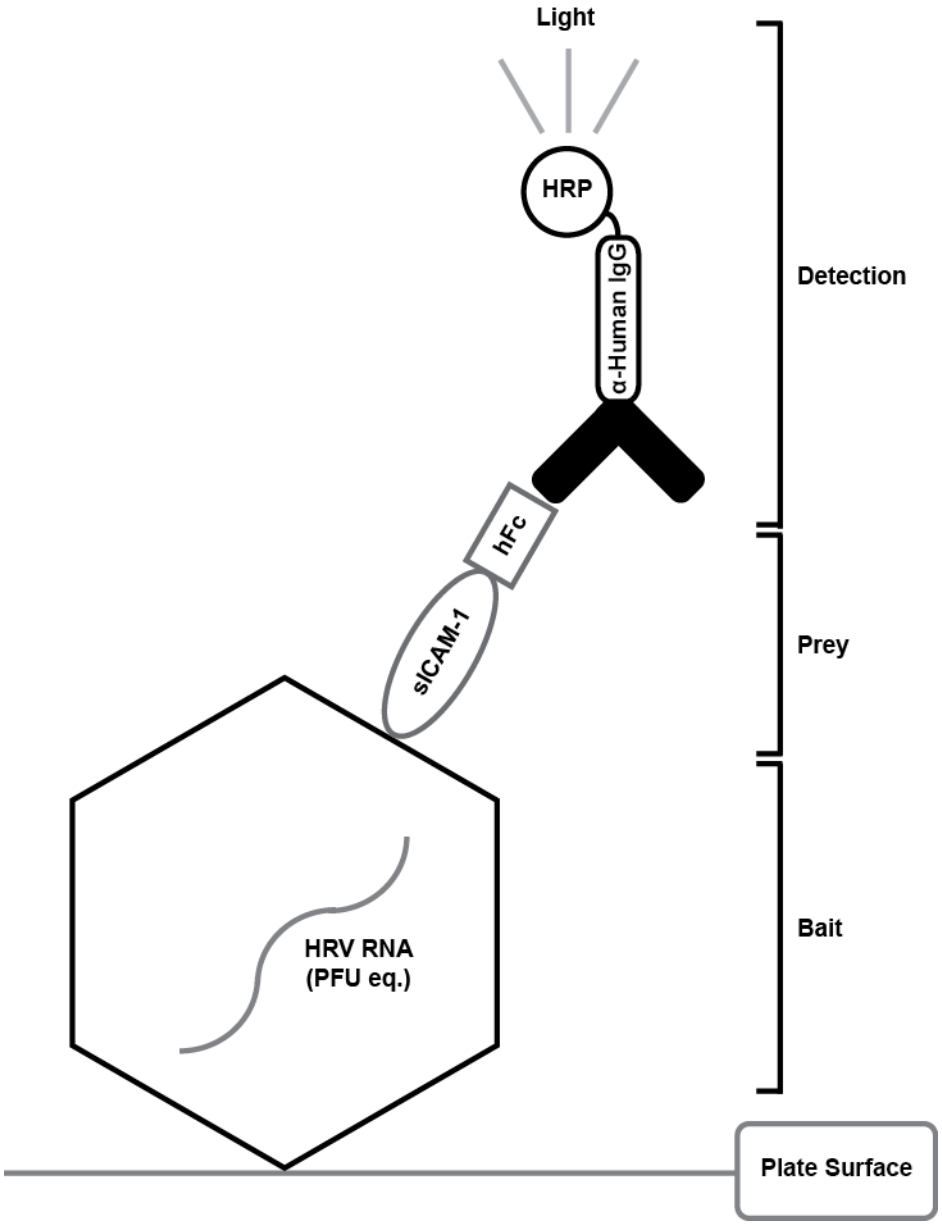

Figure A1: Modified ELISA for measurement of RV:sICAM-1 K_Ds. The experimental setup is shown. RNA genome equivalent virus (10^8 RNA copies/well) was attached to the plate surface as bait. A chimera of soluble ICAM-1 and human IgG Fc fragment was added at varying concentrations as prey (1.25-40 μg/mL). aHuman IgG linked to horseradish peroxidase was used to quantify sICAM bound to RV capsids.

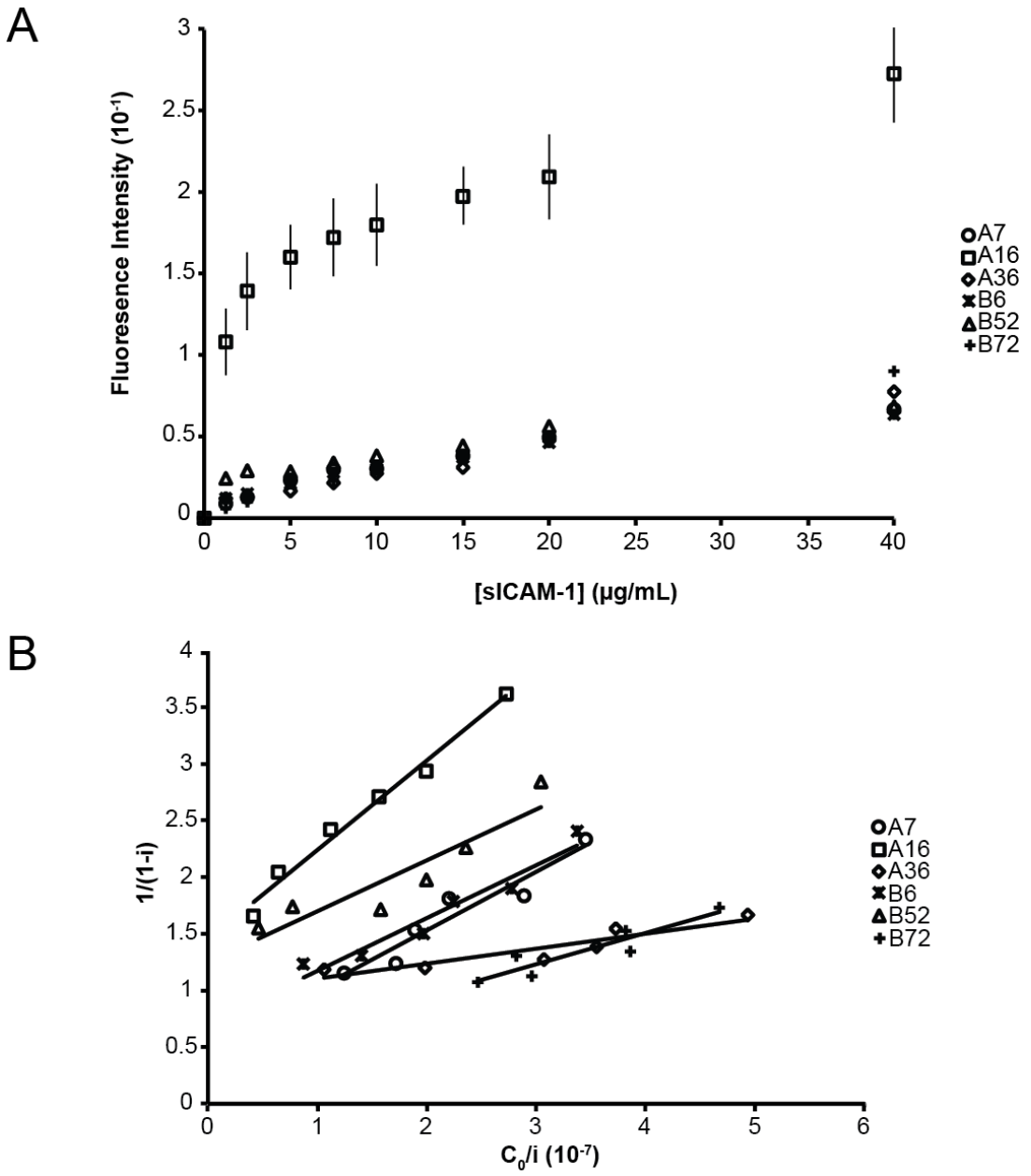

Figure A2: Raw and linearized fluorescence intensities of RV:sICAM-1. A) Fluorescence intensities at varying sICAM-1-Fc concentrations were measured and plotted. Values were normalized by subtracting the fluorescence intensity in the absence of sICAM-1-Fc. Error bars are presented for A16 (n=4), but are omitted due to low error and visual overlap for remaining viruses. B) Data were linearized as described in Materials and Methods. Best-fit lines were determined in Excel and overlaid onto data points. Slopes of the best-fit line were inverted to give the K_D of each RV.

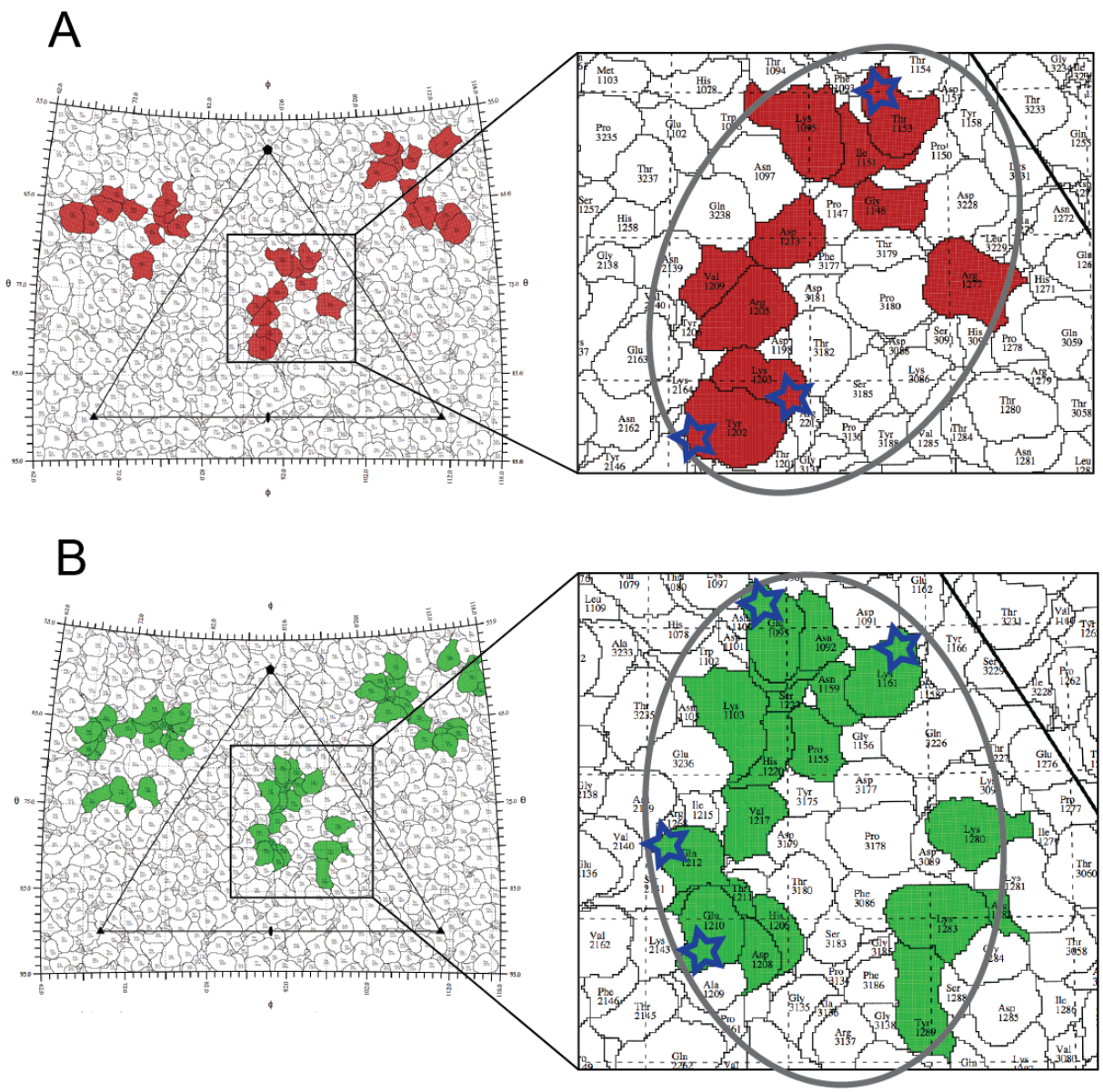

Figure A3: Roadmap of ICAM-1 contact residues in RV-A/B VP1. Roadmaps of the surface of RV-A16 (3A, PDB: 1AYM) and RV-B14 (3B, PDB: 4RHV) are shown. Five-fold (pentagon), three-fold (triangle), and two-fold (ellipse) are indicated. Residues are labeled with the first number representing which VP (1,2, or 3) peptides displayed is the source, followed by the three digit number of the residue in the VP amino acid sequence. Residues of VP1 that make contact with ICAM-1 were colored in red (A16) or green (B14). The ICAM-1 footprint is indicated as a grey oval. VP1 residues that differ from their respective species consensus are indicated with a blue star.

Virus (HRV)	[sICAM-1] (μg/mL)	Raw Fluorescence
A16 (major group)	0 (background)	0.052
	7.5	0.224
A1 (minor group)	7.5	0.050
No virus	7.5	0.051

Table A1: Controls for ELISA. Negative controls using either a blocked surface alone (no virus) or minor group virus (RV-A1) were measured for raw fluorescence and compared to that of A16 in the absence of sICAM-1-Fc (background fluorescence) and at 7.5 μg/mL.

Virus (HRV)	K_D (nM)	Best-fit line R^2	Best-fit line F-ratio
A7	190±30	0.91	42
A16	130±10	0.98	250
A36	760±160	0.84	23
B6	210±30	0.94	60
B52	220±50	0.85	22
B72	360±80	0.85	23

Table A2: RV:ICAM-1 K_Ds and statistical analyses. K_Ds for RV species/strains derived from Fig. 2 are presented. Uncertainty, R^2 value, and F-statistic, are all derived from the best-fit line determined by Excel LINEST function.

VP1 Residue	Consensus	HRV-A7	HRV-A16 (PDB: 1AYM)	HRV-A36
95	*X (T/K)*	T	K	T
148	G	G	G	G
151	*X (I/V)*	V	I	V
153	*X (K/T)*	I	T	V
202	*X (P/T)*	A	Y	A
203	*X (G/D)*	S	K	A
205	*X (R/K)*	K	R	K
209	V	V	V	V
213	D	D	D	D
277	*X (R/K)*	A	R	K

Table A3: Comparison of ICAM-1 contact residues in RV-A VP1. ICAM-1 contacting residues from aligned RV-A VP1 sequences were selected and displayed using single letter amino acid codes. Virus sequence used for RV-A roadmap in Fig 3 is indicated with PDB ID. Consensus sequence is defined as the amino acid that exceeds 51% conservation at a particular residue number. An "*X*" indicates that no amino acid exceeds 51% conservation followed by the two most frequent amino acids in parentheses.

VP1 Residue	Consensus	HRV-B6	HRV-B14 (PDB: 4RHV)	HRV-B52	HRV-B72
92	N	N	N	T	N
94	K	K	R	K	K
95	E	E	E	E	V (*A*)
103	K	K	K	K	K
155	P	P	P	P	P
159	N	N	N	N	N
161	*X (V/K)*	E	K	V	V
206	H	H	H	H	H
208	D	D (*N*)	D	D	D
210	*X (D/N&T)*	D (*N*)	E	N	N (*E*)
211	T	T	T	T	T
212	P	P	Q	Q	P (*Q*)
217	V	V	V	V	V
220	H	H	H	H	H
223	S	S	S	S	S

Table A4: Comparison of ICAM-1 contact residues in RV-B VP1. ICAM-1 contacting residues from aligned RV-B VP1 sequences were selected and displayed using single letter amino acid codes. Virus sequence used for RV-A roadmap in Fig 3 is indicated with PDB ID. Consensus sequence was determined as in Table 3.

References

1. **Svitkin YV, Herdy B, Costa-Mattioli M, Gingras AC, Raught B, Sonenberg N.** 2005. Eukaryotic translation initiation factor 4E availability controls the switch between cap-dependent and internal ribosomal entry site-mediated translation. Mol Cell Biol **25:**10556-10565.
2. **Lee CK, Wimmer E.** 1988. Proteolytic processing of poliovirus polyproteins: Elimination of $2A^{pro}$-mediated, alternative cleavage of polypeptide 3CD by in vitro mutagenesis. Virology **166:**405-414.
3. **Sommergruber W, Zorn M, Blaas D, Fessl F, Volkmann P, Maurer-Fogy I, Pallai PV, Merluzzi VJ, Matteo M, Skern T, Kuechler E.** 1989. Polypeptide 2A of human rhinovirus type 2: identification as a protease and characterization by mutational analysis. Virology **169:**68-77.
4. **Palmenberg AC.** 1989. Cleavage specificity of the EMC 3C proteinase, p. 27-32. *In* Krausslich H-G, Oroszlan S, Wimmer E (ed.), Current Communications in Molecular Biology: Viral Proteinases as Targets for Chemotherapy. Cold Spring Harbor Laboratory Press, Cold Spring Harbor, N.Y.
5. **Blinov VM, Donchenko AP, Gorbalenya AE.** 1985. Internal homology in the primary structure of the poliovirus polyprotein: the possibility of existence of two viral proteinases. Doklady Academii, nauk SSSR **281:**984-987.
6. **Donnelly ML, Luke G, Mehrotra A, Li X, Hughes LE, Gani D, Ryan MD.** 2001. Analysis of the aphthovirus 2A/2B polyprotein 'cleavage' mechanism indicates not a proteolytic reaction, but a novel translational effect: a putative ribosomal 'skip'. J Gen Virol **82:**1013-1025.
7. **Devaney MA, Vakharia VN, Lloyd RE, Ehrenfeld E, Grubman MJ.** 1988. Leader protein of foot-and-mouth disease virus is required for cleavage of the p220 component of the cap-binding protein complex. J. Virol. **62:**4407-4409.
8. **Porter FW, Palmenberg AC.** 2009. Leader-induced phosphorylation of nucleoporins correlates with nuclear trafficking inhibition of cardioviruses. J.Virol **83:**1941-1951.
9. **Porter FW, Bochkov YA, Albee AJ, Wiese C, Palmenberg AC.** 2006. A picornavirus protein interacts with Ran-GTPase and disrupts nucleocytoplasmic transport. Proc.Natl.Acad.Sci.U.S.A **103:**12417-12422
10. **Zhang YZ, Gan X, Song J, Sun P, Song QQ, Li GQ, Sheng LJ, Wang BD, Lu MZ, Li LM, Han J.** 2013. [The 2A protease of enterovirus 71 cleaves nup62 to inhibit nuclear transport]. Bing Du Xue Bao. **29:**421-425.
11. **Watters K, Palmenberg A.** 2011. Differential processing of nuclear pore complex proteins by rhinovirus 2A proteases from different species and serotypes. J.Virol. **85:**10874-10883.
12. **Castello A, Izquierdo JM, Welnowska E, Carrasco L.** 2009. RNA nuclear export is blocked by poliovirus 2A protease and is concomitant with nucleoporin cleavage. J. Cell Science **122:**3799-3809.

13. **Cho MW, Teterina N, Egger D, Bienz K, Ehrenfeld E.** 1994. Membrane rearrangement and vesicle induction by recombinant poliovirus 2C and 2BC in human cells. Virology **202:**129-145.
14. **Tolskaya EA, Romanova LI, Kolesnikova MS, Gmyl AP, Gorbalenya AE, Agol VI.** 1994. Genetic studies on the poliovirus 2C protein an NTPase: A plausible mechanism of guanidine effect on the 2C function and evidence for the importance of 2C oligomerization. J.Mol.Biol. **236:**1310-1323.
15. **Teterina NL, Gorbalenya AE, Egger D, Bienz K, Ehrenfeld E.** 1997. Poliovirus 2C protein determinants of membrane binding and rearrangements in mammalian cells. J.Virol. **71:**8962-8972.
16. **Rodriguez PL, Carrasco L.** 1993. Poliovirus protein 2C has ATPase and GTPase activities. J.Biol.Chem. **268:**8105-8110.
17. **Rodriguez PL, Carrasco L.** 1995. Poliovirus protein 2C contains two regions involved in RNA binding activity. J Biol Chem **270:**10105-10112.
18. **Morace G, Pisani G, Beneduce F, Divizia M, Pana A.** 1993. Mutations in the 3A genomic region of two cytopath strains of hepatitis A virus isolated in Italy. Virus Research **28:**187-194.
19. **Giraudo AT, Beck E, Strebel K, de Mello PA, La Torre JL, Scodeller EA, Bergmann IE.** 1990. Identification of a nucleotide deletion in parts of polypeptide 3A in two independent attenuated aphthovirus strains. Virology **177:**780-783.
20. **Flanegan JB, Pettersson RF, Ambros V, Hewlett MJ, Baltimore D.** 1977. Covalent linkage of a protein to a defined nucleotide sequence at the 5' terminus of the virion and replicative intermediate RNAs of poliovirus. Proc.Natl.Acad.Sci.U.S.A. **74:**961-965.
21. **Takegami T, Kuhn RJ, Anderson CW, Wimmer E.** 1983. Membrane-dependent uridylylation of the genome-linked protein VPg of poliovirus. Proc.Natl.Acad.Sci.U.S.A. **80:**7447-7451.
22. **Crawford NM, Baltimore D.** 1983. Genome-linked protein VPg of poliovirus present as VPg and VPg-pUpU in poliovirus-infected cells. Proc.Natl.Acad.Sci.U.S.A. **80:**7452-7455.
23. **Jore J, de Geus B, Jackson RJ, Pouwels PH, Engervalk BE.** 1988. Poliovirus protein 3CD is the active protease for processing of the precursor protein P1 in vitro. J.Gen.Virol. **69:**1627-1636.
24. **Nicklin MJH, Krausslich HG, Toyoda H, Dunn JJ, Wimmer E.** 1987. Poliovirus polypeptide precursors: Expression in vitro and processing by exogeneous 3C and 2A proteinases. Proc.Natl.Acad.Sci.U.S.A. **84:**4002-4006.
25. **Palmenberg AC.** 1987. Picornaviral processing: some new ideas. J.Cell.Biochem. **33:**191-198.
26. **de Breyne S, Bonderoff JM, Chumakov KM, Lloyd RE, Hellen CU.** 2008. Cleavage of eukaryotic initiation factor eIF5B by enterovirus 3C proteases. Virology **378:**118-122.
27. **Kundu P, Raychaudhuri S, Tsai W, Dasgupta A.** 2005. Shutoff of RNA polymerase II transcription by poliovirus involves 3C protease-mediated cleavage of the TATA-binding protein at an alternative site: incomplete shutoff of transcription interferes with efficient viral replication. J.Virol. **79:**9702-9713.

28. **Kuyumcu-Martinez NM, Joachims M, Lloyd RE.** 2002. Efficient cleavage of ribosome-associated poly(A)-binding protein by enterovirus 3C protease. Journal of Virology **76:**2062-2074.
29. **Burns CC, Lawson MA, Semler BL, Ehrenfeld E.** 1989. Effects of mutations in poliovirus 3Dpol on RNA polymerase activity and on polyprotein cleavage. J.Virol. **63:**4866-4874.
30. **Oberste MS, Flanegan JB.** 1988. Measurement of poliovirus RNA polymerase binding to poliovirion and nonviral RNAs using a filter-binding assay. Nucleic Acids Res. **16:**10339-10352.
31. **Barton DJ, Flanegan JB.** 1993. Coupled translation and replication of poliovirus RNA in vitro: Synthesis of functional 3D polymerase and infectous virus. J.Virol. **67:**822-831.
32. **Reider E, Paul AV, Kim DW, van Boom JH, Wimmer E.** 2000. Genetic and biochemical studies of poliovirus cis-acting replication element cre in relation to VPg uridylylation. J.Virol. **74:**10371-10380.
33. **Tiley L, King AM, Belsham GJ.** 2003. The foot-and-mouth disease virus cis-acting replication element (cre) can be complemented in trans within infected cells. J.Virol. **77:**2243-2246.
34. **Steil BP, Barton DJ.** 2009. Cis-active RNA elements (CREs) and picornavirus RNA replication. Virus Research **139:**240-252.
35. **Huber SA.** 1994. VCAM-1 is a receptor for encephalomyocarditis virus on a murine vascular endothelial cells. J.Virol. **68:**3453-3458.
36. **Burness ATH.** 1980. Glycophorin and sialylated components as virus receptors, p. 63-84. *In* Lonberg-Holm K, Philipson L (ed.), Receptors and Recognition. Series B, Vol. 8: Virus Receptors. Part 2: Animal Viruses. Chapman and Hall, New York.
37. **Allaway GP, Burness AT.** 1986. Site of attachment of encephalomyocarditis virus on human erythrocytes. J.Virol. **59:**768-770.
38. **Jin YM, Pardoe IV, Burness ATH, Michalak TI.** 1994. Identification of the cell surface 70 kD sialoglycoprotein(s) as a candidate receptor for encephalomyocarditis virus. J.Virol. **68:**7308-7319.
39. **DeTulleo L, Kirchhausen T.** 1998. The clathrin endocytic pathway in viral infection. EMBO **17:**4585-4593.
40. **Lopez de Quinto S, Lafuente E, Martinez-Salas E.** 2001. IRES interaction with translation initiation factors: functional characterization of novel RNA contacts with eIF3, eIF4B, and eIF4GII. RNA **7:**1213-1226.
41. **Belsham GJ, Sonenberg N.** 1996. RNA-protein interactions in regulation of picornavirus RNA translation. Microbiological Reviews **60:**499-511.
42. **Haghighat A, Svitkin Y, Novoa I, Kuechler E, Skern T, Sonenberg N.** 1996. The eIF4G-eIF4E complex is the target for direct cleavage by the rhinovirus 2A proteinase. J.Virol. **70:**8444-8450.
43. **Witherell GW, Gil A, Wimmer E.** 1993. Interaction of polypyrimidine tract binding protein with the encephalomyocarditis virus mRNA internal ribosomal entry site. Biochemistry **32:**8268-8275.

44. **Kaminski A, Hunt SL, Patton JG, Jackson RJ.** 1995. Direct evidence that polypyrimidine tract binding protein (PTB) is essential for internal initiation of translation of encephalomyocarditis virus RNA. RNA **1:**924-938.
45. **Meerovitch K.** 1992. La autoantigen functions in translation initiation of poliovirus RNA. Abstract; Translational Control,Cold Spring Harbor Symposium.
46. **Izumi RE, Valdez B, Banerjee R, Srivastava M, Dasgupta A.** 2001. Nucleolin stimulates viral internal ribosome entry site-mediated translation. Virus Res **76:**17-29.
47. **Bienz K, Egger D, Pfister T.** 1994. Characteristics of the poliovirus replication complex. Archives of Virology **9:**147-157.
48. **Bienz K, Egger D, Pfister T, Troxler M.** 1992. Structural and functional characterization of the poliovirus replication complex. J.Virol. **66:**2740-2747.
49. **Racaniello VR.** 2001. *Picornaviridae*: The viruses and their replication, p. 685-722. *In* Knipe DM, Mowley PM (ed.), Fields Virology, 4th edition ed. Lippincott Williams and Wilkins, Philadelphia, PA.
50. **Dick GWA, Smithburn KC, Haddow AJ.** 1958. Mengo encephalomyocarditis virus:Isolation and immunological properties. Brit.J.Exptl.Path. **29:**547-558.
51. **Dick GWA, Best AM, Haddow AJ, Smithburn KC.** 1948. Mengo encephalomyelitis; a hitherto unknown virus affecting man. Lancet **252:**286-289.
52. **Sanford SE, Rehmtulla AJ, Gaylan KA.** 1989. Encephalomyocarditis virus outbreak among suckling pigs. Can.Vet.J. **30:**178.
53. **Acland HM, Littlejohns IR.** 1975. Encephalomyocardits virus infection of pigs 1. An outbreak in New South Wales. Aust.Vet.J. **51:**409-415.
54. **Grobler DG, Raath JP, Braack LE.** 1995. An outbreak of encephalomyocarditis virus infection in free-ranging African elephants in Kruger National Park. Ondersteport Journal of Veterinary Research **62:**97-108.
55. **Backues KA, Hill M, Palmenberg AC, Aguilar R, Soike KF, Miller C.** 1999. Genetically engineered Mengo virus vaccination and titer development in multiple captive wildlife species. J. Wildlife Diseases **35:**384-387.
56. **Nicholson R, Pelletier J, Le SY, Sonenberg N.** 1991. Structural and functional analysis of the ribosome landing pad of poliovirus type 2: In vivo translation studies. J.Virol. **65:**5886-5894.
57. **Borman A, Jackson RJ.** 1992. Initiation of translation of human rhinovirus RNA: Mapping the internal ribosome entry site. Virology **188:**685-696.
58. **Wang C, Sarnow P, Siddiqui A.** 1993. Translation of human hepatitis C virus RNA in cultured cells is mediated by an internal ribosome-binding mechanism. J.Virol. **67:**3338-3344.
59. **Brown EA, Zajac AJ, Lemon SM.** 1994. *In vitro* characterization of an internal ribosomal entry site (IRES) present within the 5´ nontranslated region of hepatitis A virus RNA: Comparison with the IRES of encephalomyocarditis virus. J.Virol. **68:**1066-1074.
60. **Porter FW, Brown B, Palmenberg A.** 2010. Nucleoporin phosphorylation triggered by the encephalomyocarditis virus leader protein is mediated by mitogen-activated protein kinases. J.Virol. **84:**12538-12548.
61. **Groppo R, Palmenberg A.** 2007. Cardiovirus 2A protein associates with 40S but not 80S ribosome subunits during infection. J. Virol. **81:**13067-13074.

62. **Cornilescu CC, Porter FW, Zhao Q, Palmenberg AC, Markley JL.** 2008. NMR structure of the Mengovirus leader protein zinc-finger domain. FEBS Letters **582:**896-900.
63. **Bacot-Davis VR, Ciomperlik JJ, Cornilescu CC, Basta HA, Palmenberg AC.** 2014. Solution structures of Mengovirus leader protein, its phosphorylated derivatives, and in complex with RanGTPase. Proc. Nat. Acad. Sci. USA **Submitted**.
64. **Chen H-H, Kong W-P, Roos RP.** 1995. The leader peptide of Theiler's murine encephalomyelitis virus is a zinc-binding protein. J.Virol. **69:**8076-8078.
65. **Bacot-Davis VR, Palmenberg AC.** 2013. Encephalomyocarditis virus Leader protein hinge domain is responsible for interactions with Ran GTPase. Virology **443:**177-185.
66. **Basta HA, Bacot-Davis VR, Ciomperlik JJ, Palmenberg AC.** 2014. Encephalomyocarditis virus Leader is phosphorylated by CK2 and syk as a requirement for subsequent phosphorylation of cellular nucleoporins. J.Virol. **88:**2219-2226.
67. **Basta HA, Palmenberg AC.** 2014. AMP-activated protein kinase phosphorylates EMCV, TMEV, and SafV Leader proteins at different sites. Virology **262:**236-240.
68. **Zoll J, Galama JMD, van Kuppeveld FJM, Melchers WJG.** 1996. Mengovirus leader is involved in the inhibition of host cell protein synthesis. J.Virol. **70:**4948-4958.
69. **van Pesch V, van Eyll O, Michiels T.** 2001. The leader protein of Theiler's virus inhibits immediate-early alpha/beta interferon production J.Virol. **75:**7811-7817.
70. **Zoll J, Melchers WJ, Galama JM, van Kuppeveld FJ.** 2002. The mengovirus leader protein suppresses alpha/beta interferon production by inhibition of the iron/ferritin-mediated activation of NF-kappa B. J.Virol **76:**9664-9672.
71. **Ricour C, Delhaye S, Hato SV, Olenyik TD, Michel B, van Kuppeveld FJ, Gustin KE, Michiels T.** 2009. Inhibition of mRNA export and dimerization of interferon regulatory factor 3 by Theiler's virus leader protein. J Gen Virol **90:**177-186.
72. **Ricour C, Borghese F, Sorgeloos F, Hato SV, van Kuppeveld FJ, Michiels T.** 2009. Random mutagenesis defines a domain of Theiler's virus leader protein that is essential for antagonism of nucleocytoplasmic trafficking and cytokine gene expression. J.Virol. **83:**11223-11232.
73. **Borghese F, Michiels T.** 2011. The leader protein of cardioviruses inhibits stress granule assembly. J. Virol. **85:**9614-9622.
74. **Gustin KE, Sarnow P.** 2001. Effects of poliovirus infection on nucleo-cytoplasmic trafficking and nuclear pore complex composition. EMBO J. **20:**240-249.
75. **Park N, Skern T, Gustin KE.** 2010. Specific cleavge of the nuclear pore complex protein Nup62 by a viral protease. J. Biol. Chem. **285:**28796-28805.
76. **Fischer U, Huber J, Boelens WC, Mattaj IW, Luhrmann R.** 1995. The HIV-1 Rev activation domain is a nuclear export signal that accesses an export pathway used by specific cellular RNAs. Cell **82:**475-483.

77. **Askjaer P, Jensen TH, Nilsson J, Englmeier L, Kjems J.** 1998. The Specificity of the CRM1-Rev Nuclear Export Signal Interaction is Mediated by RanGTP. J Biol Chem. **273:**33414-33422.
78. **Rouquette J, Choesmel V, Gleizes P.** 2005. Nuclear export and cytoplasmic processing of precursors to teh 40S subunits in mammalian cells. EMBO **24:**2862-2872.
79. **Cullen BR.** 2003. Nuclear RNA export. J. Cell Science **116:**587-597.
80. **Groppo R, Brown BA, Palmenberg AC.** 2011. Mutational analysis of EMCV 2A protein identifies a nuclear localization signal and an eIF4E binding site. Virology **410:**257-267.
81. **Palmenberg AC, Parks GD, Hall DJ, Ingraham RH, Seng TW, Pallai PV.** 1992. Proteolytic processing of the cardioviral P2 region: 2A/2B cleavage in clone-derived precursors. Virology **190:**754-762.
82. **Zoll J, van Kuppeveld FJM, Galama JMD, Melchers WJG.** 1998. Genetic analysis of mengovirus protein 2A: its function in polyprotein processing and virus reproduction. J.Gen.Virol. **79:**17-25.
83. **Aminev AG, Amineva SP, Palmenberg AC.** 2003. Encephalomyocarditis virus (EMCV) proteins 2A and 3BCD localize to nuclei and inhibit cellular mRNA transcription but not rRNA transcription. Virus Research **95:**59-73.
84. **Schreier MH, Staehelin T.** 1973. Initiation of mammalian protein synthesis: the importance of ribosome and initiation factor quality for the efficiency of in vitro systems. J.Mol.Biol. **73:**329-349.
85. **Lawrence C, Thach RE.** 1974. Encephalomyocarditis virus infection of mouse plasmacytoma cells I. Inhibition of cellular protein synthesis. J.Virol. **14:**598-610.
86. **Hershey JWB.** 1991. Translational control in mammalian cells. Annu. Rev. Biochem. **60:**717-755.
87. **Merrick WC, Hershey JWB.** 1996. The pathway and mechanism of eukaryotic protein synthesis, p. 31-69. *In* Hershey JWB, Mathews MB, Sonenberg N (ed.), Translational Control. Cold Spring Harbor Laboratory Press.
88. **Hershey JWB, Duncan R, Mathews MB.** 1986. Introduction: Mechanisms of Translational Control, p. 1-18. *In* Mathews MB (ed.), Translational Control; Current Communications in Molecular Biology. Cold Spring Harbor Laboratory Press, New York.
89. **Gingras AC, Svitkin Y, Belsham GJ, Pause A, Sonenberg N.** 1996. Activation of the translational suppressor 4E-BP1 following infection with encephalomyocarditis virus and polio. Proc.Natl.Acad.Sci.U.S.A. **93:**5578-5583.
90. **Ryan KJ, Wente SR.** 2000. The nuclear pore complex: a protein machine bridging the nucleus and cytoplasm. Curr Opin Cell Biol **12:**361-371.
91. **Stoffler D, Fahrenkrog B, Aebi U.** 1999. The nuclear pore complex: from molecular architecture to functional dynamics. Curr Opin Cell Biol **11:**391-401.
92. **Takeuchi O, Akira S.** 2009. Innate immunity to virus infection. Immunological Reviews **227:**75-86.
93. **Hato SV, Sorgeloos F, Ricour C, Zoll J, Melchers WJ, Michiels T, Kuppeveld FJv.** 2010. Differential IFN-alpha/beta production suppressing capacities of the

leader proteins of mengovirus and food-and-mouth disease virus. Cell Microbiol **12:**310-317.

94. **Faria PA, Chakraborty P, Levay A, Barber GN, Ezelle HJ, Enninga J, Arana C, van Deursen J, Fontoura BM.** 2005. VSV disrupts the Rae1/mrnp41 mRNA nuclear export pathway. Mol Cell **17:**93-102.
95. **Cui T, Sankar S, Porter AG.** 1993. Binding of encephalomyocarditis virus RNA polymerase to the 3'-noncoding region of the viral RNA is specific and requires the 3'-poly(A) tail. J.Biol.Chem. **268:**1-6.
96. **Hato SV, Ricour C, Schulte BM, Lanke KH, de Bruijni M, Zoll J, Melchers WJ, Michiels T, van Kuppeveld FJ.** 2007. The mengovirus leader protein blocks interferon-alpha/beta gene transcription and inhibits activation of interferon regulatory factor 3. Cell Microbiol **9:**2921-2930.
97. **Gustin KE.** 2003. Inhibition of nucleo-cytoplasmic trafficking by RNA viruses: targeting the nuclear pore complex. . Virus Res. **95:**35-44.
98. **Belov GA, Evstafieva AG, Rubtsov YP, Mikitas OV, Vartapetian AB, Agol V.** 2000. Early alteration of nucleocytoplasmic traffic induced by some RNA viruses. Virology **275:**244-248.
99. **Hirasawa K, Kim A, Han HS, Han J, Jun HS, Yoon JW.** 2003. Effect of p38 mitogen-activated protein kinase on the replication of encephalomyocarditis virus. J.Virol. **77:**5649-5656.
100. **Lidsky PL, Hato S, Bardina MV, Aminev AG, Palmenberg AC, Sheval EV, Polyakov VY, van Kuppeveld FJ, Agol V.** 2006. Nucleo-cytoplasmic traffic disorder induced by cardioviruses. J. Virol. **80:**2705-2717.
101. **Bardina MV, Lidsky P, Sheval EV, Fominykh KV, van Kuppeveld FJ, Polyakov VY, Agol V.** 2009. Mengovirus-induced rearrangements of the nuclear pore complex: Hijacking cellular phosphorylation machinery. J.Virol. **83:**3150-3161.
102. **Dvorak CMT, Hall DJ, Hill M, Riddle M, Pranter A, Dillman J, Deibel M, Palmenberg AC.** 2001. Leader protein of encephalomyocarditis virus binds zinc, is phosphorylated during viral infection and affects the efficiency of genome translation. Virology **290:**261-271.
103. **Dasso M.** 2002. The Ran GTPase: theme and variations. Curr Biol **12:**502-508.
104. **Floer M, Blobel G.** 1996. The nuclear transport factor karyopherin beta binds stoichiometrically to Ran-GTP and inhibits the Ran GTPase activating protein. J Biol Chem **271:**5313-5316.
105. **Seki T, Hayashi N, Nishimoto T.** 1996. RCC1 in the Ran Pathway. J. Biochem. **120:**207-214.
106. **Wilde A, Zheng Y.** 1999. Stimulation of microtubule aster formation and spindle assembly by the small GTPase Ran. Science **284:**1359-1362.
107. **Klebe C, Prinz H, Wittinghofer A, Goody RS.** 1995. The kinetic mechanism of Ran-nucleotide exchange catalyzed by RCC1. Biochemistry **34:**12543-12552.
108. **Guttler T, Gorlich D.** 2011. Ran-dependent nuclear export mediators: a structural perspective. EMBO J. **30:**3457-3474.
109. **Gorlich D, Seewald MJ, Ribbeck K.** 2003. Characterization of Ran-driven transport and the RanGTPase system by kinetic measurements and computer simulation. EMBO J. **22:**1088-1100.

110. **Cheng Y, Prusoff WH.** 1973. Relationship between the inhibition constant (K1) and the concentration of inhibitor which causes 50 per cent inhibition (I50) of an enzymatic reaction. Biochem. Pharmacol. **22:**3099-3108.
111. **Makde RD, England JR, Yennawar HP, Tan S.** 2010. Structure of RCC1 chromatin factor bound to the nucleosome core particle. Nature **467:**562-566.
112. **Renault L, Kuhlmann J, Henkel A, Wittinghofer A.** 2001. Structural basis for guanine nucleotide exchange on Ran by the Regulator of Chromosome Condensation (RCC1). Cell **105:**245-255.
113. **Renault L, Kuhlmann J, Henkel A, Wittinghofer A.** 2001. Structural basis for guanine nucleotide exchange on Ran by the Regulator of Chromatin Condensation (RCC1). Cell **105:**245-255.
114. **Partidge JR, Schwartz TU.** 2009. Crystallographic and bochemical analysis of the Ran-binding zinc finger domain. . J Mol Biol **391:**375-389.
115. **Mosammaparast N, Pemberton LF.** 2004. Karyopherins: from nuclear-transport mediators to nuclear-function regulators. Trends in Cell Biology **14:**547-556.
116. **Aminev AG, Amineva SP, Palmenberg AC.** 2003. Encephalomyocarditis viral protein 2A localizes to nucleoli and inhibits cap-dependent mRNA translation. Virus Research **95:**45-57.
117. **Romanova L, Lidsky P, Kolesnikova M, Fominykh KV, Gmyl AP, Sheval EV, Hato SV, van Kuppeveld FJ, Agol V.** 2009. Antiapoptotic activity of the cardiovirus leader protein, a viral "security" protein. J.Virol. **83:**7273-7284.
118. **Paul S, Michiels T.** 2006. Cardiovirus leader proteins are functionally interchangeable and have evolved to adapt to virus replication fitness. J. Gen. Virol **87:**1237-1246.
119. **Pevear DC, Calenoff MA, Rozhon EJ, Lipton HL.** 1987. Analysis of the complete nucleotide sequence of the picornavirus Theiler's murine encephalomyelitis virus indicates that it is closely related to cardioviruses. J.Virol. **61:**1507-1516.
120. **Zoll J, Hulshof SE, Lanke K, Lunel FV, Melchers WJG, Ven ES-vd, Roivainen M, Galama JMD, Kuppeveld FJMv.** 2009. Saffold virus, a human Theiler's-like cardiovirus, is ubiquitous and causes infection early in life. PLoS Pathogens **5:**1-10.
121. **Martinez-Salas E, Ryan MD.** 2010. Translation and protein processing, p. 141-161. *In* Ehrenfeld E, Domingo E, Roos RP (ed.), The Picornaviruses. ASM Press, Washington D.C.
122. **Petty RV, Palmenberg AC.** 2013. Guanine-nucleotide exchange factor RCC1 facilitates a tight binding between EMCV Leader and cellular Ran GTPase. J. Virol. **87:**6517-6520.
123. **Svitkin YV, Hahn H, Gingras AC, Palmenberg AC, Sonenberg N.** 1998. Rapamycin and wortmannin enhance replication of a defective encephalomyocarditis virus. J.Virol. **72:**5811-5819.
124. **Martin LR, Neal ZC, McBride MS, Palmenberg AC.** 2000. Mengovirus and encephalomyocarditis virus poly(C) tract lengths can affect virus growth in murine cell culture. J. Virol. **74:**3074-3081.
125. **Cheng Y, Patel DJ.** 2004. An efficient system for small protein expression and refolding. Biochem. Biophys. Res. Commun. **317:**401-405.

126. **Hall DJ, Palmenberg AC.** 1996. Mengo virus 3C proteinase: Recombinant expression, intergenus substrate cleavage and localization in vivo. Virus Genes **13:**99-110.
127. **Butterworth BE, Rueckert RR.** 1972. Kinetics of synthesis and cleavage of encephalomyocarditis virus-specific polypeptides. Virology **50:**535-549.
128. **Ray BL, Brendler TG, Adya S, Daniels-McQueen S, Miller JK, Hershey JWB, Grifo JA, Merrick WC, Thach RE.** 1983. Role of mRNA competition in regulating translation: Further characterization of mRNA discriminatory initiation factors. PNAS **80:**663-667.
129. **Jen G, Thach RE.** 1982. Inhibition of host translation in encephalomyocarditis virus-infected L cells: A novel mechanism. J.Virol. **43:**250-261.
130. **Etchison D, Fout GS.** 1985. Human rhinovirus 14 infection of HeLa cells results in the proteolytic cleavage of the p220 cap-binding complex subunit and inactivates globin mRNA translation *in vitro*. J.Virol. **54:**634-638.
131. **Babiss LE, Ginsberg HS, Darnell JE.** 1985. Adenovirus E1B proteins are required for accumulation of late viral mRNA and for effects on cellular mRNA translation and transport. Mol Cell Biol **5:**2552-2558.
132. **Sonenberg N.** 1987. Regulation of translation by poliovirus. Advances in Virus Research **33:**175-204.
133. **Gradi A, Svitkin YV, Imataka H, Sonenberg N.** 1998. Proteolysis of human eukaryotic translation initiation factor eIF4GII, but not eIF4FI, coincides with the shutoff of host protein synthesis after poliovirus infection. Proc Natl Acad Sci U S A **15:**11089-11094.
134. **Wang X, Beugnet A, Murakami M, Yamanaka S, Proud CG.** 2005. Distinct signaling events downstream of mTOR cooperate to mediate the effects of amino acids and insulin on initiation factor 4E-binding proteins. Molecular and Cellular Biology **25:**2558-2572.
135. **Saitoh M, Pullen N, Brennan P, Cantrell D, Dennis P, Thomas G.** 2002. Regulation of an activated S6 kinase 1 variant reveals a novel mammalian target of rapamycin phosphorylation site. The Journal of Biological Chemistry **277:**20104-20112.
136. **Raught B, Gingras A-C.** 1999. eIF4E activity is regulated at multiple levels. Intl.J.Biochem.Cell Biol. **31:**43-57.
137. **Bochkov Y, Palmenberg AC.** 2006. Translational efficiency of an EMCV IRES in bicistronic vectors is dependent upon IRES sequence and gene location. BioTechniques **41:**238-290.
138. **Gharbi SI, Zvelebil MJ, Shuttleworth SJ, Hancox T, Saghir N, Timms JF, Waterfield MD.** 2007. Exploring the specificity of the PI3K family inhibitor LY294002. Biochemical Journal **404:**15-21.
139. **Gorbalenya AE, Chumakov KM, Agol VI.** 1978. RNA-binding properties of nonstructural polypeptide G of encephalomyocarditis virus. Virology **88:**183-185.
140. **Calenoff MA, Badshah CS, Dal Canto MC, Lipton HL, Rundell MK.** 1995. The leader polypeptide of Theiler's virus is essential for neurovirulence but not for virus growth in BHK cells. J.Virol. **69:**5544-5549.

141. **Rdondo-Munoz J, Perez-Garcia V, Rodriguez MJ, Valpuesta JM, Carrera AC.** 2014. PI3KB protects nuclear envelope integrity by controlling RCC1 localization and ran activity. American Society for Microbiology**:**1-41.
142. **Carocci M, Cordonnier N, Huet H, Romey A, Relmy A, Gorna K, Blaise-Boisseau S, Zientara S, Kassimi LB.** 2011. Encephalomyocarditis virus 2A protein is required for viral pathogenesis and inhibition of apoptosis. J.Virol. **85:**10741-10754.
143. **Li HY, Wirtz D, Zheng Y.** 2003. A mechanism of coupling RCC1 mobility to RanGTP production on the chromatin in vivo. J Cell Biol. **160:**635-644.
144. **Makde RD, England JR, Yennawar HP, Tan S.** 2010. Structure of RCC1 chromatin factor bound to the nucleosome core particle. Nature **467:**562-566.
145. **Renault L, Kuhlmann J, Henkel A, Wittinghofer A.** 2001. Structural basis for guanine nucleotide exchange on Ran by the regulator of chromosome condensation (RCC1). Cell **105:**245-255.
146. **Uchida S, Sekiguchi T, Nishitani H, Miyauchi K, Ohtsubo M, Nishimoto T.** 1990. Premature chromosome condensation is induced by a point mutation in the hamster RCC1 gene. Molecular and Cellular Biology **10:**577-584.
147. **Roy A, Kucukural A, Zhang Y.** 2010. I-TASSER: a unified platform for automated protein structure and function prediction. Nat Protoc **5:**725-738.
148. **Zhang Y.** 2009. I-TASSER: Fully automated protein structure prediction in CASP8. Proteins **77:**100-113.
149. **Zhang Y.** 2008. I-TASSER server for protein 3D structure prediction. BMC Bioinformatics **9:**40.
150. **Gern JE, Busse WW.** 2002. Relationship of viral infections to wheezing illnesses and asthma. Nat. Rev. Immunol. **2:**132-138.
151. **Lee W-M, Lemanske RF, Evans MD, Vang F, Pappas T, Gangnon R, Jackson DJ, Gern JE.** 2012. Human rhinovirus species and season of infection determine illness severity. Am. J. Respir. Crit. Care Med. **186:**886-891.
152. **Gern JE, Busse WW.** 1999. Association of rhinovirus infections with asthma. Clin Microbiol Rev **12:**9-18.
153. **Palmenberg AC, Spiro D, Kuzmickas R, Wang S, Djikeng A, Rathe JA, Fraser-Liggett CM, Liggett SB.** 2009. Sequencing and analysis of all known human rhinovirus genomes reveals structure and evolution. Science **324:**55-59.
154. **Greve JM, Davis G, Meyer AM, Forte CP, Yost SC, Malor CW, Kamarck ME, McClelland A.** 1989. The major human rhinovirus receptor is ICAM-1. Cell **56:**839-847.
155. **Staunton DE, Merluzzi VJ, Rothlein R, Barton R, Marlin SD, Springer RA.** 1989. A cell adhesion molecule, ICAM-1 is the major surface receptor for rhinoviruses. Cell **56:**849-853.
156. **Hofer F, Gruenberger M, Kowalski H, Machat H, Huettinger E, Kuechler E, Blaas D.** 1994. Members of the low density lipoprotein receptor family mediate cell entry of a minor-group common cold virus. Proc Natl Acad Sci U S A **91:**1839-1842.
157. **Martin S, Casasnovas JM, Staunton DE, Springer TA.** 1993. Efficient Neutralization adn Disruption of Rhinovirus by Chimeric ICAM-1/Immunoglobulin Molecules. J Virol **67:**3561-3568.

158. **Casasnovas JM, Springer TA.** 1995. Kinetics anf Thermodynamics of Virus Binding to Receptor. J Biol Chem. **270:**13216-13224.
159. **Casasnovas JM, Bickford JK, Springer TA.** 1998. The Domian Structure of ICAM-1 and the Kinetics of Binding Rhinovirus. J Virol **72:**6244-6246.
160. **Kim BB, Dikova EB, Sheller U, Dikov MM, Gavrilova EM, Egorov AM.** 1990. Evaluation of dissociation constants of antigen-antibody complexes by ELISA. J Immunol Methods **131:**213-222.
161. **Liliom K, Orosz F, Horvath L, Ovadi J.** 1991. Quantitative evaluation of indirect ELISA. J Immunol Methods **143:**119-125.
162. **Nakagome K, Bochkov YA, Ashraf S, Brockman-Schneider RA, Evans MD, Pasic TR, Gern JE.** 2014. Effects of rhinovirus species on viral replication and cytokine production. American Academy of Allergy, Asthma & Immunology **134:**332-341.
163. **Bochkov YA, Palmenberg AC, Lee W-M, Rathe JA, Amineva SP, Sun X, Pasic TR, Jarjour NN, Liggett SB, Gern JE.** 2011. Molecular modeling, organ culture and reverse genetics for a newly identified human rhinovirus C. Nature Medicine **17:**627-632.
164. **Ashraf S, Brockman-Schneider R, Bochkov YA, Pasic TR, Gern JE.** 2013. Biological characteristics and propagation of human rhinovirus-C in differentiated sinus epithelial cells. Virology **436:**143-149.
165. **Lee WM, Wang W, Rueckert RR.** 1995. Complete sequence of the RNA genome of human rhinovirus 16, a clinically useful common cold virus belonging to the ICAM-1 receptor group. Virus Genes **9:**177-181.
166. **Lee WM, Monroe SS, Rueckert RR.** 1993. Role of maturation cleavage in infectivity of picornaviruses: Activation of an infectosome. J.Virol. **67:**2110-2122.
167. **Palmenberg AC, Rathe J, Liggett S.** 2010. Analysis of the complete genome sequences of human rhinovirus. J. Allergy and Clinical Immunology **125:**1190-1199.
168. **Basta HA, Sgro J-Y, Palmenberg AC.** 2014. Modeling of the human rhinovirus C capsid suggests a novel topology with insights on receptor preference and immunogenicity. Virology **448:**176-184.
169. **Smith TJ, Olson NH, Ceng RH, Liu H, Chase ES, Lee WM, Leippe DM, Mosser AG, Rueckert RR, Baker TS.** 1993. Structure of human rhinovirus complexed with Fab fragments from a neutralizing antibody. J.Virol. **67:**1148-1158.
170. **Tormo J, Stadler E, Skern T, Auer H, Kanzler O, Betzel C, Blaas D, Fita I.** 1992. Three-dimensional structure of the Fab fragment of a neutralizing antibody to human rhinovirus serotype 2. Protein Sci. **1:**1154-1161.
171. **Colonno RJ, Callahan PL, Long WJ.** 1986. Isolation of a monoclonal antibody that blocks attachment of the major group of human rhinoviruses. J.Virol. **57:**7-12.
172. **Jang YJ, Kwon HJ, Lee BJ.** 2006. Effect of clarithromycin on rhinovirus-16 infection in A549 cells. Eur Respir J **27:**12-19.
173. **Funkhouser AW, Kang JA, Tan A, Li J, Zhuo L, Abe MK, Solway J, Hershenson MB.** 2004. Rhinovirus 16 3C protease induces interleukin-8 and

granulocyte-macrophage colony-stimulating factor expression in human bronchial epithelial cells. Pediatr Res **55:**13-18.

174. **Oliveira MA, Zhao R, Lee W, Kremer MJ, Minor I, Rueckert RR, Diana GD, Pevear DC, Dutko FJ, McKinlay MA.** 1993. The structure of human rhinovirus 16. Structure **1:**51-68.
175. **Hadfield AT, Oliveira MA, Kim KH, Minor I, Kremer MJ, Heinz BA, Shepard D, Pevear DC, Rueckert RR, Rossmann MG.** 1995. Structural studies on human rhinovirus 14 drug-resistant compensation mutants. J Mol Biol **253:**61-73.
176. **Rossmann MG.** 1989. The canyon hypothesis. J.Biol.Chem. **264:**14587-14590.